New Astronomy 114 (2025) 102297

Contents lists available at ScienceDirect

New Astronomy

journal homepage: www.elsevier.com/locate/newast

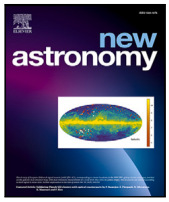

Discovery of 226 δ Scuti and γ Doradus Stars near NGC 6871 with *TESS*

Ai-Ying Zhou *

National Astronomical Observatories, Chinese Academy of Sciences, A20 Datun Road, Chaoyang District, Beijing, 100101, PR China
Key Laboratory of Radio Astronomy and Technology (CAS), Beijing, PR China

ARTICLE INFO

This research is dedicated to my wife Jingyun Zhang who has been supporting my works all the time.

Keywords:
Stars: oscillation (pulsation)
Stars: variables: δ Scuti
γ Doradus
Techniques: photometric
Stars: individual: HD 191025
HD 227647
HD 227941
TYC 2682-863-1
HD 227505

ABSTRACT

We present the discovery of 269 pulsating variable stars of δ Scuti, γ Doradus, and Maia types in the vicinity of the open cluster NGC 6871, using data from the Transiting Exoplanet Survey Satellite (*TESS*). Our small-scale regional survey centered on the δ Scuti star V1821 Cyg in the open cluster NGC 6871, covering a radius of one degree. The results include a remarkable total of 1512 newly classified variable stars, comprising the following categories: 105 δ Scuti stars, 121 γ Doradus stars, 50 Maia variables, 198 eclipsing binary systems, with 12 exhibiting pulsating or rotating components, 500+ rotating variable stars, and dozens of other types. Out of 1512 newly discovered variable stars, 108 are confirmed members of NGC 6871 with a membership probability exceeding 50%. Notably, dedicated Fourier analyses were applied to eight representative stars from the newly discovered variables. Among these, one star exhibits a rich and complex pulsation spectrum characterized by amplitude variations in dominant pulsations. To contextualize the new pulsators, we plotted them in the Hertzsprung–Russell diagrams alongside the largest known group of class member stars. Surprisingly, both δ Scuti and γ Doradus stars occupy nearly the same region in the diagrams, hinting at a potential unified pulsation mechanism. This study contributes valuable insights into the variability census of NGC 6871 and sheds light on the pulsation behavior of different stellar types. Further investigations into the physical properties and evolutionary status of these stars are warranted.

1. Introduction

Variable star analysis and classification is an important task in understanding stellar features and processes. Several all-sky variability surveys on ground together with the advent of high-precision space-based photometry projects have revolutionized the identification and classification of variable stars. Both automated classification employing supervised machine learning techniques and traditional visual inspection play crucial roles in this endeavor. Notable projects such as, OGLE-IV (Soszyński et al., 2021; Pietrukowicz et al., 2020), ASAS-SN Catalog of Variable Stars X (Christy et al., 2022), ZTF (Bellm et al., 2019; Masci et al., 2019; Ofek et al., 2020; Chen et al., 2020), the *Kepler* variables (Bass and Borne, 2016; McQuillan et al., 2014; Slawson et al., 2011; Uytterhoeven et al., 2011) and the *TESS* variables (Fetherolf et al., 2023; Prša et al., 2022; Balona, 2022b,a; Balona and Ozuyar, 2020; Antoci et al., 2019), alongside the expansive *Gaia* DR2 Variability Results of 363 969 records (Gaia Collaboration et al., 2018a), and *Gaia* DR3 Part.4 Variability catalogs of 9 976 881 variables (Gaia Collaboration et al., 2023), have amassed an unprecedented volume of variable stars. These stars, meticulously categorized by their variability mechanisms, are invaluable astrophysical probes for unraveling the structure and evolution of the Milky Way Galaxy and the cosmos at large.

Main-sequence stars of spectral types A and F (hereafter 'AF' stars), stand out as prime subjects for pulsational variability studies. However, their inherent rotation – often with periods documented in sources such as McQuillan et al. (2014), Nielsen et al. (2013) – may also lead to observable brightness fluctuations. These variations are attributed to starspots with heterogeneous distributions across the stellar surface. Moreover, the current sensitivity threshold of photometric observations could potentially obscure the detection of some forms of intrinsic variability.

The NASA's Transiting Exoplanet Survey Satellite (*TESS*, Ricker et al. 2015) data offer an unparalleled opportunity to examine the light variations of numerous stars with exceptional precision. In pursuit of this, we embarked on a mission to identify new variables using space-borne photometry, achieving a precision of a few parts per million (ppm). Our goal is to refine the distribution and incidence rate of variables across the sky and map their populations across the stages of stellar evolution on the Hertzsprung–Russell (H–R) diagram. Our survey zeroes in on the discovery of new pulsating AF variables within the

* Correspondence to: National Astronomical Observatories, Chinese Academy of Sciences, A20 Datun Road, Chaoyang District, Beijing, 100101, PR China.
E-mail address: aiying@nao.cas.cn.

https://doi.org/10.1016/j.newast.2024.102297
Received 8 May 2024; Received in revised form 15 July 2024; Accepted 21 August 2024
Available online 14 September 2024
1384-1076/© 2024 Elsevier B.V. All rights are reserved, including those for text and data mining, AI training, and similar technologies.

lower portion of the instability strip, with a focus on the realms of δ Scuti stars and γ Doradus stars.

Utilizing *TESS* data, we conducted a search for new variables within a 60-arcminute radius centered on the δ Scuti star V1821 Cyg, situated in the open cluster NGC 6871 in the Cygnus constellation. The preliminary findings of this targeted regional survey are summarized in the research note by Zhou (2023b).

This paper details the final results of our comprehensive survey. Section 2 introduces the sample of targets, followed by an exposition of the analyzed light curves data and the analysis methods in Sections 3 and 4. The following sections present the results in Section 5, discussions of cluster membership and contamination issues of *TESS* light curves are presented in Section 6, and the conclusions in the final section.

2. Sample of targets

The affiliation of a star with a stellar cluster provides independent measures of its age and distance. When such a member is also a pulsating variable, it becomes possible to ascertain an asteroseismic age. The young Galactic stellar open cluster NGC 6871 harbors a rich population of δ Scuti stars, with at least 15 including V1821 Cyg and V2238 Cyg (Jeon et al., 2012). Unfortunately, Simbad does not index the other stars' variabilities properly, while six of these variables HD 227942, HD 227876, TYC 2683-2756-1, TYC 2679-1381-1, UCAC4 629-090838 are listed as *Gaia* DR3 pulsators (Gaia Collaboration et al., 2023). These six stars' δ Sct type is confirmed in this work. A search within a 60-arcminute radius centered on NGC 6871 in the Simbad database revealed 6126 objects. This population includes a variety of variable types, with 29 explicitly classified as 'dS*' (δ Sct), 47 as RR Lyrae, 284 as BY Draconis, 460 as RS CVn, 737 as eclipsing binaries, etc. Interestingly, no γ Doradus stars were found in this search. However, further inspection of the 29 δ Sct stars revealed that 28 stars are designated as ZTF variables (Chen et al., 2020), and four of them were previously classified as pulsators with ATO identifiers by Heinze et al. (2018). Actually, there are more than 33 known δ Sct recognized in this list. Despite its modest apparent angular size of about 32 arcminutes in diameter (Tadross, 2011) and a membership of fewer than five hundred stars (see Section 6.2 for details), the region surrounding NGC 6871 is a fertile field for the discovery of pulsating variables due to several factors that make it particularly conducive to such a search:

- Discovery Connection: The observation of the known δ Sct star V1821 Cyg (Zhou et al., 2001a) within the open cluster NGC 6871 led to the serendipitous discovery of another δ Sct star, GSC 2683-3076 (also known as V2238 Cyg), by the author (Zhou et al., 2001b). However, neither star is a member of NGC 6871 (Zhou et al., 2001b; Reimann, 1989; Delgado et al., 1984).
- Optimal Age: NGC 6871 is a young open cluster with an age range determined between 5.5 and 11.6 Myr (Casado and Hendy, 2023; Dias et al., 2021; Cantat-Gaudin et al., 2020; Southworth et al., 2004; Loktin et al., 1994). This young age range, rich in massive hot stars, makes it a prime hunting field for astronomers seeking pulsating variable stars. Many types of pulsating variables, like β Cephei and Slowly Pulsating B-type (SPB) stars, δ Scuti and γ Doradus stars, are most active in this age range before they evolve into more stable burning phases. Studies by Kang et al. (2007) and Viskum et al. (1997) have shown that open clusters with intermediate ages between 0.3 and 1.0 Gyr and distances between 1 and 2 kpc are prime targets for asteroseismological investigations of δ Scuti stars. This preference is due to the well-understood relationship between a star's age and its oscillation frequencies and the versatile application of a color-magnitude diagram (CMD) for a cluster, as demonstrated by Kjeldsen (2000).
- Metallicity Influence: Given the stellar mass and chemical composition of a Zero-Age Main Sequence (ZAMS) star, the stellar modeling can, in principle, predict the stellar evolutionary track. Metallicity refers to the abundance of elements heavier than hydrogen and helium in a celestial object. NGC 6871 is known to have a relatively low metallicity, with [Fe/H] = -0.33 ± 0.10 dex (equivalent to $Z = 0.009$, Paunzen et al. 2010, Tadross 2003) or a metal abundance of $Z = 0.018$ (Casado and Hendy, 2023), contrasts with the solar value $Z_{\odot} = 0.0152$. Southworth et al. (2004) used normal solar helium and metal abundances, a chemical composition of (Z, Y) = (0.02, 0.28), when modeling a NGC 6871 member, the detached eclipsing binary V453 Cygni. Lower metallicity affects a star's ability to transport radiation from its core to its surface, influencing the conditions for pulsations and driving pulsational instabilities (Catelan and Smith, 2015). Studying pulsators being cluster members helps validate theories about the relationship between pulsation, rotational velocity, and metallicity for normal main-sequence Population I pulsators (see e.g. section IV of Breger, 1979), and the period-luminosity-metallicity relations for RR Lyrae stars, Population II Cepheids, anomalous Cepheids and SX Phe stars pulsating in the fundamental and first-overtone modes (Nemec et al., 1994).
- Field of View: NGC 6871 offers a balance between a rich stellar population and a relatively sparse field to minimize blending in CCD observations. However, regarding the *TESS* CCD cameras, the cluster's density can still lead to some contamination by nearby objects in certain stars (see Figs. 1, 2, and 9). This highlights the need for careful analysis to disentangle the signals from individual stars.

TESS is designed to monitor approximately ~150 million stars brighter than *TESS* magnitude ($T_{\rm mag}$) of roughly 16, delivering photometric precision from 60 ppm to 3%. To capitalize on the highest photometric quality, our sample is confined to stars with $T_{\rm mag}$ between 16 and 6. From *TESS* Input Catalog (TIC v8.2, Paegert et al., 2021), we extracted 52,681 stars within a 60-arcminute radius centered on the δ Scuti star V1821 Cyg, ensuring alignment with *TESS* premium targets known for their superior photometry.

Our survey's target selection relied upon objects unreported for variability, specifically those of spectral types A and F. This led to a further refinement based on effective temperatures, filtering for a range between 10,000 and 6000 K — roughly corresponding to main sequence stars of spectral types A to F, which include the domains of δ Sct and γ Dor stars on H–R diagram. Consequently, we obtained 13,980 stars within the desired temperature bracket. An additional 9468 stars, initially lacking effective temperature data in *TESS* Input Catalog (TIC v8.2, Paegert et al., 2021), underwent cross-referencing with Gaia DR2 (Gaia Collaboration et al., 2016, 2018b) and DR3 (Gaia Collaboration et al., 2023) for temperature verification and subsequent filtering. After excluding known variables, we isolated 4,726 candidate AF stars with uncharted variability and accessible *TESS* light curves. The spectral classification was primarily sourced from Simbad or, when unavailable, was empirically deduced from the effective temperature.

3. The data

3.1. TESS data

The Transiting Exoplanet Survey Satellite (*TESS*, Ricker et al. 2015) is an MIT-led NASA mission dedicated to discovering transiting exoplanets orbiting nearby bright stars by an all-sky photometry survey. *TESS* rotates every ~13.7 days per orbit, and it is equipped with four identical cameras with a combined field-of-view (FOV) of 24° ×96° (known as an observing sector). A brief description of *TESS* was encapsulated in Zhou (2024). Readers can refer to the details in both the *TESS*

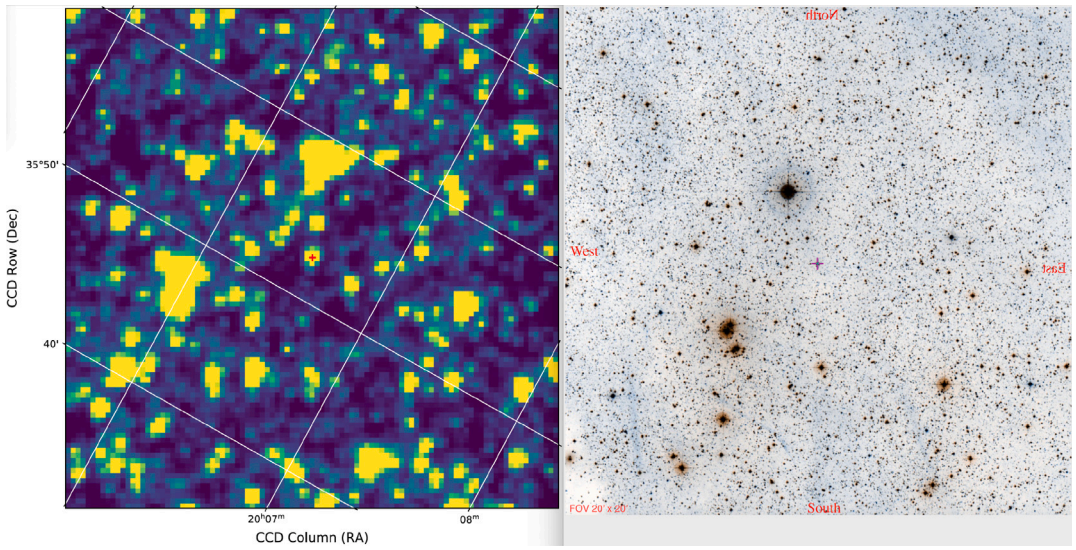

Fig. 1. Comparison of *TESS* images cutout from Full Frame Images (FFI, Sector 55, Camera 3 and CCD 1) with the Digitized Sky Survey image (DSS). Both images are centered on V1821 Cyg (red cross) and have the same size (99 × 99 pixels), corresponding to a field of view with a radius of approximately 20 arc minutes, but slightly rotated orientations. FFI cutouts are requested via Astrocut (Brasseur et al., 2019).

Science Data Products Description Document[1] and the "Characteristics of the *TESS* space telescope" web page.[2]

The *TESS* space telescope's 16 2 K × 2 K frame transfer CCDs are engineered to capture and output images incessantly at 2-second intervals. These frames, however, undergo on-board processing by the data handling unit (DHU), which stacks 2-second exposures into sets of 60, 300 or 900, thus generating images with 2-minute, 10-minute, and 30-minute cadences for the primary observational data. The amassed data on spacecraft are relayed to Earth as the spacecraft approaches its orbital perigee, which occurs roughly every ∼13.7 days. Each celestial sector undergoes a dual observation cycle spanning 27.4 days, punctuated by a systematic intermission ranging from about half a day to one and a half days between consecutive orbits. Acknowledging the intricacies of the spacecraft's timing structure is paramount when embarking on frequency domain data analysis.

TESS observed the NGC 6871 field in Sectors 14, 15, 41, 54, 55, 74, and 75. For each star, the shortest-exposure light curves are downloaded from the latest observation (Sectors 1-75), prioritizing products of 20-second and 2-minute cadences SPOC (MAST Team, 2021a,b), TESS-SPOC (Caldwell et al., 2020), QLP (Huang, 2020), and TASOC (Handberg et al., 2019) available at Mikulski Archive for Space Telescopes (MAST[3])

TESS has an exceptionally large image scale of 21″ per pixel, i.e. the cameras map a 21 arcsecond^2 sky area onto a pixel (Ricker et al., 2014), causing most *TESS* light curves resulted from aperture photometry of the combined light of multiple stars. *TESS* images are highly susceptible to crowding, blending, and source confusion. When analyzing *TESS* light curves, there is considerable risk of attributing detected variability to the wrong source, which would invalidate any analysis. During our search and classification of new variables, blending occasionally occurs. We indeed encountered at least six stars forming three pairs, each pair exhibits seemingly identical light curves and periodograms (see Figs. 2 and 9). One blending case is investigated in Section 5.2. During the identification process, visualization of both light curves and periodograms has helped mark such cases. Methods for pinpointing the true variability source are discussed in Section 6.3.

[1] https://archive.stsci.edu/missions-and-data/tess
[2] https://heasarc.gsfc.nasa.gov/docs/tess/the-tess-space-telescope.html
[3] https://mast.stsci.edu/portal/Mashup/Clients/Mast/Portal.html

3.2. Gaia and TIC v8.2 data

Both *Gaia* (DR2/DR3, Gaia Collaboration et al., 2016, 2018b, 2023) archive and *TESS* Input Catalog (TIC v8.2, Paegert et al., 2021) are employed to retrieve astronomical and stellar parameters for evaluating stellar properties and their locations on H–R diagram.

4. Data analysis, methodology and identification

The classification of variability types hinges on the integration of light curve morphology, periodogram analysis, and astrophysical parameters. This triad elucidates the positioning of stars on the H–R diagram specific to pulsating variables. Our survey leveraged an interactive approach, utilizing a Python program refined from Zhou (2023c), which facilitated the entire data processing sequence.

Prior to the acquisition of light curves, we conducted a preliminary variability check for each candidate against a comprehensive database of known variable stars. This database included the extensive *Gaia* DR3 Part.4 Variability (9 976 881 objects, Gaia Collaboration et al. 2023), *Gaia* DR2 Variability Results of 363 969 records (Gaia Collaboration et al., 2018a), 378 861 variables in ASAS-SN Catalog of Variable Stars X (Christy et al., 2023), 123 841 and 84 206 *TESS* variables (Balona, 2022a; Fetherolf et al., 2023), among other scholarly sources. Subsequent verification was performed programmatically via online resources such as Simbad and VSX to confirm non-inclusion. We systematically excluded known variables, stars lacking *TESS* data, and those not classified as A or F spectral types. The remaining candidates, unreported for variability, constituted the final selection pool. The intricate steps of the classification process are outlined in Zhou (2023a,c).

4.1. Light curve morphology of related stars

The light curve morphology of typical γ Dor stars is readily discernible when visualized through one-sector *TESS* data on a computer display. This clarity also extends to eclipsing binary systems, RR Lyr stars of RRab subtype, heartbeat stars, and rotating variables such as ACV, ELL, and SXARI subtypes. However, for δ Sct stars, the application of Fourier analyses or periodograms is often indispensable to visibly delineate their frequency spectrum. Given the H–R diagram overlap between GDOR and solar-like stars, coupled with occasionally ambiguous

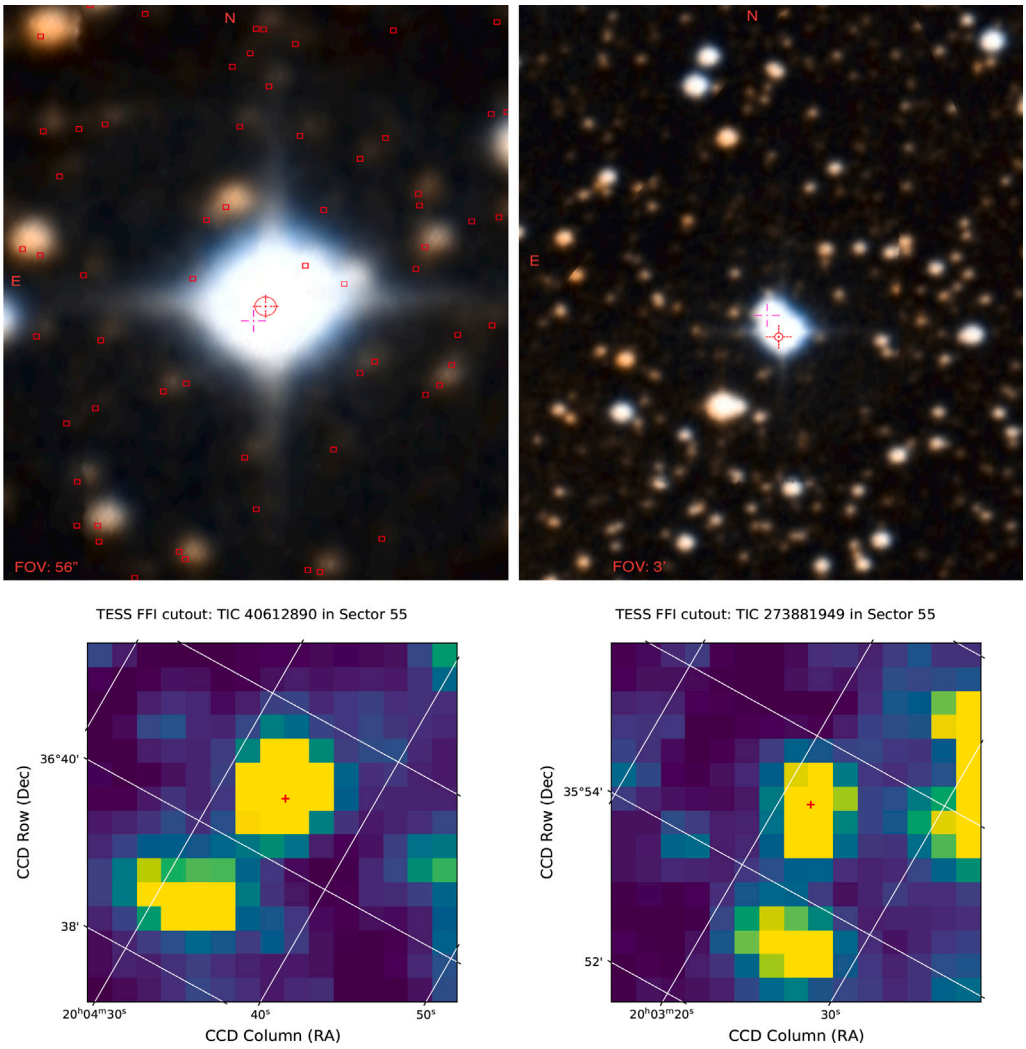

Fig. 2. Stars blending in NGC 6871 field, which leads to the same *TESS* light curves and periodograms. Left: a new δ Sct star TIC 40612890 (= TIC 1966659741 = HD 227487, $T_{\rm mag}$ = 9.m397, red Sun cross), blended by TIC 1966659713 on its lower left (red cross, $T_{\rm mag}$ = 10.m43), while two TIC stars (40612895, 1966659735, red circles on its upper right) are fainter than 16.m2; Right: a new Maia star TIC 273881949 (= HD 227369, $T_{\rm mag}$ = 10.m07, Red Sun cross) blended by TIC 273881940 ($T_{\rm mag}$ = 12.m43, red cross) on its upper left. In these cases, the Target Pixel Files at bottom are unable to tell real source of variability. The DSS images were captured from the Astroview window in MAST while searching the TIC catalog. TPFs are FFI cutout sized 15 × 15 pixels, equivalent to FOV of $3' \times 3'$, comparable with the top right DSS image.

light curves, frequency analysis emerges as a necessary and beneficial tool.

Recent models by Xiong et al. (2016) suggest that pulsational driving of low degree modes in δ Sct stars does not occur for effective temperatures exceeding 9000 K. Consequently, Maia variables have been categorized as either hot and anomalous γ Dor stars, hot hybrid δ Sct-γ Dor stars, or cool B stars with high-frequency pulsations, following the observational definition of Maia variables as a hotter extension of δ Sct stars (Balona, 2023; Balona and Ozuyar, 2020). However, the classification of Maia variables remains a topic of dispute among astronomers (Kahraman Aliçavuş et al., 2024).

In our study, which concentrates on DSCT and GDOR types, stars demonstrating solar-like rotational modulation, classified as 'solar_rm' by Gaia DR3, and general various rotating stars classified as 'ACV|CP|MCP|ROAM|ROAP|SXARI' by Gaia DR3 are collectively designated as 'ROT' type. This follows the precedent set by Balona and Ozuyar (2020), Balona (2022a), and typically, further subclassifications is not pursued.

Distinguishing between certain variable star classes can be challenging, particularly for EB/EW/ELL, DSCT/RRc, and GDOR/ROT(solar-like). To address these potential ambiguities, two classifications are assigned during the identification process. A classification of 'Variable' is applied when a definitive variability type cannot be assigned. The 'unclear' is assigned to serve as a placeholder for uncertain variability cases. These stars are finally abandoned. However, a crucial strategy is employed throughout the identification process: we prioritize avoiding ambiguous classifications for DSCT and GDOR stars, which are our primary targets of interest.

4.2. Frequency analysis and pulsation spectra of related stars

For identification purpose, we employ the Lomb–Scargle Periodogram available in Lightkurve (Lightkurve Collaboration et al., 2018) to obtain the Fourier spectrum in real-time. In the pulsation analyses of the eight example stars featured in Section 5, we utilized the PERIOD04 software package (Lenz and Breger, 2005) for Fourier analysis of their light curves, adhering to the protocol delineated in Zhou (2024). Initially, a classical Fourier transform is applied to the processed light curves, producing an amplitude spectrum that graphically represents the signal's intensity across various frequencies. Subsequent prewhitenings are conducted to isolate significant frequencies. This iterative process involves subtracting the best-fitting sine waves from the light curve and recalculating the Fourier transform on the residuals. With each newly identified frequency, we optimize the parameters of

Table 1
Eight representative discoveries of new variable stars. Candidates marked '?' require further investigation.

SN	TIC	Simbad main identifier	Variability Status
01	TIC 41189624	HD 191025	DSCT/Maia
02	TIC 40831024	HD 227647	DSCT
03	TIC 42254956	HD 227941	DSCT
04	TIC 91945834	–	DSCT: mono-periodic
05	TIC 1966084202	–	DSCT+GDOR(?)
06	TIC 274636885	TYC 2682-863-1	GDOR
07	TIC 1966186334	–	GDOR
08	TIC 89119933	HD 227505	GDOR

all accumulated sine waves through a least-squares fitting procedure. The prewhitening process continues until the amplitude spectrum is devoid of significant peaks.

While the initial Fourier spectrum already displays all extractable frequencies, prewhitening is not strictly necessary for classification purposes and is thus omitted during the screening process. However, in detailed analyses, prewhitening is instrumental in verifying that the identified peaks are genuine and not the result of aliasing. The final step involves recalculating the signal-to-noise ratio (SNR) based on the residuals, with all significant frequencies prewhitened.

4.3. Location on H-R diagram of related stars

Our focal subjects, DSCT and GDOR stars, reside in the lower region of the classical instability trip, on and near the main-sequence evolutionary stage, with some stars just transitioning off the MS. These stars typically possess masses ranging from 1 to 2 solar masses and exhibit luminosities below 50 $L_{\odot}$, with effective temperatures ($T_{\rm eff}$) spanning from 6500 to 8500 K, corresponding to spectral types from A2 to late F. Special consideration is given to stars at the extremities of this range: those cooler than 6500 K, which verge into G-type or solar-like stars, and those hotter than 8500 K, which approach the Slowly Pulsating B-type (SPB) domain. In instances of higher luminosity, alternative classifications are explored.

5. Results

Utilizing data from the Transiting Exoplanet Survey Satellite (*TESS*), the author meticulously examined a targeted area centered on V1821 Cyg around the open cluster NGC 6871. The selection of survey sample stars was strategic, focusing on those with *TESS* magnitudes ($T_{\rm mag}$) ranging from 6 to 16 mag, matching the *TESS* premium targets with high-quality photometry. These stars also fell within the effective temperature range of 10000 and 6000 K, roughly corresponding to main sequence stars of spectral types A to F, which includes the domains of δ Sct and γ Dor stars.

Out of the 4726 candidates examined, a remarkable 1512 new variable stars were identified, categorized as follows: 105 δ Sct stars; 121 γ Dor stars; 50 Maia variables; 198 eclipsing binary systems, with 12 exhibiting pulsating or rotating components; over 500 rotating variables; and a few others.

Comprehensive details for all the newly discovered variables are available on Zenodo DOI: 10.5281/zenodo.10215618. Below, we present Fourier analyses on eight exemplary cases from these discoveries (refer to Table 1), along with two dozens additional representative examples of the new variables in Appendix D, Figs. D.19–D.21. All reported dependent frequencies fall within the adopted frequency resolution.

5.1. Four representative δ Sct stars

5.1.1. δ Sct: HD 191025

HD 191025 (= TIC 41189624, V = 8$^{\rm m}$.75, A5V) was observed by *TESS* in Sectors 14, 15, 41, 54, and 55, with 2-minute cadence. No variability was found in the literature, Simbad/CDS and VSX. We selected the light curves in the three sectors in proximity: 41, 54, and 55, a Fourier analysis was conducted and resulted in multiple frequencies (Fig. 3). We noted the presence of several pulsation frequencies lower than 5 d^{-1}. This star exhibits characteristics of a low-amplitude hybrid δ Sct-γ Dor pulsating variable, but with wider dispersed pulsations being typical to Maia stars. More than 39 significant pulsation frequencies are resolved over signal-to-noise level 4.9, see Fig. 3 and Table 2. We investigated its effective temperature from TIC v8.2, *Gaia* DR2 and DR3. These sources provide values of 8137, 8228, and 10253 K, respectively. If the higher temperature from *Gaia* DR3 is accurate, this star would be classified as a Maia variable.

5.1.2. δ Sct: HD 227647

HD 227647 (= TIC 40831024, V = 10$^{\rm m}$.29, A2) was observed in *TESS* Sectors 14, 15, 41, 54, and 55. No variability was reported in the literature. By a Fourier analysis of the light variations, it is identified to be a new high-frequency δ Sct pulsating variable star. Table 3 reports the 16 pulsation frequencies detected over a significant level of SNR=4.9 in the range of 36–65 d^{-1}, and Fig. 4 shows the light curves and Fourier spectrum based on the data in Sector 41. Since no significant peaks were observed below 36 d^{-1} and relatively simple pulsational spectrum, only one sector's data were analyzed.

5.1.3. δ Sct: HD 227941

HD 227941 (A5 D, B = 9$^{\rm m}$.41, V = 9$^{\rm m}$.23, = TIC 42254956) was observed by *TESS* in Sectors 14, 15, 41, 54, and 55, during 2019.07.18 UT 20:34:00 and 2022.09.01 UT 18:23:16, i.e. BJD 24571683.35775–24572824.26696. We used the TESS-SPOC light curve products at MAST. The star is now identified to be a new δ Sct star with dense low-amplitude pulsation frequencies where the dominant pulsation's amplitude varied over the time. Fig. 5 displays the periodograms obtained for Sectors 41, 54, and 55, respectively. The variation in the strength of the main frequencies across sectors is particularly interesting. Due to Sectors 14 and 15 are 30-minute cadence data, there are aliases beyond the Nyquist frequency of about 24 d^{-1}. For resolving pulsation frequencies, a Fourier analysis was performed on the combination of the 10-minute cadence data in three Sectors 41, 54, and 55, and the result is shown in Fig. 6. According to TIC v8.2, $T_{\rm eff}$ = 7901 ± 166 K, $\log g$= 4.184 ± 0.073, stellar radius: 1.84 ± 0.05 $R_{\odot}$, stellar mass: 1.891 ± 0.296 $M_{\odot}$, stellar luminosity: 11.925 ± 0.761 $L_{\odot}$, and *Gaia* DR3 parameters $T_{\rm eff}$ = 7751.96 K and $\log g$ = 4.075, this star is a representative δ Sct (see Table 4).

5.1.4. TIC 91945834

TIC 91945834 has a *TESS* magnitude of 13$^{\rm m}$.4526, with stellar parameters well in DSCT domain: $T_{\rm eff}$ = 6748 (TIC), $L/L_{\odot}$= 15.966 (GDR3), $\log g$= 3.665 (GDR3), Mass = 1.44 $M_{\odot}$, Radius = 2.924 $R_{\odot}$ (GDR2). It is not indexed in Simbad. A Fourier analysis identified the star to be a mono-periodic DSCT with presence of harmonics. See Fig. 7 and Table 5.

5.2. δ Sct-γ Dor hybrid candidate TIC 1966084202

This star has *TESS* magnitude 13$^{\rm m}$.475, it is not indexed in Simbad, TIC v8.2 cross-matched it with a *Gaia* DR2 identifier 2058936510610300032. The stellar parameters in known databases as follows would well place the star in the DSCT-GDOR intersection: $T_{\rm eff}$ = 6766 ± 122 K (TIC); $L/L_{\odot}$= 6.621 (GDR3); $\log g$= 4.055 (GDR3); Mass = 1.45 $M_{\odot}$; Radius = 1.873 $R_{\odot}$(GDR2). Fig. 8 and Table 6 present the periodogram and frequency solution.

Table 2
Frequency solution of HD 191025 (= TIC 41189624) based on *TESS* Sectors 41, 54, and 55. The digits in parentheses represent the error in the last two or three decimal places. The amplitude units are milli-magnitudes (mmag), with typical uncertainties of 0.0042 mmag.

Frequency (d^{-1})	μHz	Amplitude (mmag)	Phase (0-1)	SNR
f_0 = 24.146127(11)	279.47	0.510	0.6232(13)	73.9
f_1 = 3.350263(28)	38.78	0.208	0.1016(33)	17.8
f_2 = 21.153533(30)	244.83	0.196	0.0929(34)	26.8
f_3 = 44.753728(47)	517.98	0.143	0.9444(55)	24.0
f_4 = 2.788548(42)	32.27	0.139	0.1089(49)	11.8
f_5 = 32.119706(47)	371.76	0.124	0.8884(54)	16.8
f_6 = 20.615291(48)	238.60	0.120	0.6293(56)	15.7
f_7 = 27.047572(49)	313.05	0.118	0.9449(57)	18.0
f_8 = 47.625447(49)	551.22	0.118	0.7419(57)	20.4
f_9 = 12.874784(53)	149.01	0.109	0.4016(62)	16.1
f_{10} = 35.459085(54)	410.41	0.108	0.3879(63)	13.2
f_{11} = 34.939945(54)	404.40	0.107	0.3964(63)	13.3
f_{12} = 6.684206(61)	77.36	0.095	0.7357(71)	10.3
f_{13} = 17.719891(61)	205.09	0.094	0.0794(72)	13.2
f_{14} = 3.311107(64)	38.32	0.090	0.9816(75)	7.7
f_{15} = 20.809056(66)	240.85	0.087	0.8483(77)	11.4
f_{16} = 37.488160(67)	433.89	0.087	0.2466(78)	11.3
f_{17} = 15.129634(67)	175.11	0.086	0.3322(78)	14.2
f_{18} = 44.334185(72)	513.13	0.081	0.6519(84)	13.6
f_{19} = 47.698735(74)	552.07	0.078	0.1271(86)	13.5
f_{20}= 33.654781(76)	389.52	0.076	0.6846(89)	10.2
f_{21} = 40.889432(80)	473.26	0.072	0.0828(94)	10.4
f_{22} = 61.841870(81)	715.76	0.071	0.6681(95)	14.4
f_{23} = 6.559791(84)	75.92	0.069	0.7524(98)	7.4
f_{24} = 19.997839(84)	231.46	0.069	0.5249(97)	10.8
f_{25} = 18.127672(85)	209.81	0.068	0.5808(99)	11.0
f_{26} = 59.508675(86)	688.76	0.067	0.7409(101)	13.9
f_{27} = 50.302000(95)	582.20	0.061	0.9875(111)	9.5
f_{28} = 12.613404(104)	145.99	0.056	0.8051(121)	8.2
f_{29} = 20.012099(103)	231.62	0.056	0.7147(120)	7.4
f_{30} = 54.317689(103)	628.68	0.056	0.8646(120)	9.9
f_{31} = 75.894121(109)	878.40	0.053	0.1613(127)	12.1
f_{32} = 58.004516(112)	671.35	0.052	0.2812(131)	9.9
f_{33} = 55.612520(124)	643.66	0.047	0.8318(145)	8.0
f_{34} = 19.179440(125)	221.98	0.046	0.6502(146)	7.2
f_{35} = 50.959060(128)	589.80	0.045	0.1334(150)	7.0
f_{36} = 54.336811(207)	628.90	0.028	0.4186(241)	4.9
Dependent frequencies within the effective frequency resolution 0.0122 d^{-1} =0.14 μHz				
$f_{37} = f_1$ + 0.005419	38.84	0.163	0.4401(41)	13.9
$f_{38} = f_0$ + 0.004445	279.52	0.073	0.2024(93)	10.5
Theoretic frequency resolution: 0.0025 d^{-1} = 0.03 μHz				
Zeropoint: −0.00000005 mag				
Residuals: 0.0007048 mag				

Table 3
Frequency solution of HD 227647 (= TIC 40831024) based on *TESS* Sector 41. The digits in parentheses represent the error in the last two or three decimal places. The amplitude units are milli-magnitudes (mmag), with typical uncertainties of 0.0132 mmag.

Frequency (d^{-1})	μHz	Amplitude (mmag)	Phase (0-1)	SNR
f_0 = 51.624848(114)	597.51	2.395	0.9475(09)	135.7
f_1 = 61.912960(154)	716.59	1.782	0.2072(12)	107.7
f_2 = 44.992391(402)	520.75	0.682	0.7256(31)	36.6
f_3 = 48.396062(457)	560.14	0.600	0.6113(35)	33.3
f_4 = 48.258787(617)	558.55	0.444	0.0635(47)	24.7
f_5 = 41.61505(114)	481.66	0.242	0.8656(87)	13.6
f_6 = 36.67878(118)	424.52	0.232	0.2688(91)	13.3
f_7 = 45.33276(125)	524.68	0.219	0.4648(96)	12.0
f_8 = 42.35219(172)	490.19	0.159	0.1299(132)	9.3
f_9 = 41.25964(173)	477.54	0.158	0.9813(133)	8.9
f_{10} = 48.76652(217)	564.43	0.127	0.8011(166)	7.0
f_{11} = 48.71574(267)	563.84	0.103	0.2526(205)	5.7
f_{12} = 43.13448(266)	499.24	0.103	0.1423(204)	5.4
f_{13} = 38.72099(283)	448.16	0.097	0.7813(217)	5.8
f_{14} = 38.64765(285)	447.31	0.096	0.8084(219)	5.8
f_{15} = 38.55739(324)	446.27	0.085	0.0880(249)	5.1
Theoretical frequency resolution: 0.03761 d^{-1} = 0.44 μHz				
Zeropoint: 9.95198413 mag				
Residuals: 0.001264941 mag				

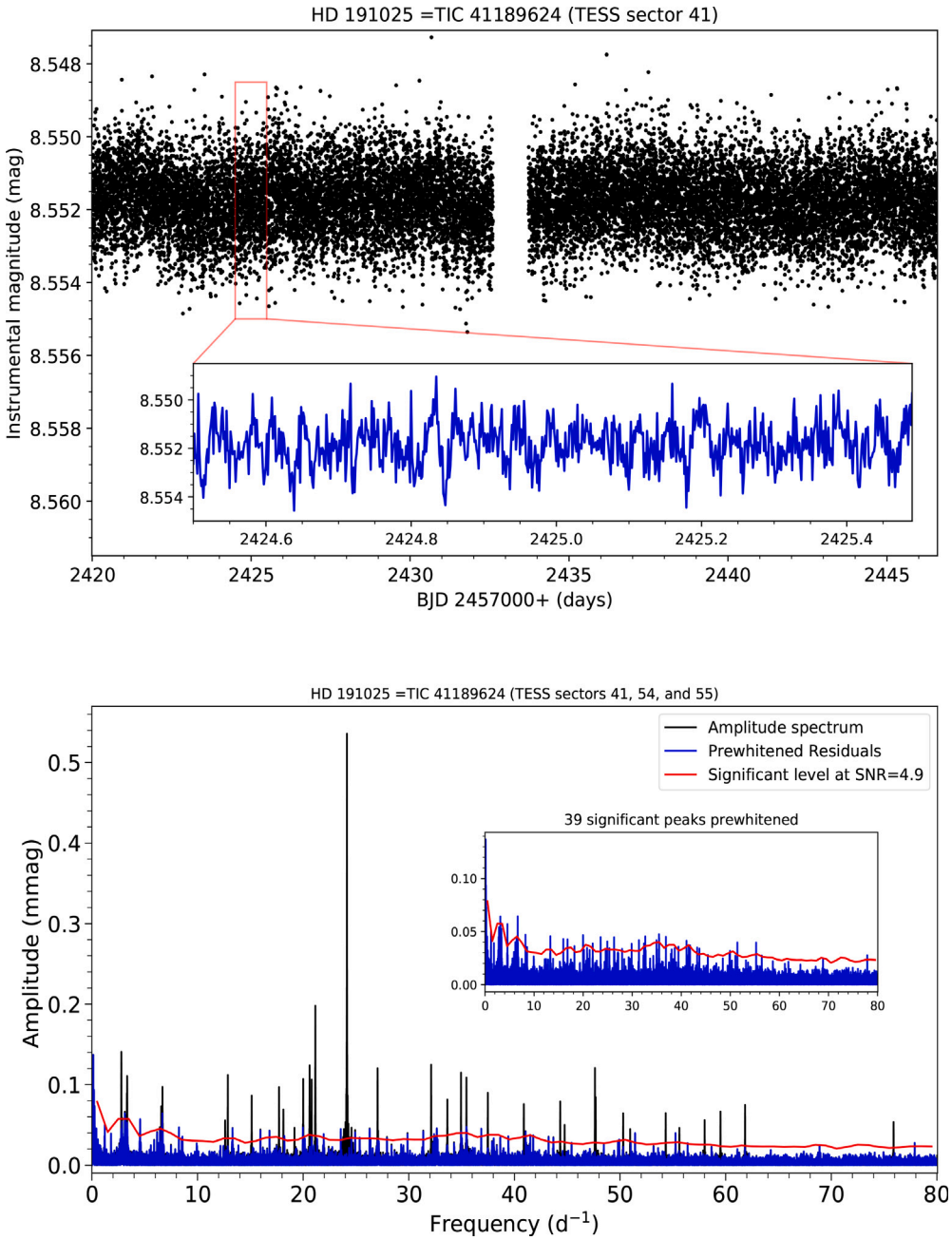

Fig. 3. *TESS* light curves and amplitude spectrum of δ Sct or Maia star HD 191025 (=TIC 41189624).

Due to the star's location in a crowded region, it is blended with two similar bright stars: the nearest, TIC 92309924 ('star A', $T_{\rm mag} = 13\overset{\rm m}{.}61$), separated by 3.5″; TIC 378823684 ('star B', $T_{\rm mag} = 13\overset{\rm m}{.}23$) separated by 11″, on a single pixel of the CCD detector, and contaminated by multiple stars fainter than $16\overset{\rm m}{.}0$ within the aperture mask (see Figs. 9 and 18). Furthermore, there are three faint RS CVn variables identified by ZTF within 60″ from the target. These faint variables would contribute little light to the target in view of the profile of light variations and periodicities different from that of RS Cvn. We did not screen the two closest bright stars in our initial search because of their low effective temperatures ($T_{\rm eff,A} = 3669.6$ K [GDR2]; 4461 K[TIC v8.2]; $T_{\rm eff,B} = 4570$ K [GDR3]; 4094 K[TIC v8.2]), which are impossible causing the detected pulsation. They are also background stars of the target (1326 pc) for their farther distance (3956 and 4611 pc).

Unfortunately, when searching the *TESS* light curve database at MAST for star A, yielded no data. This suggests significant blending with TIC 1966084202. To address this, we downloaded the FFI cutout images from *TESS* Sector 55 (because of no TPF available). By creating a custom aperture mask with threshold of 9, we were able to extract light curves for the blended stars (see Fig. 9). The light curves, despite the blending, still exhibit characteristics indicative of γ Dor pulsations. Notably, the periodogram of the extracted light curve matched that of the target star, further supporting the presence of γ Dor variability. We further examined the light curves for star B, the periodograms showed almost the same as that of TIC 1966084202. These indicate that both stars A and B were blended with TIC 1966084202 in *TESS* images.

The close proximity of these stars, captured within a single pixel of the CCD detector, precludes the discrimination of their true individual variability using standard aperture photometry — technically, the minimal aperture is one pixel. So the light variation observed by *TESS* was a combined signal from all three stars. Moreover, the strong peaks around 1.06 d^{-1} in the periodogram disappeared for Sector 54 data

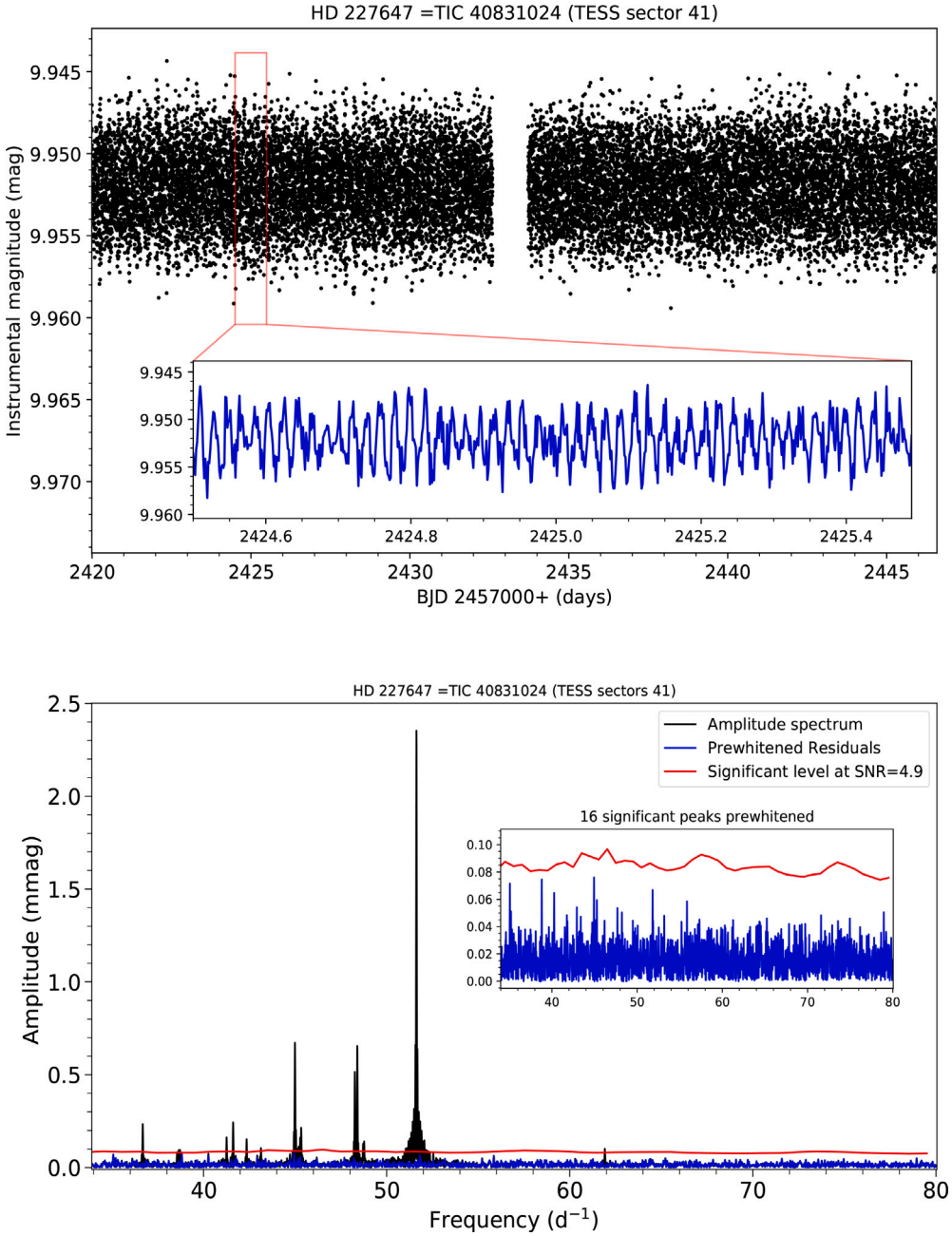

Fig. 4. *TESS* light curves and amplitude spectrum of HD 227647 (= TIC 40831024).

of TIC 1966084202 alone. This would suggest these peaks probably originate from blended objects and contamination lights. Regarding their temperatures, both stars are unlikely the real source of the pulsational variability between 8 and 11 d^{-1}, but they could contribute to the variability observed lower than 2 d^{-1}, which is typically used to identify γ Dor pulsations. Other methods such as higher spatial resolution CCD photometry would be helpful to further pinpoint the true variability origin, and to eliminate the blending and contamination issues.

The true origin of the observed δ Sct-γ Dor hybrid variability remains inconclusive. The inability to distinguish between TIC 1966084202 and its blended neighbors using current data hinders a definitive assessment. Considering the effective temperatures of the blended stars, TIC 1966084202 emerges as the most likely physical source of the observed δ Sct-γ Dor hybrid pulsation.

5.3. Three representative γ Dor stars

5.3.1. γ Dor star: TIC 274636885

TIC 274636885 (= TYC 2682-863-1, $B = 10\overset{m}{.}98$, $V = 10\overset{m}{.}72$, F2V) with stellar parameters from TIC v8.2 and Gaia DR3: $T_{\rm eff}$ = 7155.535 (GDR2), 7080.370 (GDR3), 7267.0 (TIC); $L/L_{\odot}$= 5.143 (GDR3, GDR2), 6.1616 (TIC); $\log g$= 4.170 (GDR3), 4.263 (TIC); Radius = 1.476 $R_{\odot}$ (GDR2), 1.566 $R_{\odot}$(TIC); Mass = 1.638 $M_{\odot}$(TIC); Parallax = 2.825 mas; Distance = 345.44 pc. An initial Fourier calculation was first applied to the 10-minute cadence data in the three *TESS* Sectors 41, 54, and 55 in the frequency range from 0 to 100 d^{-1}, and we found no peaks beyond 6 d^{-1}. Thus subsequent Fourier analyses are conducted in frequency range of 0–15 d^{-1}. Actually all significant peaks are lower than 6 d^{-1}. It is now identified to be a new γ Dor star. Fig. 10 shows the light curves in Sector 41 and the periodograms resulted from the 10-minute

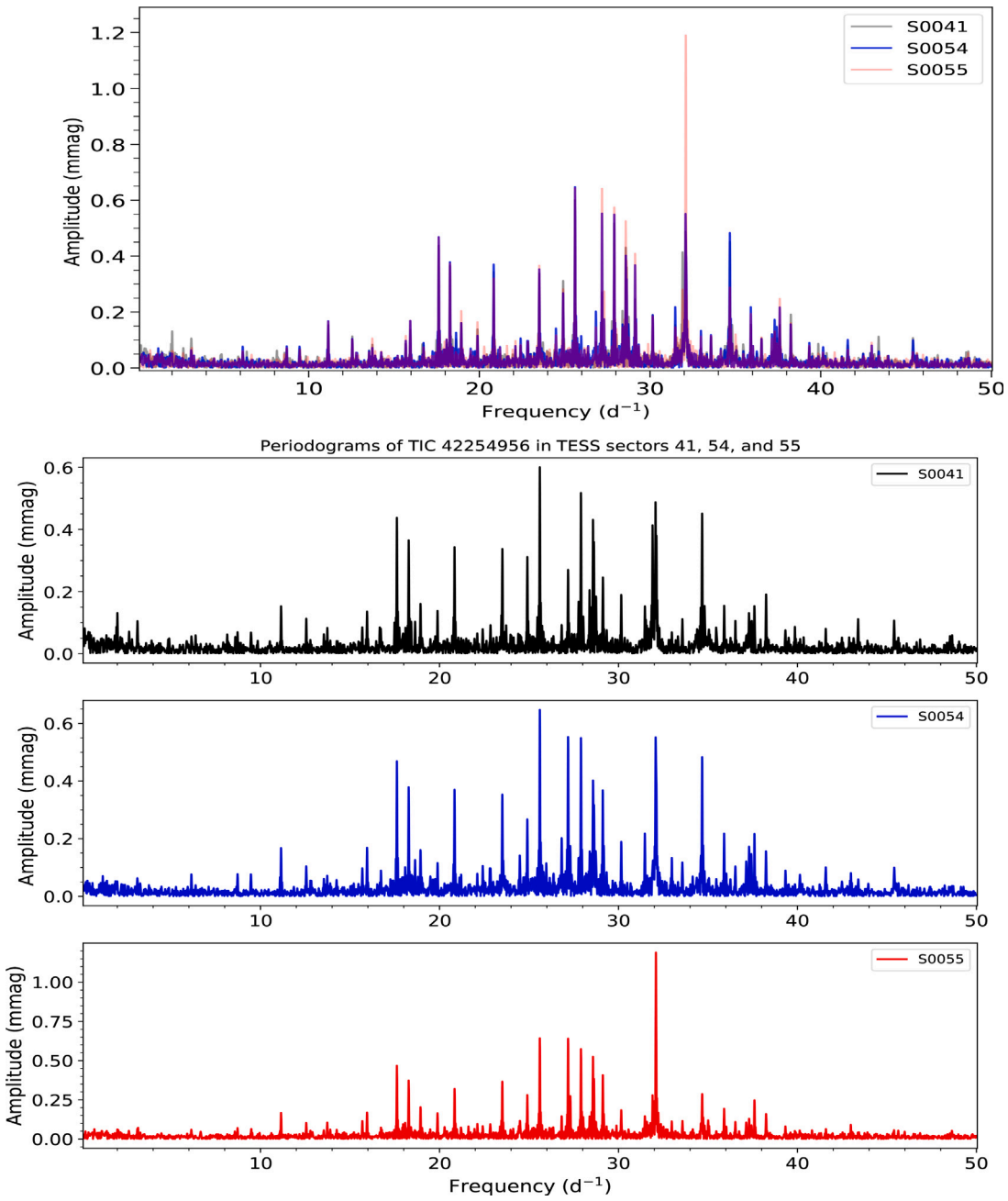

Fig. 5. Amplitude spectrum patterns change over time: HD 227941 (= TIC 42254956).

cadence data in Sectors 41, 54, and 55. Table 7 provides the frequency solution.

5.3.2. γ Dor star: TIC 1966186334

This star has four identifiers in Simbad: UCAC4 629-090129, TIC 1966186334, [MJD95] J200704.70+354006.5 (Massey et al., 1995), and *Gaia* DR3 2059047286405057152. In terms of the stellar parameters from TIC v8.2 and Gaia DR3: $T_{\rm eff}$ = 7862.33 K (GDR2, roughly corresponds to spectral type of A7), 8860.0 K (TIC); $L/L_{\odot}$= 13.103$L_{\odot}$ (GDR3), 25.120$L_{\odot}$(TIC); log g= 4.131 (TIC); Mass = 2.23 $M_{\odot}$; Radius = 1.951 $R_{\odot}$(GDR2), 2.127 $R_{\odot}$(TIC), together with all the detected pulsation frequencies lower than 5 d^{-1}, the star is a hot GDOR or a Maia variable. Table 8 gives the three detected frequencies and Fig. 11 displays the typical GDOR light curves and periodograms based on the data in the three 10-minute cadence Sectors 41, 54 and 55.

This star is very closely surrounded by an S star IRAS 20051+3531 (= TIC 90463637) on upper right, which is an evolved post-MS star (mostly AGB or RGB) and a constant star 2MASS J20070431+3540334 directly above it (see Fig. 18). There is a very faint star TIC 1966186338 ($T_{\rm mag}$=18$^{\rm m}$.49) invisible between TIC 1966186334 and TIC 90463637. Fortunately, contamination did not significantly impact the variability of TIC 1966186334.

5.3.3. γ Dor star: TIC 89119933

HD 227505 (= TIC 89119933, B = 11$^{\rm m}$.37, V = 10$^{\rm m}$.72) has *TESS* light curve products available at MAST in Sectors 14, 15, 41, 54, 55, 74, and 75. The star was observed during 2019-07-18 UT 20:34:00 (Sector 14) and 2024-02-26 UT 23:29:53 (Sector 75), i.e. BJD 24571683.35775 through 2460367.4799. In Sector 41, observations started on 2021-07-24 UT 11:53:44 (BJD 2459419.9964). Sectors 41, 54 and 55 have 10-minute cadence light curves, while Sectors 74 and 75 are in 2-minute cadence, Sectors 14 and 15 in 30-minute cadence. The star's light variations exhibit characteristics typical of γ Doradus pulsations

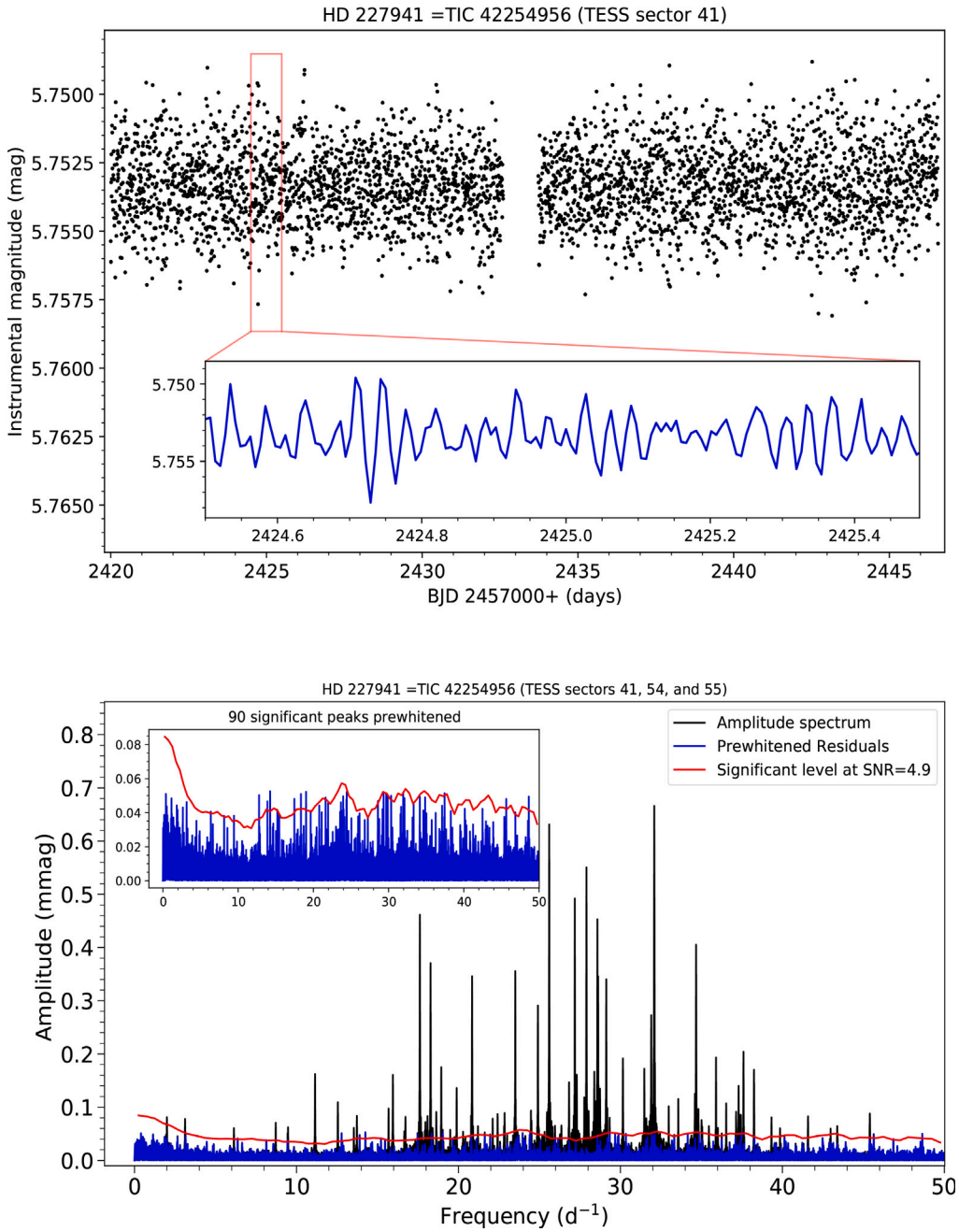

Fig. 6. *TESS* light curves and amplitude spectrum of HD 227941 (= TIC 42254956).

(see Fig. 12). The variability type is further corroborated by the following stellar parameters: Effective temperature $T_{\rm eff}$ = 6717 K (spectral type F5), Luminosity = 10.846$L_{\odot}$(GDR3), Mass = 1.43 $M_{\odot}$, surface gravity $\log g$= 3.822 (GDR3), Radius = 2.432 $R_{\odot}$(GDR2). Light curves in last five Sectors (41–75, spanning 947.4835 days) are analyzed for resolving pulsations. No significant peaks beyond 3 d^{-1}. Table 9 gives the detected frequencies over SNR = 4.9 and Fig. 13 displays the periodograms based on the data in five Sectors 41, 54, 55, 74 and 75.

6. Discussions

6.1. H-R diagram

Exploiting the extensive catalogs of δ Sct stars and γ Dor stars (Zhou, 2024), where the effective temperature, luminosity, surface gravity, and other stellar parameters are adopted from the *TESS* Input Catalog (TIC v8.2, Paegert et al., 2021) and *Gaia* DR2/DR3, we have plotted the newly identified variables from our regional survey around NGC 6871 on the Hertzsprung–Russell diagram, juxtaposed with previously known sources for comparison (Fig. 14). This comparative illustration marks a pioneering endeavor, showcasing both types of stars in a substantial collective for the first time.

Fig. 14 shows that the distributions of δ Sct and γ Dor variables exhibit significantly larger extents compared to their classical instability domains. This discrepancy may arise from several factors. One possibility is the presence of inaccurate stellar parameters within databases. In particular, lower luminosities and effective temperatures compared to solar values might be influencing the results ($\log L/L_{\odot} < 0$ and $\log T_{\rm eff} < 3.76, T_{\rm eff} < 5780$ K). Additionally, the observed distributions might be affected by the potential inclusion of Maia variables within

Table 4
Frequency solution of HD 227941(= TIC 42254956) based on *TESS* Sectors 41, 54, and 55. The digits in parentheses represent the error in the last two or three decimal places. The amplitude units are milli-magnitudes (mmag), with typical uncertainties of 0.0071 mmag.

Frequency (d^{-1})	μHz	Amplitude (mmag)	Phase (0-1)	SNR
f_0 = 32.089337(14)	371.40	0.715	0.9614(16)	64.8
f_1 = 25.603527(15)	296.34	0.635	0.7297(18)	75.9
f_2 = 27.902698(18)	322.95	0.540	0.6423(21)	63.5
f_3 = 32.103750(18)	371.57	0.540	0.4902(21)	49.0
f_4 = 27.183373(21)	314.62	0.459	0.9329(25)	60.8
f_5 = 17.619107(21)	203.92	0.458	0.6461(25)	53.5
f_6 = 28.577518(23)	330.76	0.431	0.5253(26)	44.8
f_7 = 34.670907(26)	401.28	0.381	0.6122(30)	35.4
f_8 = 18.278468(26)	211.56	0.371	0.9993(31)	43.2
f_9 = 23.509531(27)	272.10	0.359	0.8940(32)	30.8
f_{10} = 20.840446(28)	241.21	0.349	0.0394(33)	37.1
f_{11} = 29.125902(29)	337.11	0.335	0.8374(34)	31.4
f_{12} = 31.906129(32)	369.28	0.302	0.4192(38)	29.5
f_{13} = 28.625207(33)	331.31	0.296	0.0596(39)	30.7
f_{14} = 24.905673(34)	288.26	0.291	0.9202(39)	28.8
f_{15} = 37.596786(49)	435.15	0.199	0.2337(57)	19.1
f_{16} = 30.153213(50)	349.00	0.194	0.1038(59)	19.9
f_{17} = 35.902523(52)	415.54	0.187	0.1454(61)	19.3
f_{18} = 31.473863(54)	364.28	0.181	0.2886(63)	17.3
f_{19} = 18.939638(54)	219.21	0.180	0.1347(63)	20.9
f_{20} = 38.245666(58)	442.66	0.168	0.9404(68)	18.5
f_{21} = 11.147687(61)	129.02	0.162	0.7149(71)	24.8
f_{22} = 28.386941(61)	328.55	0.159	0.8847(72)	18.3
f_{23} = 15.952415(62)	184.63	0.158	0.8425(72)	21.0
f_{24} = 26.828519(68)	310.52	0.145	0.1553(79)	16.8
f_{25} = 34.599976(69)	400.46	0.141	0.2125(81)	13.1
f_{26} = 19.890787(71)	230.22	0.138	0.2792(82)	16.7
f_{27} = 37.294737(72)	431.65	0.136	0.5100(84)	13.4
f_{28} = 28.510837(74)	329.99	0.131	0.0234(87)	13.6
f_{29} = 32.057988(80)	371.04	0.123	0.1797(98)	11.1
f_{30} = 12.554842(90)	145.31	0.109	0.7907(91)	14.8
f_{31} = 33.568032(93)	388.52	0.105	0.9797(108)	10.8
f_{32} = 36.529143(94)	422.79	0.105	0.5470(109)	10.2
f_{33} = 28.738612(95)	332.62	0.103	0.7166(111)	10.7
f_{34} = 32.982412(98)	381.74	0.100	0.2378(114)	9.5
f_{35} = 15.686176(101)	181.55	0.097	0.4882(118)	12.9
f_{36} = 37.143236(104)	429.90	0.094	0.3505(122)	9.3
f_{37} = 27.310304(105)	316.09	0.093	0.7034(122)	12.4
f_{38} = 24.474815(109)	283.27	0.090	0.8182(128)	7.8
f_{39} = 45.398958(109)	525.45	0.090	0.2375(127)	10.3
f_{40} = 22.849366(111)	264.46	0.089	0.4690(129)	8.9
f_{41} = 34.654261(110)	401.09	0.089	0.9507(128)	8.3
f_{42} = 29.161287(112)	337.51	0.088	0.7920(130)	8.2
f_{43} = 37.385981(112)	432.71	0.087	0.2097(131)	8.6
f_{44} = 13.729855(115)	158.91	0.085	0.1654(134)	9.9
f_{45} = 22.418179(118)	259.47	0.083	0.1962(137)	9.0
f_{46} = 41.582549(119)	481.28	0.082	0.9855(139)	9.3
f_{47} = 27.773559(120)	321.45	0.082	0.4881(140)	9.6
f_{48} = 18.629932(120)	215.62	0.082	0.3526(140)	9.5
f_{49} = 16.728376(121)	193.62	0.081	0.2129(141)	10.5
f_{50} = 2.001252(122)	23.16	0.080	0.6276(142)	6.0
f_{51} = 3.122016(125)	36.13	0.078	0.9551(146)	7.7
f_{52} = 18.088109(127)	209.35	0.077	0.3359(148)	9.0
f_{53} = 39.325647(127)	455.16	0.077	0.3323(148)	8.4
f_{54} = 24.507359(130)	283.65	0.075	0.1601(152)	7.4
f_{55} = 37.415777(132)	433.05	0.074	0.1412(154)	7.3
f_{56} = 22.112404(132)	255.93	0.074	0.0008(155)	8.0
f_{57} = 31.790620(134)	367.95	0.073	0.5274(156)	7.1
f_{58} = 28.029419(137)	324.41	0.072	0.8770(159)	8.2
f_{59} = 8.719233(137)	100.92	0.071	0.4775(160)	9.2
f_{60} = 34.749362(142)	402.19	0.069	0.7076(166)	6.4
f_{61} = 18.415252(142)	213.14	0.069	0.3976(166)	8.0
f_{62} = 25.391616(143)	293.88	0.068	0.3606(167)	7.0
f_{63} = 34.821869(149)	403.03	0.066	0.8999(174)	6.1
f_{64} = 35.009751(148)	405.21	0.066	0.6164(173)	6.4
⋮				
f_{83} = 36.013411(180)	416.82	0.054	0.9435(210)	5.8
f_{84} = 20.284129(181)	234.77	0.054	0.3725(211)	6.0
Dependent frequencies within the effective frequency resolution 0.012165 d^{-1} = 0.14 μHz				
$f_{85} = 3f_0 - 2f_3$		0.310	0.0628	28.1
$f_{86} = f_4 + 0.003803$	314.67	0.174	0.2085(66)	23.0
$f_{87} = 3f_0 - 2f_3$		0.123	0.1797	11.1
$f_{88} = 3f_0 - 3f_2$		0.109	0.7907	14.8
$f_{89} = f_{37} - 0.0038$	316.05	0.105	0.3781(109)	13.9
$f_{90} = f_{11} + 0.006307$	337.18	0.091	0.0851(126)	8.5
Theoretical frequency resolution: 0.002474 d^{-1} = 0.03 μHz				
Zeropoint: −0.000000767 mag				
Residuals: 0.0005319982 mag				

the δ Sct and γ Dor samples. Furthermore, some γ Dor stars might be misclassified solar-like oscillators or rotating stars.

In addition, using the G, BP, RP magnitudes and distance from *Gaia* DR2 and DR3 (Gaia Collaboration et al., 2023, 2018b), we have created a *Gaia* color–magnitude diagram for both δ Sct and γ Dor stars in Fig. 15). We also compare the new variables with the general *Gaia* stars in Fig. 16.

These diagrams provide a robust comparison for investigating group properties. Fig. 14 demonstrates that γ Dor stars occupy the same region of the H–R diagram as δ Sct stars. The pattern is aligns with previous findings where the γ Dor instability domain is shown to be encompassed within the δ Sct instability region (Balona, 2018). This overlap hints at a potential unification of the stellar variability classes, suggesting they may share a pulsation mechanism – a hypothesis that

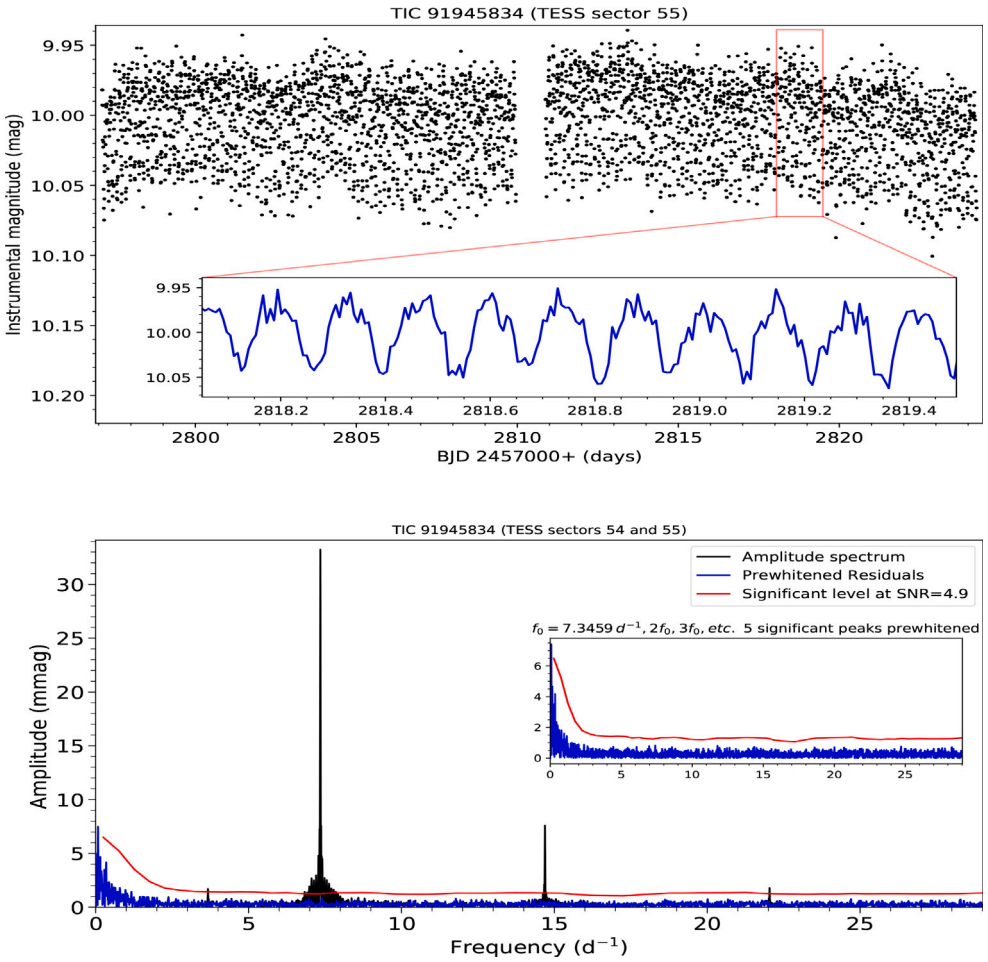

Fig. 7. *TESS* light curves and amplitude spectrum of TIC 91945834.

Table 5
Frequency solution of TIC 91945834 based on *TESS* Sectors 54 and 55. The digits in parentheses represent the error in the last one or two decimal places. The amplitude units are milli-magnitudes (mmag), with typical uncertainties of 0.262 mmag.

Frequency (d^{-1})	μHz	Amplitude (mmag)	Phase (0-1)	SNR
f_0 = 7.34592(12)	85.02	22.120	0.532(2)	87.3
$f_1 = f_0$ −0.00166		14.422	0.030	56.9
$f_2 = 2f_0$		7.563	0.270	28.2
2 $f_3 = 3f_0$		1.806	0.980	7.1
$f_4 = 0.5f_0$		1.756	0.805	6.0
Theoretical frequency resolution: 0.018395 d^{-1} = 0.21 μHz				
Zeropoint: −0.000146166 mag				
Residuals: 0.0159355335 mag				

Table 6
Frequency solution TIC 1966084202 based on *TESS* Sectors 41 and 55. The digits in parentheses represent the error in the last two decimal places. The amplitude units are milli-magnitudes (mmag), with typical uncertainties of 0.8098 mmag.

Frequency (d^{-1})	μHz	Amplitude (mmag)	Phase (0-1)	SNR
f_0 = 1.001636(45)	11.59	24.712	0.3630(52)	7.1
f_1 = 1.071979(45)	12.41	24.603	0.0961(52)	7.0
f_2 = 10.119851(55)	117.13	20.239	0.5771(64)	25.9
f_3 = 9.744688(55)	112.79	19.963	0.0682(65)	25.3
f_4 = 8.290741(57)	95.96	19.387	0.1737(66)	21.8
f_5 = 1.549968(71)	17.94	15.589	0.5415(83)	6.9
Theoretical frequency resolution: 0.002474 d^{-1} = 0.03 μHz				
Zeropoint: 0.0002316531 mag				
Residuals: 0.0494063688 mag				

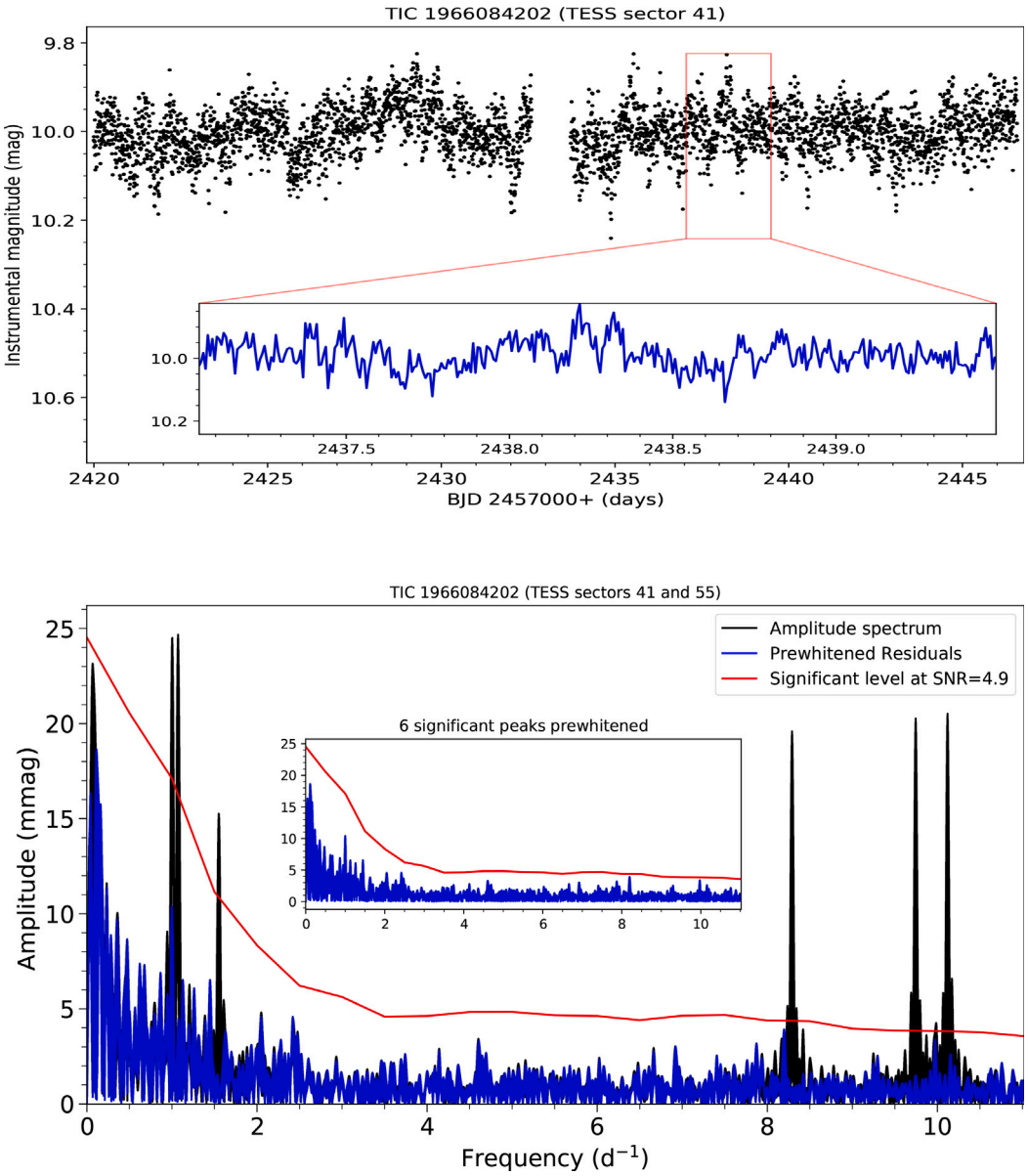

Fig. 8. *TESS* light curves in Sector 41 and the amplitude spectrum of TIC 1966084202 based on the data in Sectors 41 and 55.

Table 7
Frequency solution of TYC 2682-863-1(= TIC 274636885) based on *TESS* Sectors 41, 54, and 55. The digits in parentheses represent the error in the last two or three decimal places. The amplitude units are milli-magnitudes (mmag), with typical uncertainties of 0.0145 mmag.

Frequency (d^{-1})	μHz	Amplitude	Phase (0-1)	SNR
f_0 = 0.613712(12)	7.10	1.638	0.4158(14)	24.5
f_1 = 2.582101(15)	29.89	1.308	0.9269(18)	45.8
f_2 = 2.954093(19)	34.19	1.046	0.2881(22)	36.6
f_3 = 2.606653(25)	30.17	0.784	0.7402(29)	27.4
f_4 = 2.724872(40)	31.54	0.495	0.5217(47)	17.3
Dependent frequencies within the effective frequency resolution 0.012165 d^{-1} = 0.14 μHz				
$f_5 = 2f_2$		0.220	0.0991(105)	11.4
$f_6 = 2f_1$		0.208	0.5944(111)	10.1
$f_7 = f_1 + f_2$		0.163	0.6739(142)	8.5
$f_8 = f_1 - f_0$		0.226	0.4078(102)	5.7
$f_9 = 2f_3$		0.111	0.4919(208)	5.4
Theoretical frequency resolution: 0.002474 d^{-1} = 0.029 μHz				
Zeropoint: 0.00000518864 mag				
Residuals: 0.00107623963 mag				

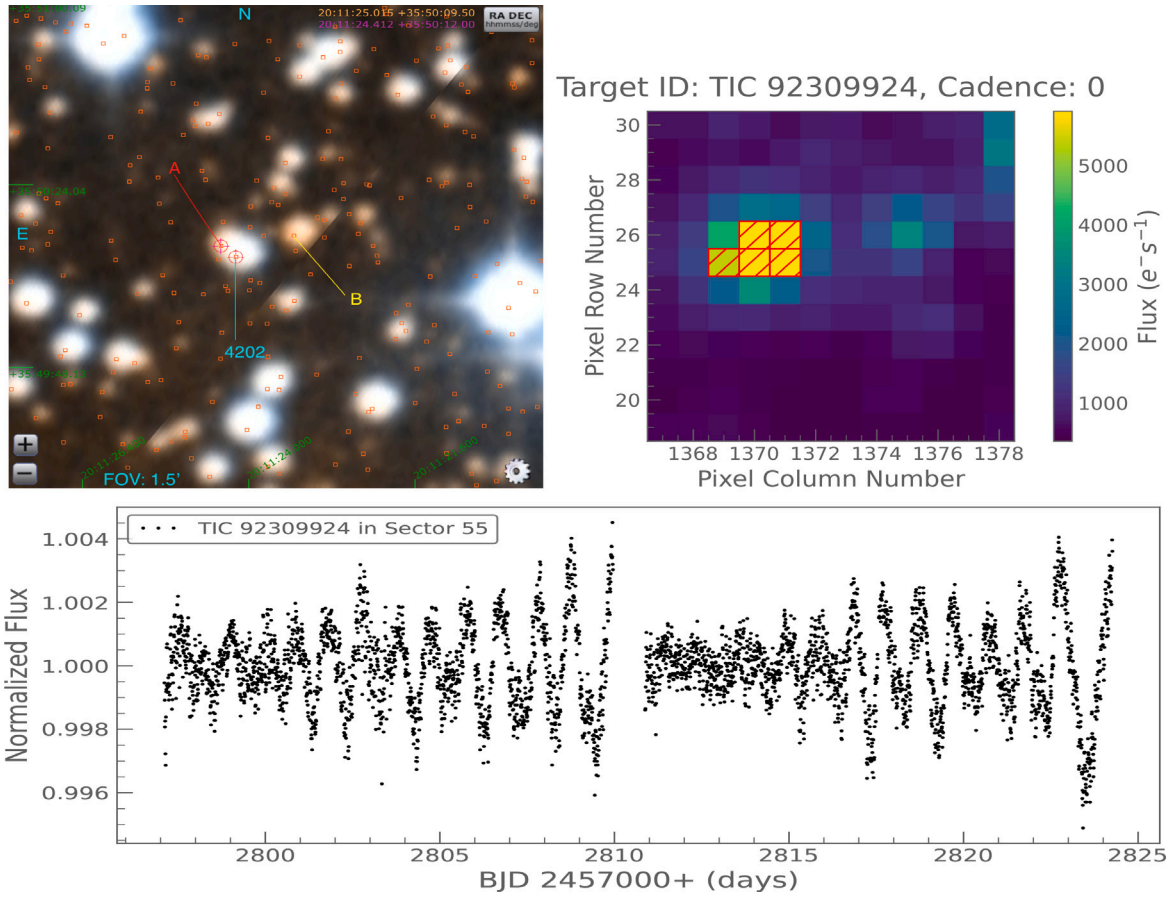

Fig. 9. Top left: Finding chart for TIC 1966084202 marked for blending with A and B in *TESS* images. The DSS image is a screenshot of the Astroview window when searching the MAST catalogs. Top right: *TESS* FFI cutout image from which the light curves extracted at bottom panel. Compare this cutout with that for TIC 1966084202 on the top left in Fig. 18.

Table 8
Frequency solution of TIC 1966186334 based on *TESS* Sectors 41, 54, and 55. The digits in parentheses represent the error in the last two decimal places. The amplitude units are milli-magnitudes (mmag), with typical uncertainties of 1.028 mmag.

Frequency (d^{-1})	μHz	Amplitude	Phase (0-1)	SNR
f_0 = 2.299060(16)	26.61	87.330	0.7428(19)	21.3
f_1 = 2.192518(22)	25.38	62.993	0.9294(26)	15.4
Dependent frequencies within the effective frequency resolution 0.012165 d^{-1} = 0.14 μHz				
$f_3 = 0.5 f_0$		42.605	0.4765(38)	6.3
Theoretical frequency resolution: 0.002474 d^{-1} = 0.03 μHz				
Zeropoint: −0.0187591899 mag				
Residuals: 0.0764090924 mag				

could reshape our understanding of stellar pulsations. This significant overlap presented in our H–R diagrams support the notion of a singular pulsation source and proposes a unified explanation for the diverse frequency range observed in pulsating stars, including Maia variables, δ Sct, and γ Dor stars. Such a unification could have profound implications for the classification and study of stellar pulsations.

The low-frequency (0.3–5 d^{-1}) gravity-mode pulsations in γ Dor stars are driven by the modulation of the radiative flux by convection at the base of a deep envelope convection zone (Guzik et al., 2000). However, it is not known whether a single excitation mechanism can be responsible for both the p and g modes in hybrid δ Sct/γ Dor stars (Balona et al., 2015). Recalling the findings of Kurtz et al. (2015), who proposed a unified explanation for SPB, γ Dor and Be stars, Xiong et al. (2016) employed a non-local and time-dependent convection theory to calculate radial and low-degree non-radial oscillations for stellar evolutionary models with $M \approx 1.4-3.0\,M_{\odot}$. This recent theoretic study concluded that the oscillations of δ Sct and γ Dor stars are both due to the combination of the κ-mechanism and the coupling between convection and oscillations. Their results demonstrated that the theoretical instability regions for δ Sct and γ Dor stars significantly overlap. δ Sct and γ Dor stars belong to the same class of variables at the low-luminosity part of the Cepheid instability strip. Within the δ Sct-γ Dor instability strip, most of the pulsating variables are very likely hybrids that are excited in both p and g modes (Xiong et al., 2016).

Pulsators crossing the effective temperature range of 10000–6000 K involve SPB, Maia, DSCT, GDOR, and solar-like oscillators. Either separate individual models with interplay in effect, or one universally applicable model is urgently needed for the interpretation of the pulsations observed in this part of the H–R diagram region.

6.2. Membership of NGC 6871

In addition, we investigated whether these newly discovered variable stars are members of the NGC 6871 cluster. Galactic stellar clusters

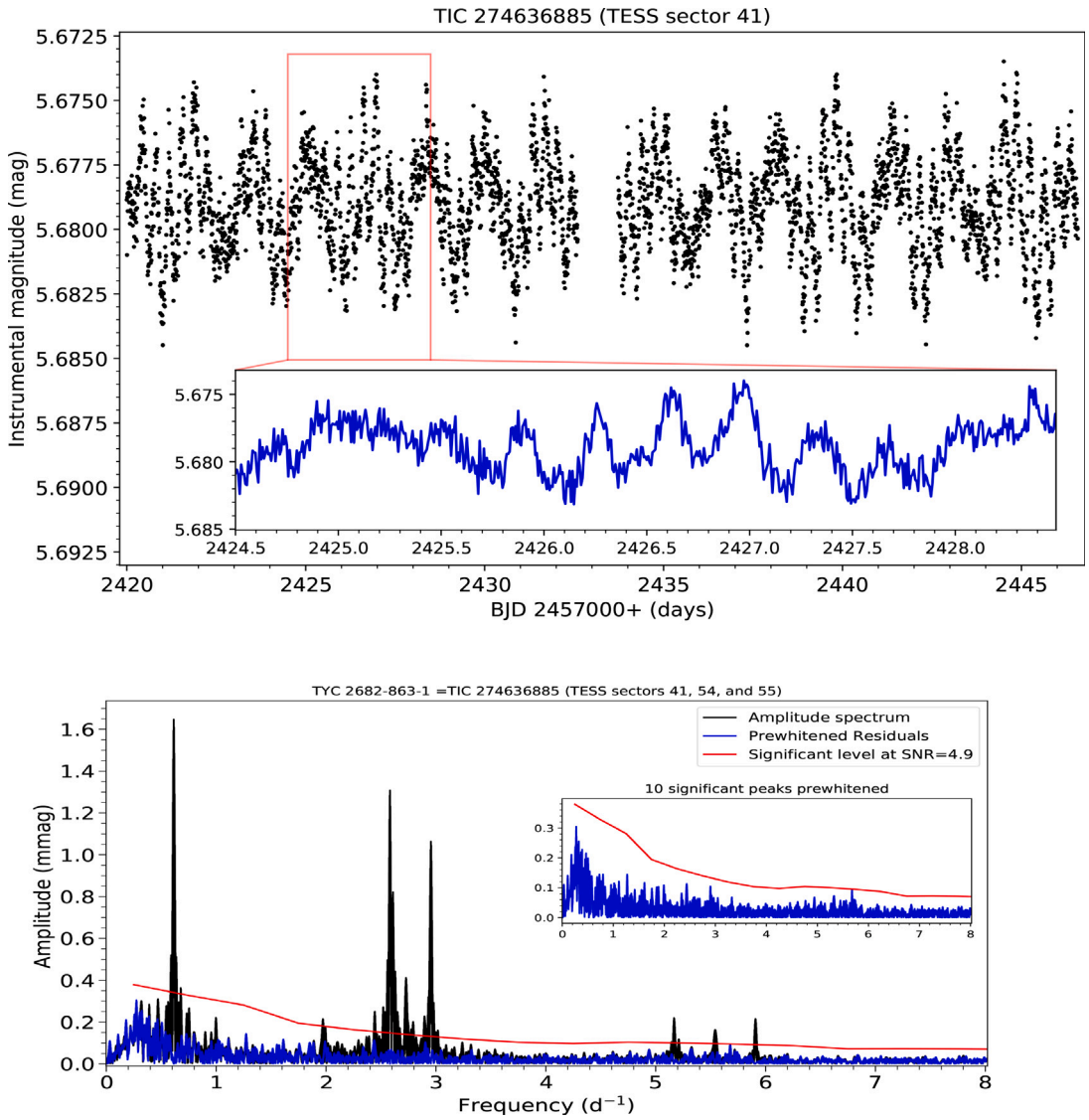

Fig. 10. *TESS* light curves and amplitude spectrum of TIC 274636885.

Table 9
Frequency solution of HD 227505 (= TIC 89119933) based on *TESS* Sectors 41, 54, and 55. The digits in parentheses represent the error in the last two decimal places. The amplitude units are milli-magnitudes (mmag), with typical uncertainties of 0.0189 mmag.

Frequency (d^{-1})	μHz	Amplitude (mmag)	Phase (0-1)	SNR
f_0 = 0.589161(02)	6.82	6.475	0.7235(05)	31.7
f_1 = 0.542232(02)	6.28	6.264	0.3323(05)	30.6
f_2 = 0.446937(04)	5.17	2.805	0.4018(11)	12.5
f_3 = 1.718473(12)	19.89	0.913	0.2577(33)	6.4
f_4 = 0.502132(11)	5.81	0.983	0.5349(31)	4.8
Dependent frequencies within the theoretical frequency resolution 0.00106 d^{-1} = 0.01 μHz				
$f_5 = f_0 + f_1$		3.295	0.242	18.9
$f_6 = f_0 + f_3$		1.648	0.424	9.5
$f_7 = f_0 + f_1 + f_3$		0.892	0.973	6.3
$f_8 = f_0 + 2f_1$		0.862	0.903	6.1
$f_9 = 2f_0 + 2f_1$		0.661	0.898	6.0
$f_{10} = f_2 + f_0 + f_3$		0.608	0.735	5.5
Zeropoint: 0.00011892429 mag				
Residuals: 0.00283699622 mag				

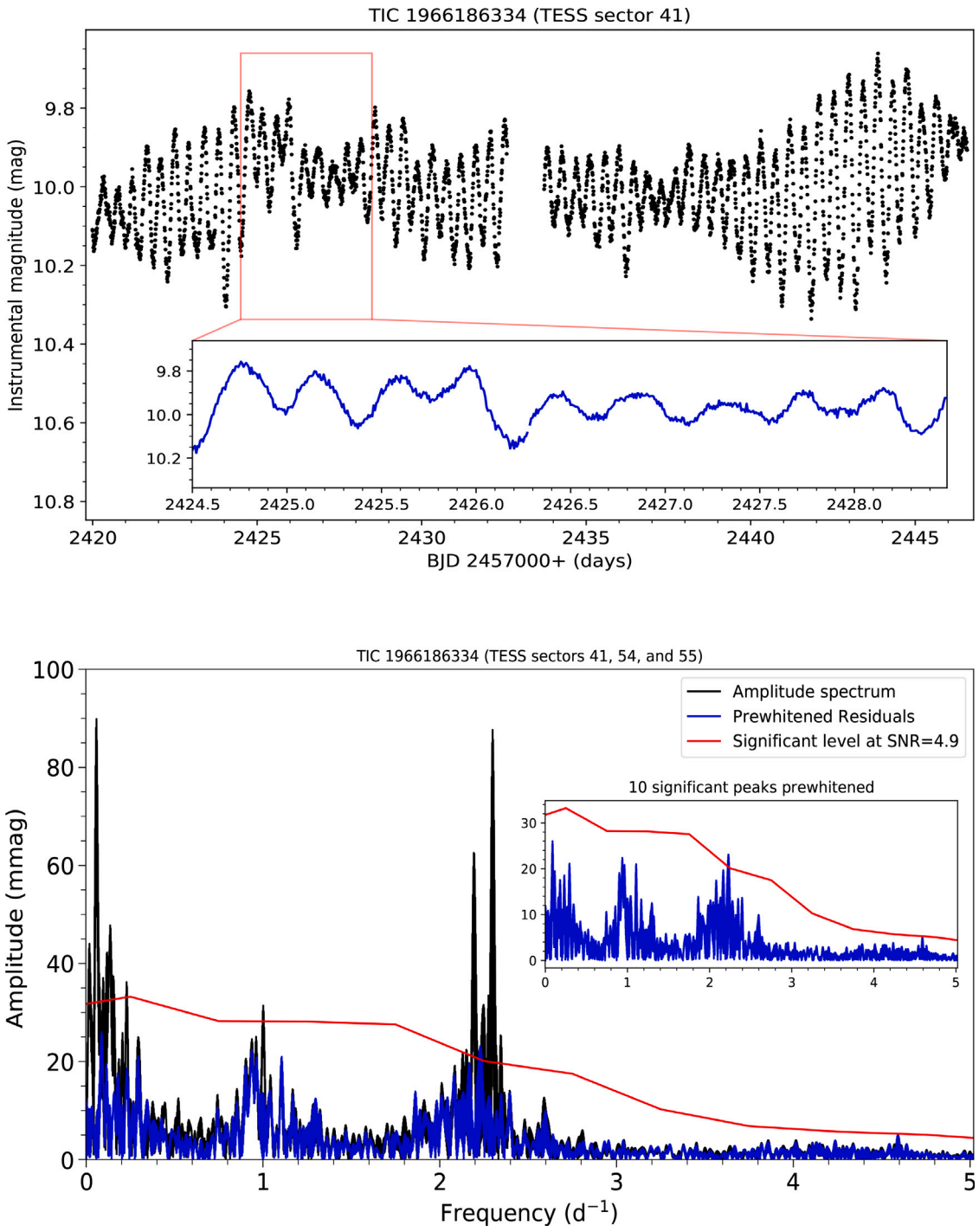

Fig. 11. *TESS* light curves and amplitude spectrum of TIC 1966186334.

where members are assumed to be born at the same time (in stellar evolution timescales) and from the same molecular cloud and thus share the same initial chemical conditions. To determine if a star belongs to a cluster, no single piece of evidence is definitive, but at least one of the following key factors should be considered: (1) A star's proper motion, i.e. its apparent movement across the sky over time. Stars in a cluster are known to share a common origin and move through space together, so cluster members will have similar proper motions, while foreground/background stars not belonging to the cluster will have different proper motions; (2) Distance: Stars within a cluster are roughly at the same distance from Earth or Sun. Cluster members typically exhibit a range of distances as they share a similar location in space. (3) Age: Stars in a cluster are believed to have formed around the same time, so member stars should have similar ages. The age of a star can only be measured in some very specific cases (Soderblom, 2010), we usually rely on stellar evolution models for this quantity. However, a star's age can be estimated using various methods, including precise astrometry and photometry (color magnitudes, luminosity, reddening), stellar isochrones fitting (Jørgensen and Lindegren, 2005; Meynet et al., 1993), asteroseismology (Palakkatharappil and Creevey, 2023; Pamos Ortega et al., 2022; Creevey et al., 2017), etc.; (4) Metallicity: Stars in a cluster are thought to have formed from the same cloud of gas and dust, leading to similar abundances of elements heavier than hydrogen and helium. (5) Radial velocity: This measures a star's motion directly

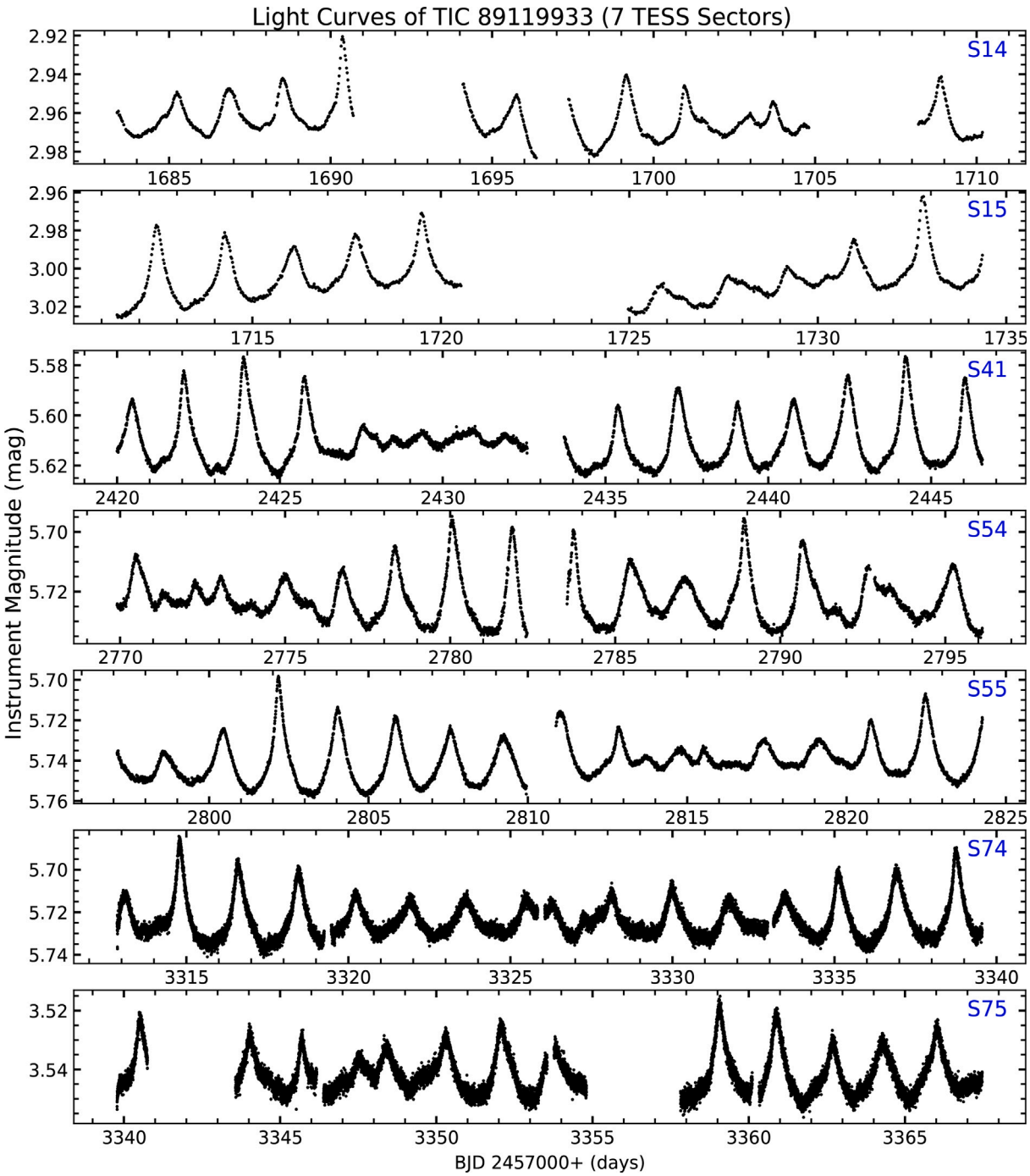

Fig. 12. *TESS* light curves of HD 227505 (= TIC 89119933) in Sectors 14, 15, 41, 54, 55, 74, and 75 from top to bottom.

towards or away from Earth. A cluster's members might exhibit similar radial velocities due to their shared motion.

Membership determination ideally involves a comprehensive analysis that considers all relevant factors. Stars exhibiting consistency with known NGC 6871 members in these parameters are considered strong candidates for membership. However, due to limitations of this work, the three factors, age, metallicity, and radial velocity were not considered in the current assessment. In practice, stars with significantly discrepant proper motion or distance estimates compared to established cluster members are excluded from membership.

Thanks to the *Gaia* DR2 open clusters in the Milky Way (Cantat-Gaudin et al., 2018; Cantat-Gaudin and Anders, 2020), which makes the identification of membership readily easy. We adopted mean parameter values of cluster members in Table 10. Based on *Gaia* archive at https://gea.esac.esa.int/archive/, parallax and proper motion data are extracted manually first for the eight example variables as well as six cluster members chosen within a region of 22-arcminute radius of NGC 6871's center (containing half the members) for comparison in Table 11. Distances are calculated from reciprocal of parallax when GSP-Phot distances unavailable in *Gaia* DR3 archive. For single

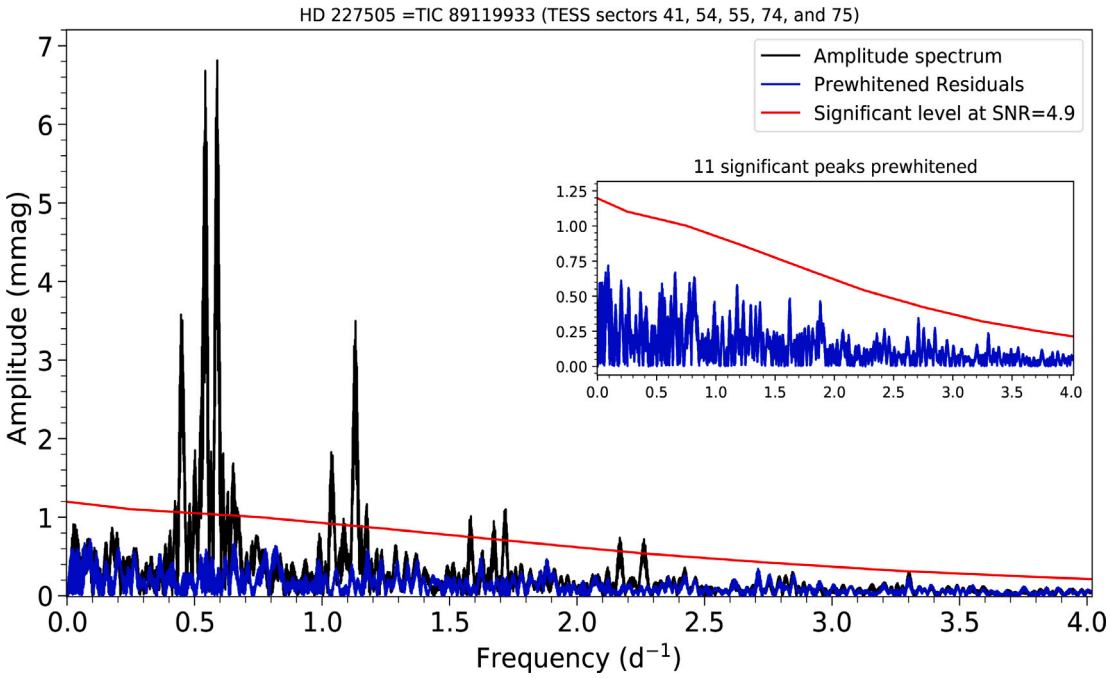

Fig. 13. Amplitude spectrum of HD 227505 (= TIC 89119933) based on *TESS* Sectors 41, 54, 55, 74, and 75.

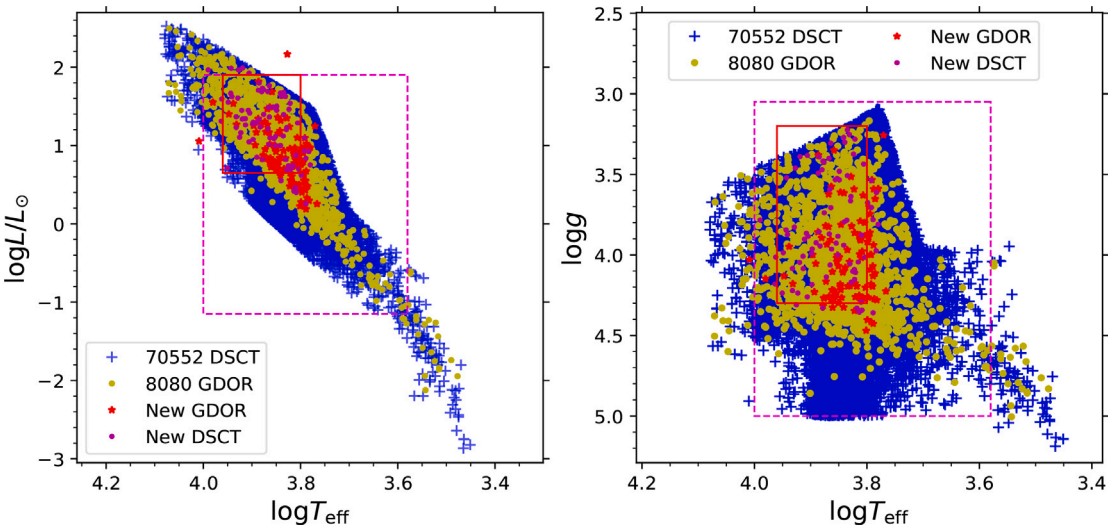

Fig. 14. Newly discovered pulsating variable stars of γ Dor and δ Sct types (red asterisks and dots, respectively) plotted contrast with the known stars. Red squares refer to classical δ Sct domain: $T_{\rm eff}$ in [6300, 9100], $\log T_{\rm eff}$ in [3.80, 3.96], $\log g$ in [3.2, 4.3], $\log L/L_\odot$ in [0.65, 1.90] consistent with the H–R diagram of pulsators given by Handler (2009), Jeffery (2008), Breger (2000). Magenta dashed squares refer to an extended domain: $T_{\rm eff}$ in [3800, 10000], $\log T_{\rm eff}$ in [3.58, 4.00], $\log g$ in [3.05, 5.0], $\log L/L_\odot$ in [−1.15, 1.90]. See comments in Section 6.1.

stars, GSP-Phot provides reliable distances out to ∼2 kpc. Beyond this limit, GSP-Phot can systematically underestimate distance depending on the fractional parallax uncertainty (*Gaia* DR3 documentation, Part III, Chapter 11, 11.4.3 Distances, Ulla et al., 2022).[4] Our analysis suggests that none of the eight example variables are members of NGC 6871. They are likely foreground stars.

We compared our list of 1512 new variables with the catalog of *Gaia* DR2 open clusters in the Milky Way by Cantat-Gaudin and Anders (2020), 160 stars were matched among the 2014 candidate members of NGC 6871 at all probabilities, based on their parallax and proper motion. 87 of these stars have membership probability exceeding 0.5, strongly suggesting they are members of the cluster NGC 6871. The remaining 73 stars have lower probabilities (0.1–0.49). For the 87 high-probability members, the average parallax is 0.513 mas, with proper motions along right ascension and declination of $\mu_\alpha = -3.105$ and $\mu_\delta = -6.416$ mas/yr, respectively. These parameter values fall within the ranges $[0.436, 0.615]$ mas for parallax, $[-3.412, -2.673]$ mas/yr for μ_α, and $[-6.951, -5.923]$ mas/yr for μ_δ, respectively.

To assess membership for the remaining unmatched stars, we programmatically retrieved parallax and proper motion data for all the new variables presented in this work. Utilizing the established parameter ranges above, we independently identified 108 members, among all the 1512 new variables. If taking parallax exceeding 0.666 mas (corresponding distance within 1500 pc) and parallax less than 0.425 mas (distance over 2352 pc) for foreground and background objects, respectively, and parallax values in between [0.425, 0.666] mas as candidates,

[4] https://gea.esac.esa.int/archive/documentation/GDR3/

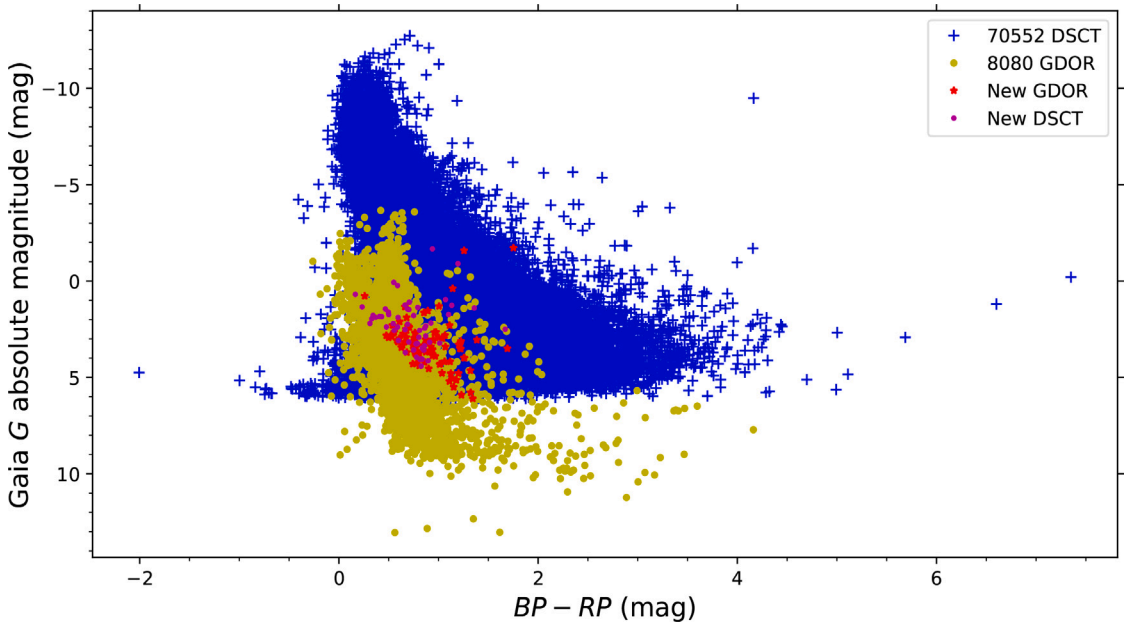

Fig. 15. Present new δ Sct and γ Dor stars in the *Gaia* color-magnitude diagram, plotted contrast with the up-to-date collection of known member stars.

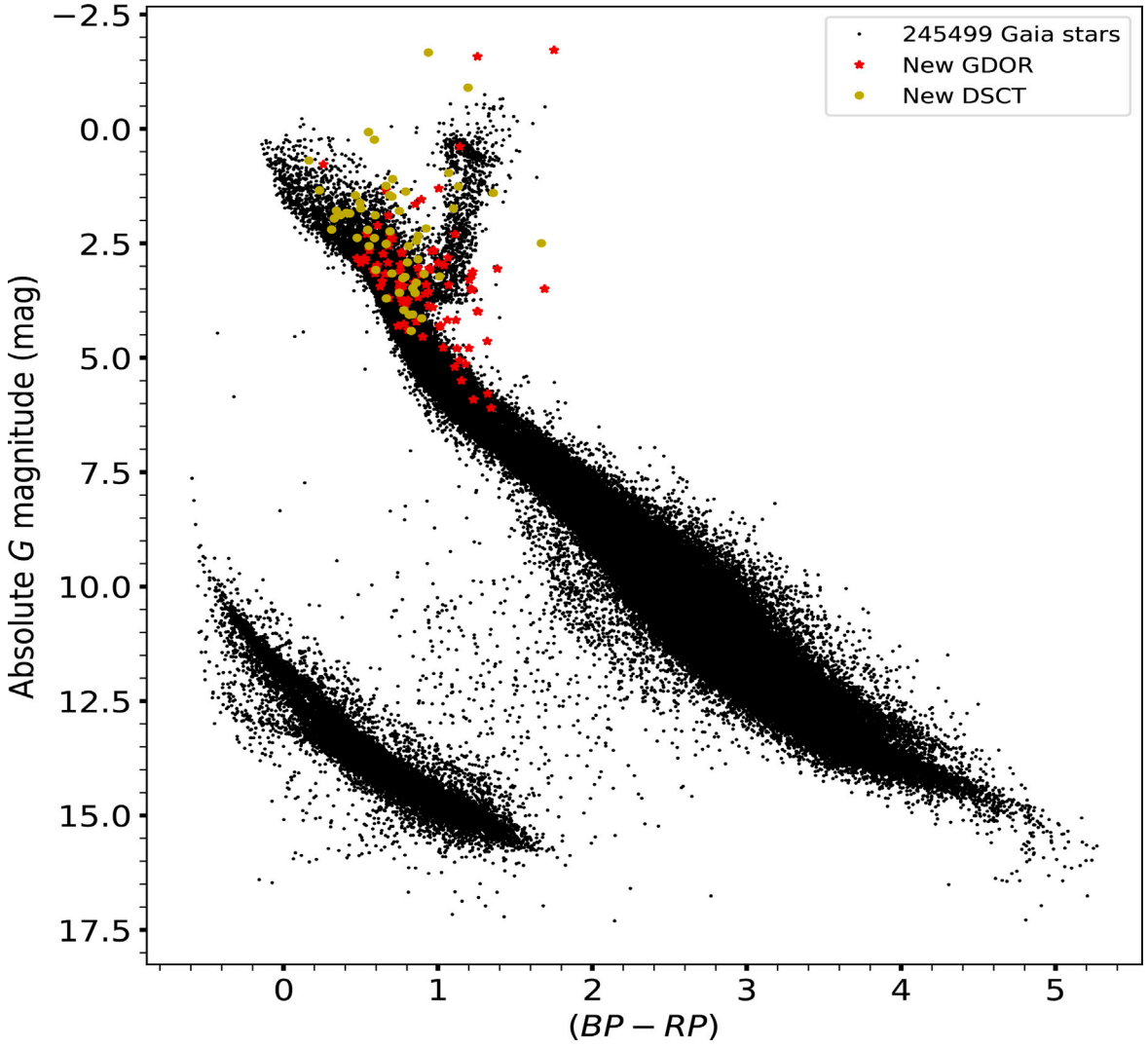

Fig. 16. Present new δ Sct and γ Dor stars in the *Gaia* color-magnitude diagram, plotted to compare with the *Gaia* stars.

Table 10
Mean parameters of NGC 6871 cluster members adopted from *Gaia* DR2 (Cantat-Gaudin and Anders, 2020).

Parameters	Mean values of members
Center coordinates (RA, Dec)	20:06:11.52 +35:45:54.0
Galactic Longitude and Latitude	l = 72.658°, b = 2.012°
Parallax (plx)	0.514 ± 0.002 mas
Distance (d)	1841.0 pc (in [1554.8, 2256.5][a]); 1741 ± 69 pc[c]
Proper motion along RA(μ_α)	−3.129 ± 0.006 mas/yr
Proper motion along Dec(μ_δ)	−6.437 ± 0.010 mas/yr
Radius containing half the members	0.371°
Number of members	594/2014 (probability over 0.5/0.1)
Age	7.064 ± 0.062 Myr[c]
Metallicity [Fe/H]	0.104±0.125[c]
Number of Simbad objects	6126 (1° radius on cluster center)
Ranges of 87 members: μ_α[−3.415, −2.673], μ_δ[−6.951, −5.926], plx [0.436, 0.615]	
Interstellar Reddening	$E(B-V)$ = 0.46, $E(b-y)$ = 0.34[b]

[a] An earlier value is 1580 pc ($m - M$ = 12.18) given by Becker and Fenkart (1971).
[b] Zhou et al. (2001b), Crawford and Barnes (1974).
[c] Adopted from Dias et al. (2021), which also reports other parameters with consistent values.

Table 11
Parallax and proper motion of the eight example stars and six NGC 6871 members from *Gaia* DR3. Non-members are labeled either as foreground (F) or background (B) stars. Membership probability is given in last column.

SN	TIC	Simbad main ID	*Gaia* DR3 ID	Parallax (mas)	Distance (pc)	Proper Motion (mas/yr)			VarType	Membership
						μ_α	μ_δ			
01	TIC 41189624	HD 191025	2059982829034485376	4.379	303.86	4.350	−9.948	10.86	DSCT	F
02	TIC 40831024	HD 227647	2060006507222471808	2.641	378.64	2.741	0.049	2.74	DSCT	F
03	TIC 42254956	HD 227941	2059151258972495744	4.046	242.32	2.287	22.938	23.05	DSCT	F
04	TIC 91945834	–	2058937816280872576	0.5923	1688.33	−4.757	−7.130	8.57	DSCT	F
05	TIC 1966084202	–	2058936510610300032	0.729	1287.99	1.466	−4.567	4.79	DSCT+GDOR (?)	F
06	TIC 274636885	TYC 2682-863-1	2059899094352017920	2.8252	345.44	3.795	0.762	3.87	GDOR	F
07	TIC 1966186334	–	2059047286405057152	0.663	1509.43	0.561	−1.085	1.22	GDOR	F
08	TIC 89119933	HD 227505	2059079653284766848	1.466	776.94	−1.184	−3.929	4.10	GDOR	F
15	TIC 89758057	NGC 6871 23	2059075869382941696	0.478	2061.87	−3.056	−6.582	7.26	star	yes: 0.70
18	TIC 89758088	NGC 6871 21	2059075804989882496	0.485	1940.92	−3.154	−6.455	7.18	star	yes: 0.80
34	TIC 89758053	HD 227634	2059075873709364864	0.520	1921.60	−3.054	−6.555	7.23	star	yes: 1.00
48	TIC 89758076	BD+35 3956	2059075839349023104	0.546	2324.44	−2.914	−6.320	6.96	star	yes: 1.00
982	TIC 89753650	HD 190864	2059070135632404992	0.526	2283.55	−3.062	−6.638	7.31	star	yes: 1.00
1093	TIC 40736299	NGC 6871 26	2059113875581888768	0.481	1816.56	−3.167	−6.638	7.36	star	yes: 1.00

then we obtained 587, 393, and 424 for each of the three subgroups, respectively. Membership results are included in the final catalogs.

6.3. Contamination issue

Because the *TESS* pixels are large, 21 arcsecond^2 on sky per pixel, the *TESS* photometry for many targets will be contaminated by nearby objects in a crowded field. A significant challenge in the hunt for transiting exoplanets (the *TESS* mission) arises when the observed dimming of a star (transit signal) does not originate from the target star itself, but instead come from contamination of a neighboring eclipsing binary. This would lead to false positive identification of an exoplanet. Therefore, properly assessing blending is crucial in the exoplanet detection process. Researchers employ various techniques to vet potential blending scenarios, such as `vetting` and `contaminante` Python tools including a target centroid model developed by Hedges et al. (2021), Hedges (2021). Only after confidently ruling out blending can a transit signal be definitively attributed to an exoplanet candidate. This attribution then requires further verification steps for confirmation.

In the cases of intrinsic stellar variabilities contaminated by nearby objects, various methods have been developed to address the challenges of source blending and to resolve the contamination issue. Colman et al. (2017) employed a combination of periodogram analysis and visual inspection to identify the origin of signals, distinguishing between the target star and nearby contaminants. Based on difference imaging analysis, Oelkers and Stassun (2018) developed an open-source tool to extract precision light curves from *TESS* Full Frame Images (FFIs). The public domain Python package **TESS_localize**, developed by Higgins and Bell (2023), offers a sophisticated tool for diagnosing blending and localizing sources of variability in crowded *TESS* photometry. This tool uses measured frequencies of variability (derived from periodograms) and analyzes whether the best-fit sinusoid amplitudes to raw light curves extracted from each pixel are distributed in the same way as light from the variable source, under the assumption that other neighboring stars are not variable at the same frequencies. This package effectively identifies the location of the true variable source. Studies like Pedersen and Bell (2023) have successfully utilized this method in exploring the impact of light curve contamination on the detection of fast yellow pulsating supergiant stars. A pulsating white dwarf (RX J2117.1+3412 =TIC 117070953) contaminated by a nearby eclipsing binary is identified using this tool by Córsico et al. (2021).

When classifying variability type for new variables, if the light of an object were contaminated by the light of nearby stars, this would lead to the same periodograms for the objects enclosed in the aperture. Which one is the true variable is an issue needed to be solved. The methodologies employed by Skarka and Henzl (2024), Skarka et al. (2022) are applicable in this context.

While a detailed inspection of neighboring stars for all objects in our sample is beyond the scope of this paper, it is crucial for in-depth studies of individual stars. To ensure reliable results, contamination from nearby objects affecting the detected variability needs to be excluded, and the source of the true variations must be confirmed when studying a specific star with *TESS* data.

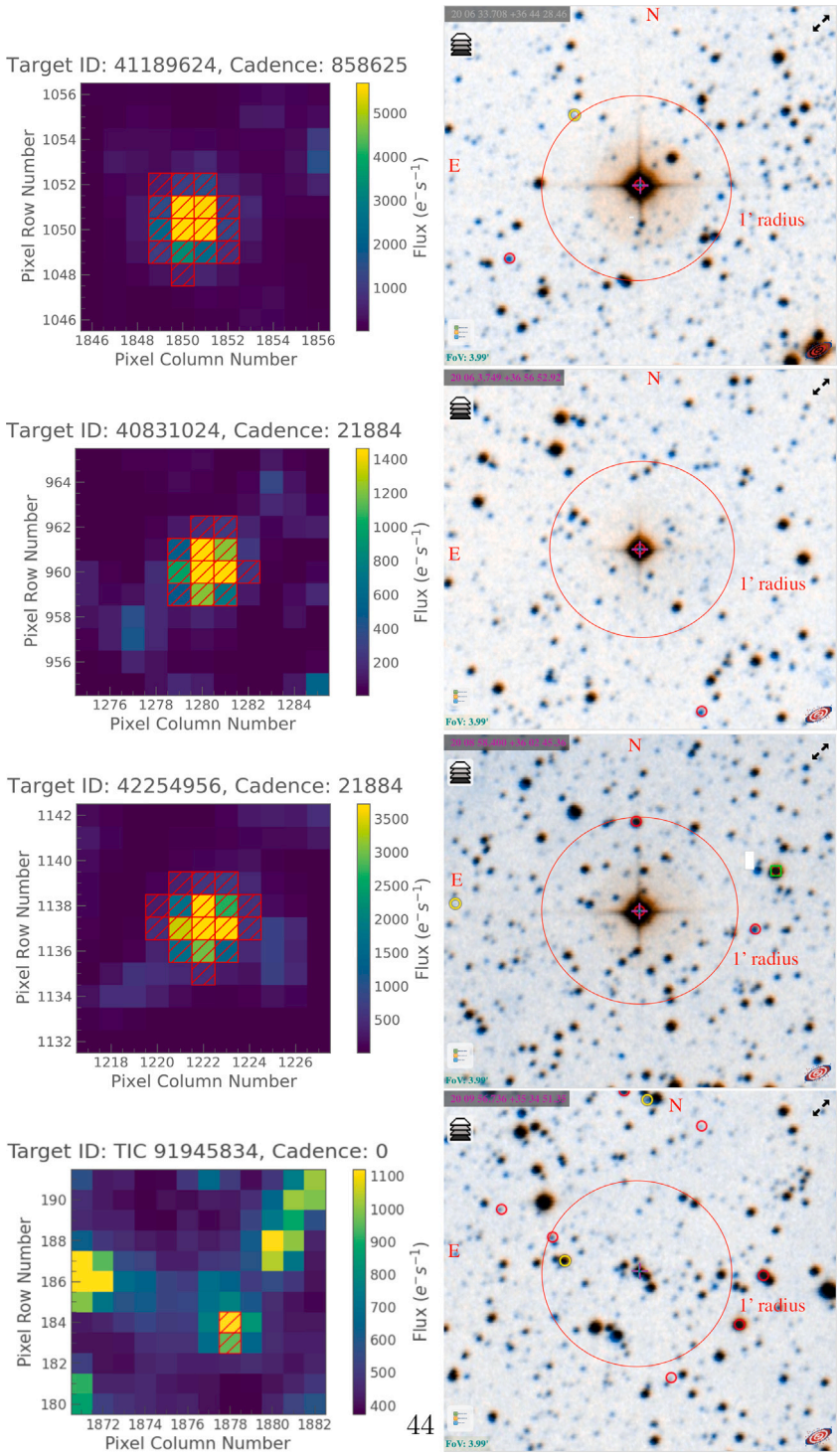

Fig. 17. *TESS* Target Pixel Files (11 × 11 pixels, ≈ 3.85′) and aperture masks (striped red squares) in photometry versus DSS images with a comparable scale of 3.99′. The largest aperture (5 × 5 pixels) corresponds to a circle with a 1′ radius. These targets are surrounded by multiple faint stars, but they are distinct from the Simbad objects (marked in red circles).

In this work, we examined the *TESS* Target Pixel Files (TPFs), Digital Sky Survey (DSS) images and periodograms for each example star, to identify any potential blending with nearby objects within the photometry aperture. TPFs are typically the first port of call when studying a star with *TESS*. They offer a visual representation of the data source and allow us to see where our data is coming from, and help us identify potential sources of noise or contamination. TPFs indicate the pixels on the CCD camera, with which a star was observed (Figs. 17 and 18). TPFs can be thought of as stacks of images, with one image for every telescopic time-stamp. Each time-stamp is referred to as a cadence. The color indicates the amount of flux in each pixel, in electrons per second. Shown here is the first observation cadence in the sector, except the 0-cadence images which are cutout from FFIs by a threshold of 5. A star's brightness (flux) is the summation of electron counts on all pixels in the photometry aperture mask.

Notably, the *TESS* data processing pipeline acknowledges this potential issue and has included a keyword in the resulting light curve

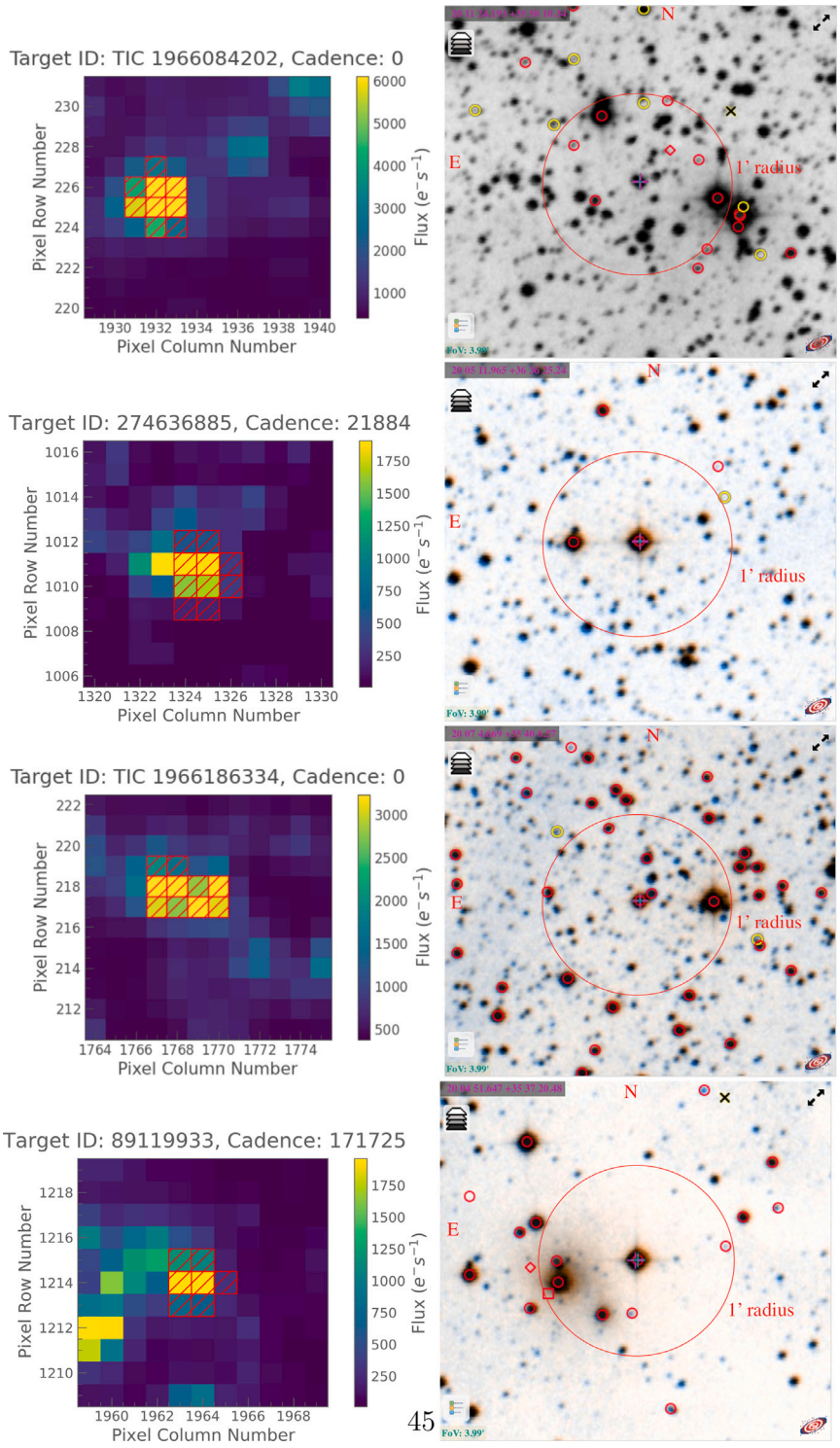

Fig. 18. *TESS* Target Pixel Files (11 × 11 pixels, ≈ 3.85′) and aperture masks (striped red squares) in photometry versus DSS images with a comparable scale of 3.99′. The largest aperture (5 × 5 pixels) corresponds to a circle with a 1′ radius. The two stars in the first and third rows might be highly contaminated by nearby stars. See text for details.

metadata. The amount of contamination for each target is approximated by the CROWDSAP keyword value in the *TESS* FITS file headers, which gives the ratio of target star flux to total flux in the optimal aperture. CROWDSAP's value close to 1 signifies that most of the measured flux (light or signal) originates from the target object itself, indicates that the observation successfully isolated the target and minimized contamination from surrounding celestial objects.

Based on our analysis of TPF images, CROWDSAP keyword values, and anomalous peaks in periodograms, the *TESS* light curves of seven of the eight example stars exhibit minimal to no contamination from nearby objects (see Figs. 17 and 18). This evidence strongly supports the identification of intrinsic variability in these stars. However, one star TIC 1966084202, its variability is ultimately inconclusive due to unsolved blending issue at this stage (see Section 5.2 for details). For the remaining new variable stars, we flagged potential blending issues based on similarities in their light curves and periodograms. However, definitive confirmation of these suspicions requires further individual investigation.

Table A.1
Catalog of 105 New δ Sct stars (reduced demo version). Full table in a CSV file is on the Supplementary Data.

TIC	Simbad main identifier	Gaia DR3	RA Dec (deg, J2000)	B	V	$T_{\rm eff}$(TIC)	$T_{\rm eff}$(Gaia)	log g(TIC)	log g(Gaia)	… …
TIC 89756626	–	2059113531984492544	301.487784 35.963387	15.62	13.942	7561.0	6825.04	4.3307	4.0646	… …
TIC 89758153	2MASS J20060031+3545156	2059075839349011200	301.501317 35.754336	16.684	13.445	8027.0	nan	3.8854	nan	… …
TIC 89758078	NGC 6871 29	2059076045507486848	301.480645 35.762069	13.221	12.859	8734.0	nan	3.874	nan	… …
TIC 90462180	TYC 2683-2890-1	2059056597894705408	301.851572 35.840411	11.628	11.032	7316.0	nan	3.3066	nan	… …
TIC 90461968	–	2059056834093348736	301.856888 35.866138	nan	11.106	7957.0	8810.39	nan	3.4269	… …
⋮										

Table A.2
Catalog of 121 New γ Dor stars (reduced demo version). Full table in a CSV file is available on the Supplementary Data.

TIC	Simbad main identifier	Gaia DR3	RA Dec (deg, J2000)	B	V	$T_{\rm eff}$(TIC)	$T_{\rm eff}$(Gaia)	log g(TIC)	log g(Gaia)	… …
TIC 89757254	–	2059100642754303104	301.534845 35.855827	12.794	12.333	6230.0	nan	3.7452	nan	… …
TIC 90349696	–	2059048763873903360	301.724275 35.751581	12.837	12.386	7000.0	6814.35	4.2649	4.121	… …
TIC 91106707	–	2059055532742634624	301.906252 35.82067	14.45	13.997	8547.0	9716.65	4.1794	3.9769	… …
TIC 89754909	2MASS J20053691+3544526	2059074911636219264	301.403811 35.747996	13.903	13.173	6515.0	6184.42	3.877	3.9433	… …
TIC 1966205980	–	2059071063345128448	301.56892 35.653105	nan	13.3377	6502.0	6242.9	nan	3.9379	… …
⋮										

Table A.3
Catalog of 198 New Eclipsing Binary Systems and others (reduced demo version). Full table in a CSV file is available on the Supplementary Data.

TIC	Simbad main identifier	Gaia DR3	RA Dec (deg, J2000)	$T_{\rm mag}$	$T_{\rm eff}$	SpType	$L/L_{\odot}$	log g	$M/M_{\odot}$	VarType
TIC 91573072	–	2058795601311864832	302.184024 35.089003	13.415	9269	A1	94.437	3.6568	2.35	EA
TIC 42843054	–	2059173146127143680	302.644287 36.307849	12.302	7607	A7	51.236	3.4560	1.77	EA
TIC 90975785	–	2058804844081177088	301.99698 34.986173	12.8484	5568	G5	2.117	4.0419	0.98	EA
TIC 90975729	–	2058804775361696640	301.996475 34.980243	13.0605	5682	G2V	3.443	3.8782	1.01	EA
TIC 90975113	–	2058798453169900416	301.883745 34.90696	13.9184	6742	F5	nan	nan	nan	EA
TIC 104213242	–	2059473209722261248	300.407436 35.855348	12.8209	6996	F2	15.150	3.7793	1.54	EA
TIC 106229161	TYC 2678-83-1	2058623733900094976	301.16124 34.959434	11.4978	8287	A5	nan	nan	nan	EA+ROT
TIC 90461796	2MASS J20071338+3553369	2059103876897664896	301.80577 35.893601	13.3356	7152	F0	5.290	4.2884	1.59	EA+GDOR
TIC 90980715	2MASS J20073329+3536371	2059044503266096512	301.888706 35.610319	13.4575	7885	A7	14.544	4.0914	1.88	EA+GDOR
TIC 106236194	–	2059836667040378240	301.085212 35.841442	12.9158	9849	A0	nan	nan	nan	EA+Maia
TIC 104914249	–	2059461252532749440	300.625412 35.671854	12.8061	6696	F5	5.280	4.1256	1.42	Quad-EA
TIC 91111661	–	2058839306900025984	302.104805 35.434893	13.3867	6438	F7	15.348	3.5556	1.30	EB
⋮										

7. Conclusions

The unparalleled continuous and high-precision photometry provided by *TESS* has been instrumental in revealing the subtle light variations of stars, allowing for a deeper understanding of their true nature. This focused survey, centering on V1821 Cyg within the NGC 6871 cluster, utilized *TESS* data to meticulously screen stars with $T_{\rm mag}$ values between 6 and 16 mag, matching the *TESS* premium targets with good quality photometry. These stars, with effective temperatures ranging from 10000 to 6000 K, represent main sequence stars of spectral types A to F, which include the domains of both δ Sct and γ Dor stars. Despite previous extensive studies of the NGC 6871 region, this survey has successfully identified over 1500 new variable stars from a pool of 4726 candidates. This impressive yield includes 105 δ Sct and 121 γ Dor stars, underscoring the exceptional quality of *TESS* data. The present impressive discoveries attribute to the perfect *TESS* data. The results of this survey advocate for an expanded exploration to fully leverage the *TESS* archive.

However, *TESS* data presents a challenge for variability studies due to blending and contamination. The large CCD pixels (21″/pixel on sky) often combine light from nearby stars, hindering the isolation of individual variability. Existing community approaches mentioned in Section 6.3 offer valuable tools for tackling this challenge. For a specific variable involved blending, ground-based higher resolution observations can spatially resolve blended stars, enabling independent light curve measurements and mitigating these issues.

Key highlights of this study include:

- Discovery of 269 pulsators of types δ Sct, γ Dor, and Maia;
- Discovery of 198 eclipsing binaries, with 12 featuring pulsating components;
- Detailed analyses of eight exemplary stars, revealed that: (1) initial investigations of contamination issue lead to an inconclusive hybrid δ Sct-γ Dor pulsation of TIC 1966084202, its variability source needs to be confirmed; while other seven stars' variabilities are validated. (2) Maia or hybrid δ Sct-γ Dor pulsational features in HD 191025; (3) more than 90 rich pulsation frequencies in the new δ Sct star HD 227941 and the amplitude variations of dominant pulsations over time.
- Based on parallax and proper motion data from *Gaia* DR3, we performed an initial assessment of membership of NGC 6871 for the newly identified variables. This analysis identified 108 out of the 1512 new variables (7%) as probable members of the cluster NGC 6871. These include 6 δ Sct and 11 γ Dor belong to NGC 6871 with membership probability exceeding 50%.
- Our initial assessment of blending and contamination in a limited sample of identified variables underscores the complexities these issues pose for detailed stellar characterization. While disentangling blended light curves can be challenging, as these initial results suggest, addressing blending and contamination remains crucial for accurate analysis of individual stars.
- The combined H–R diagrams (Figs. 14 and 15) for new δ Sct and γ Dor stars compared with known class members suggest a potential united pulsation mechanism valid for the two classes.
- This work not only contributes to the catalog of known variable stars but also provides a foundation for future studies aiming to unravel the complexities of stellar pulsations.

CRediT authorship contribution statement

Ai-Ying Zhou: Writing – review & editing, Writing – original draft, Visualization, Validation, Supervision, Software, Resources, Project administration, Methodology, Investigation, Formal analysis, Data curation, Conceptualization.

Declaration of competing interest

The authors declare that they have no known competing financial interests or personal relationships that could have appeared to influence the work reported in this paper.

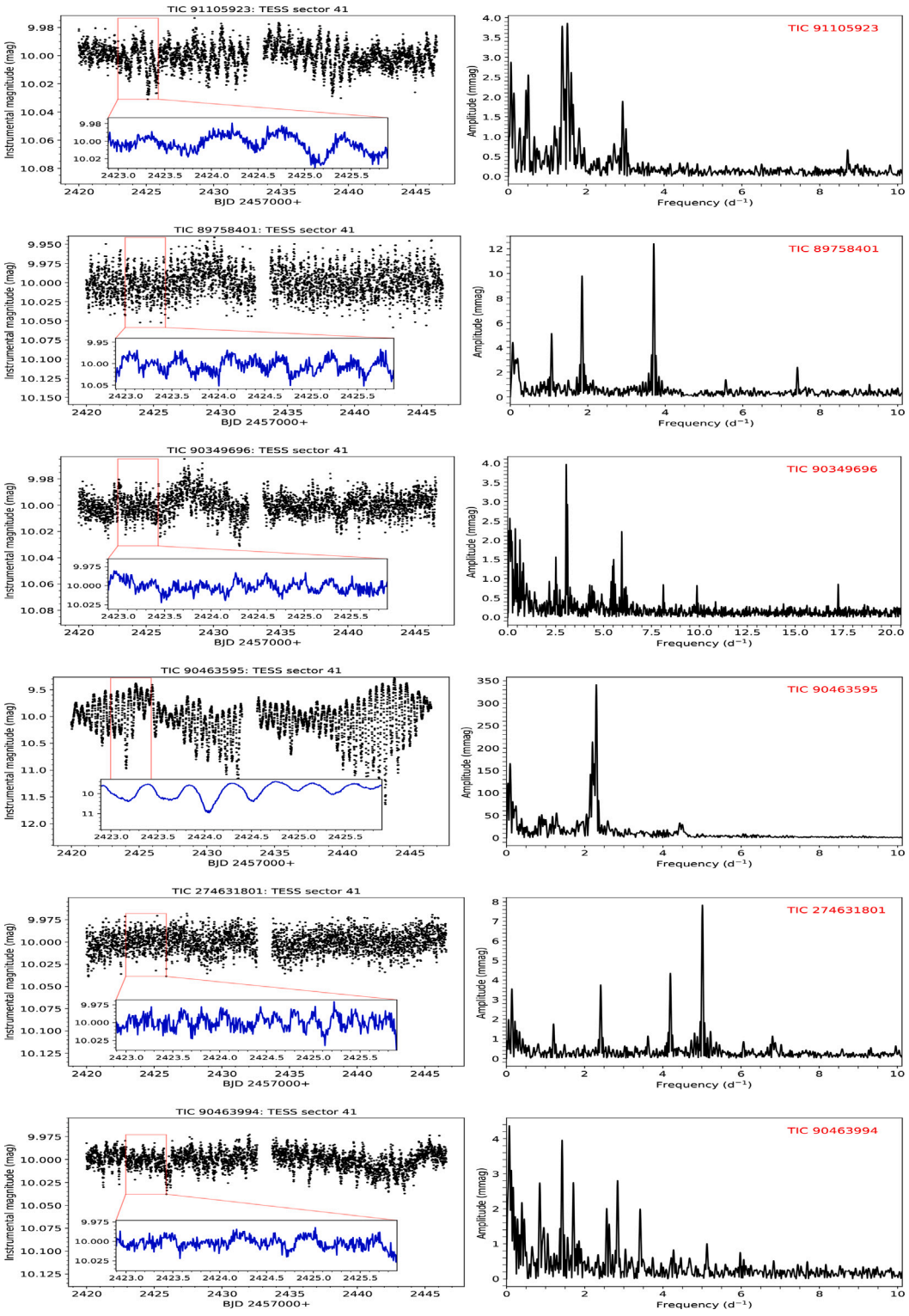

Fig. D.19. Sample *TESS* light curves and amplitude spectra of six new γ Dor variables.

Data availability

Data will be made available on request.

Acknowledgments

I appreciate the anonymous referee for their careful reading, constructive comments, and insightful suggestions. These, especially regarding the blending issue and cluster membership, significantly strengthened the manuscript's clarity and rigor. I am indebted to my wife Jingyun Zhang for her unwavering support throughout my research. This work could not have been done without her continuous support. This paper includes data collected with the *TESS* mission and obtained from the MAST data archive at the Space Telescope Science Institute (STScI). Funding for the *TESS* mission is provided by the NASA Explorer Program. STScI is operated by the Association of Universities for Research in Astronomy, Inc., under NASA contract NAS 5–26555.

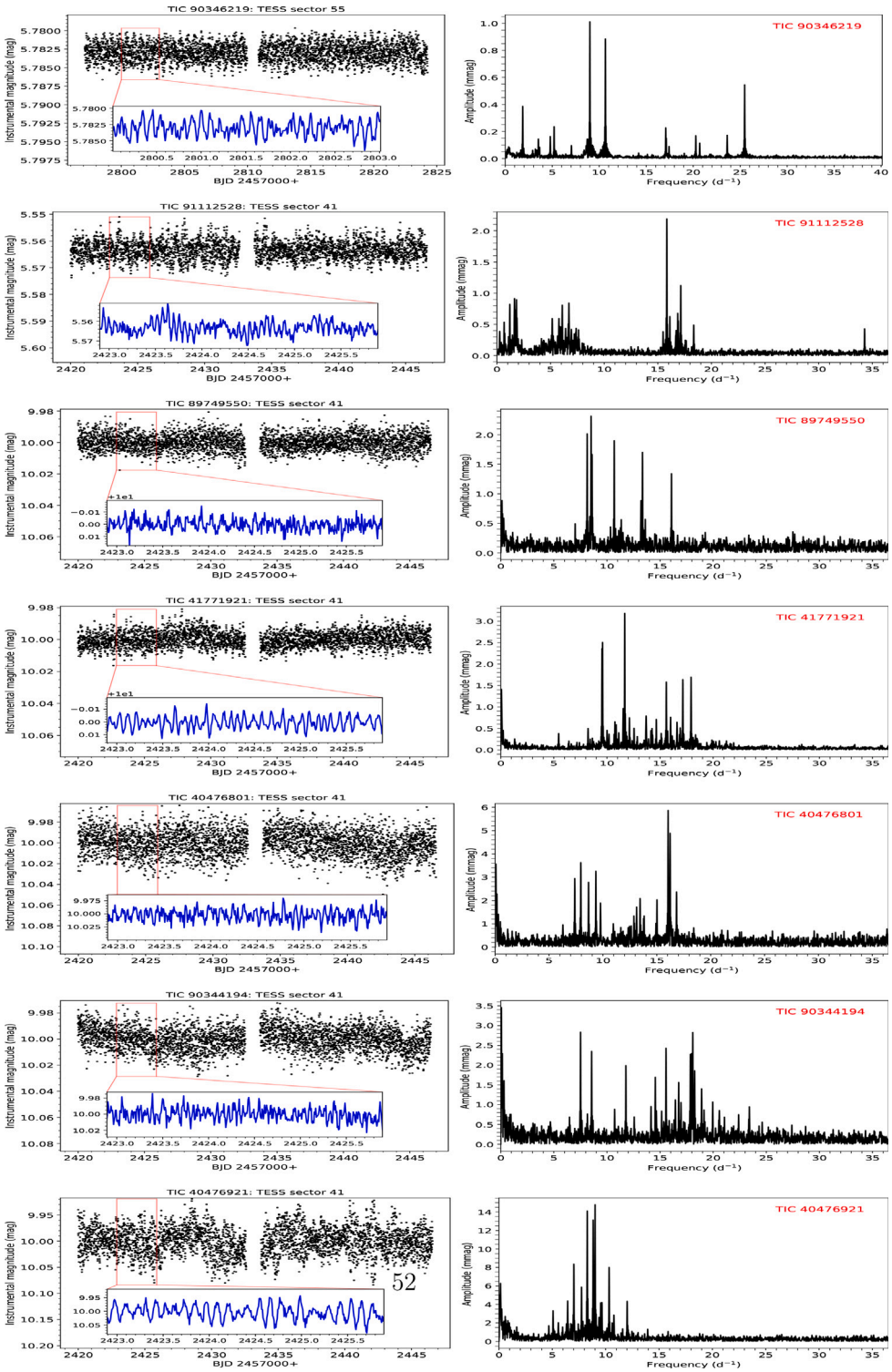

Fig. D.20. Sample *TESS* light curves and amplitude spectra of seven new δ Sct variables.

We acknowledge the use of *TESS* data, which are derived from pipelines at the *TESS* Science Processing Operations Center (SPOC). *TESS* High Level Science Products (HLSP) produced by the Quick-Look Pipeline (QLP) at the *TESS* Science Office at MIT, which are publicly available from the Mikulski Archive for Space Telescopes (MAST). This research has made use of the SIMBAD/VizieR databases, operated at CDS, Strasbourg, France. This research has made use of the International Variable Star Index (VSX) database, operated at AAVSO, Cambridge, Massachusetts, USA. This work has made use of data from the European Space Agency (ESA) mission *Gaia* (https://www.cosmos.esa.int/gaia), processed by the *Gaia* Data Processing and Analysis Consortium (DPAC, https://www.cosmos.esa.int/web/gaia/dpac/consortium). Funding for the DPAC has been provided by national institutions, in particular the institutions participating in the *Gaia* Multilateral Agreement. This work made use of *Astropy*[5]: a community-developed core Python package and

[5] http://www.astropy.org

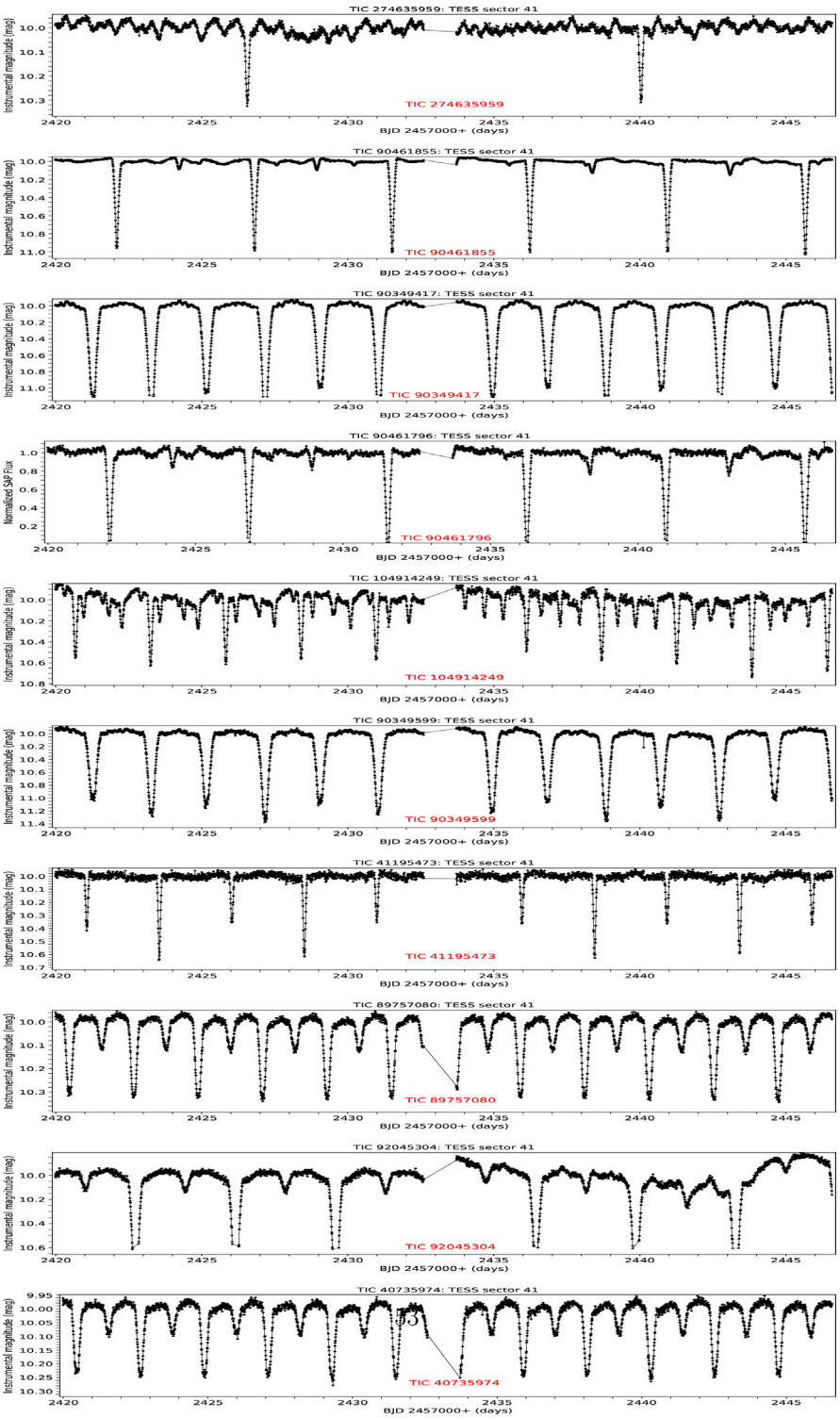

Fig. D.21. Sample *TESS* light curves of ten newly identified eclipsing binary stars.

an ecosystem of tools and resources for astronomy (Astropy Collaboration et al., 2013, 2018, 2022); Astroquery (Ginsburg et al., 2019); Lightkurve (Lightkurve Collaboration et al., 2018); Matplotlib (Hunter, 2007); SciPy (Virtanen et al., 2020); NumPy (Harris et al., 2020).

Appendix A. Table of new δ Scuti stars

Each entry in the catalog is comprised of 28 columns: TIC, Simbad main identifier, *Gaia* DR3, RA_Dec, B, V, $T_{\rm eff}$_TIC, $T_{\rm eff}$_Gaia, $\log g$_TIC, $\log g$_Gaia, Mass_TIC, R_TIC, R_Gaia, L_TIC, L_Gaia, parallax, distance, M_V, $\log T_{\rm eff}$_TIC, $\log L$_TIC, G_mag, BP_mag, RP_mag, $BP-RP$, $BP-G$, $G-RP$, Radial_Velocity_Gaia and reference source.

The whole catalog in its entirety is provided as online materials in machine-readable text format (CSV file). A reduced demo is given in Table A.1.

Appendix B. Table of newly identified γ Doradus stars

We have compiled a catalog for the new γ Dor stars. The whole catalog in its entirety is provided as online materials in a machine-readable text format (CSV file). A reduced demo is given in Table A.2.

Appendix C. Table of new eclipsing binaries and others

The new variables other than DSCT and GDOR are compiled together in a machine-readable text format (CSV file). A reduced demo is given in Table A.3.

Appendix D. Additional representative examples of classifications

See Figs. D.19–D.21.

Appendix E. Supplementary data

Supplementary material related to this article can be found online at https://doi.org/10.1016/j.newast.2024.102297.

References

Antoci, V., Cunha, M.S., Bowman, D.M., Murphy, S.J., Kurtz, D.W., Bedding, T.R., Borre, C.C., Christophe, S., Daszyńska-Daszkiewicz, J., Fox-Machado, L., García Hernández, A., Ghasemi, H., Handberg, R., Hansen, H., Hasanzadeh, A., Houdek, G., Johnston, C., Justesen, A.B., Kahraman Alicavus, F., Kotysz, K., Latham, D., Matthews, J.M., Mønster, J., Niemczura, E., Paunzen, E., Sánchez Arias, J.P., Pigulski, A., Pepper, J., Richey-Yowell, T., Safari, H., Seager, S., Smalley, B., Shutt, T., Sódor, A., Suárez, J.C., Tkachenko, A., Wu, T., Zwintz, K., Barceló Forteza, S., Brunsden, E., Bognár, Z., Buzasi, D.L., Chowdhury, S., De Cat, P., Evans, J.A., Guo, Z., Guzik, J.A., Jevtic, N., Lampens, P., Lares Martiz, M., Lovekin, C., Li, G., Mirouh, G.M., Mkrtichian, D., Monteiro, M.J.P.F.G., Nemec, J.M., Ouazzani, R.M., Pascual-Granado, J., Reese, D.R., Rieutord, M., Rodon, J.R., Skarka, M., Sowicka, P., Stateva, I., Szabó, R., Weiss, W.W., 2019. The first view of δ Scuti and γ Doradus stars with the TESS mission. Mon. Not. R. Astron. Soc. 490, 4040–4059. http://dx.doi.org/10.1093/mnras/stz2787, arXiv:1909.12018.

Astropy Collaboration, Price-Whelan, A.M., Lim, P.L., Earl, N., Starkman, N., Bradley, L., Shupe, D.L., Patil, A.A., Corrales, L., Brasseur, C.E., Nöthe, M., Donath, A., Tollerud, E., Morris, B.M., Ginsburg, A., Vaher, E., Weaver, B.A., Tocknell, J., Jamieson, W., van Kerkwijk, M.H., Robitaille, T.P., Merry, B., Bachetti, M., Günther, H.M., Aldcroft, T.L., Alvarado-Montes, J.A., Archibald, A.M., Bódi, A., Bapat, S., Barentsen, G., Bazán, J., Biswas, M., Boquien, M., Burke, D.J., Cara, D., Cara, M., Conroy, K.E., Conseil, S., Craig, M.W., Cross, R.M., Cruz, K.L., D'Eugenio, F., Dencheva, N., Devillepoix, H.A.R., Dietrich, J.P., Eigenbrot, A.D., Erben, T., Ferreira, L., Foreman-Mackey, D., Fox, R., Freij, N., Garg, S., Geda, R., Glattly, L., Gondhalekar, Y., Gordon, K.D., Grant, D., Greenfield, P., Groener, A.M., Guest, S., Gurovich, S., Handberg, R., Hart, A., Hatfield-Dodds, Z., Homeier, D., Hosseinzadeh, G., Jenness, T., Jones, C.K., Joseph, P., Kalmbach, J.B., Karamehmetoglu, E., Kałuszyński, M., Kelley, M.S.P., Kern, N., Kerzendorf, W.E., Koch, E.W., Kulumani, S., Lee, A., Ly, C., Ma, Z., MacBride, C., Maljaars, J.M., Muna, D., Murphy, N.A., Norman, H., O'Steen, R., Oman, K.A., Pacifici, C., Pascual, S., Pascual-Granado, J., Patil, R.R., Perren, G.I., Pickering, T.E., Rastogi, T., Roulston, B.R., Ryan, D.F., Rykoff, E.S., Sabater, J., Sakurikar, P., Salgado, J., Sanghi, A., Saunders, N., Savchenko, V., Schwardt, L., Seifert-Eckert, M., Shih, A.Y., Jain, A.S., Shukla, G., Sick, J., Simpson, C., Singanamalla, S., Singer, L.P., Singhal, J., Sinha, M., Sipőcz, B.M., Spitler, L.R., Stansby, D., Streicher, O., Šumak, J., Swinbank, J.D., Taranu, D.S., Tewary, N., Tremblay, G.R., Val-Borro, M.d., Van Kooten, S.J., Vasović, Z., Verma, S., de Miranda Cardoso, J.V., Williams, P.K.G., Wilson, T.J., Winkel, B., Wood-Vasey, W.M., Xue, R., Yoachim, P., Zhang, C., Zonca, A., Astropy Project Contributors, 2022. The astropy project: Sustaining and growing a community-oriented open-source project and the latest major release (v5.0) of the core package. Astrophys. J. 935, 167. http://dx.doi.org/10.3847/1538-4357/ac7c74, arXiv:2206.14220.

Astropy Collaboration, Price-Whelan, A.M., Sipőcz, B.M., Günther, H.M., Lim, P.L., Crawford, S.M., Conseil, S., Shupe, D.L., Craig, M.W., Dencheva, N., Ginsburg, A., VanderPlas, J.T., Bradley, L.D., Pérez-Suárez, D., de Val-Borro, M., Aldcroft, T.L., Cruz, K.L., Robitaille, T.P., Tollerud, E.J., Ardelean, C., Babej, T., Bach, Y.P., Bachetti, M., Bakanov, A.V., Bamford, S.P., Barentsen, G., Barmby, P., Baumbach, A., Berry, K.L., Biscani, F., Boquien, M., Bostroem, K.A., Bouma, L.G., Brammer, G.B., Bray, E.M., Breytenbach, H., Buddelmeijer, H., Burke, D.J., Calderone, G., Cano Rodríguez, J.L., Cara, M., Cardoso, J.V.M., Cheedella, S., Copin, Y., Corrales, L., Crichton, D., D'Avella, D., Deil, C., Depagne, É., Dietrich, J.P., Donath, A., Droettboom, M., Earl, N., Erben, T., Fabbro, S., Ferreira, L.A., Finethy, T., Fox, R.T., Garrison, L.H., Gibbons, S.L.J., Goldstein, D.A., Gommers, R., Greco, J.P., Greenfield, P., Groener, A.M., Grollier, F., Hagen, A., Hirst, P., Homeier, D., Horton, A.J., Hosseinzadeh, G., Hu, L., Hunkeler, J.S., Ivezić, Ž., Jain, A., Jenness, T., Kanarek, G., Kendrew, S., Kern, N.S., Kerzendorf, W.E., Khvalko, A., King, J., Kirkby, D., Kulkarni, A.M., Kumar, A., Lee, A., Lenz, D., Littlefair, S.P., Ma, Z., Macleod, D.M., Mastropietro, M., McCully, C., Montagnac, S., Morris, B.M., Mueller, M., Mumford, S.J., Muna, D., Murphy, N.A., Nelson, S., Nguyen, G.H., Ninan, J.P., Nöthe, M., Ogaz, S., Oh, S., Parejko, J.K., Parley, N., Pascual, S., Patil, R., Patil, A.A., Plunkett, A.L., Prochaska, J.X., Rastogi, T., Reddy Janga, V., Sabater, J., Sakurikar, P., Seifert, M., Sherbert, L.E., Sherwood-Taylor, H., Shih, A.Y., Sick, J., Silbiger, M.T., Singanamalla, S., Singer, L.P., Sladen, P.H., Sooley, K.A., Sornarajah, S., Streicher, O., Teuben, P., Thomas, S.W., Tremblay, G.R., Turner, J.E.H., Terrón, V., van Kerkwijk, M.H., de la Vega, A., Watkins, L.L., Weaver, B.A., Whitmore, J.B., Woillez, J., Zabalza, V., Astropy Contributors, 2018. The Astropy Project: Building an Open-science Project and Status of the v2.0 Core Package. Astron. J. 156, 123. http://dx.doi.org/10.3847/1538-3881/aabc4f, arXiv:1801.02634.

Astropy Collaboration, Robitaille, T.P., Tollerud, E.J., Greenfield, P., Droettboom, M., Bray, E., Aldcroft, T., Davis, M., Ginsburg, A., Price-Whelan, A.M., Kerzendorf, W.E., Conley, A., Crighton, N., Barbary, K., Muna, D., Ferguson, H., Grollier, F., Parikh, M.M., Nair, P.H., Unther, H.M., Deil, C., Woillez, J., Conseil, S., Kramer, R., Turner, J.E.H., Singer, L., Fox, R., Weaver, B.A., Zabalza, V., Edwards, Z.I., Azalee Bostroem, K., Burke, D.J., Casey, A.R., Crawford, S.M., Dencheva, N., Ely, J., Jenness, T., Labrie, K., Lim, P.L., Pierfederici, F., Pontzen, A., Ptak, A., Refsdal, B., Servillat, M., Streicher, O., 2013. Astropy: A community python package for astronomy. Astron. Astrophys. 558, A33. http://dx.doi.org/10.1051/0004-6361/201322068, arXiv:1307.6212.

Balona, L.A., 2018. Gaia luminosities of pulsating A-F stars in the Kepler field. Mon. Not. R. Astron. Soc. 479, 183–191. http://dx.doi.org/10.1093/mnras/sty1511, arXiv:1806.02622.

Balona, L.A., 2022a. Identification and classification of TESS variable stars. arXiv e-prints, arXiv:2212.10776, arXiv:2212.10776.

Balona, L.A., 2022b. Rapidly oscillating TESS A-F main-sequence stars: are the roap stars a distinct class? Mon. Not. R. Astron. Soc. 510, 5743–5759. http://dx.doi.org/10.1093/mnras/stac011, arXiv:2109.02246.

Balona, L.A., 2023. Maia variables and other anomalies among pulsating stars. Front. Astron. Space Sci. 10, 1266750. http://dx.doi.org/10.3389/fspas.2023.1266750.

Balona, L.A., Daszyńska-Daszkiewicz, J., Pamyatnykh, A.A., 2015. Pulsation frequency distribution in δ Scuti stars. Mon. Not. R. Astron. Soc. 452, 3073–3084. http://dx.doi.org/10.1093/mnras/stv1513, arXiv:1505.07216.

Balona, L.A., Ozuyar, D., 2020. Pulsation among TESS A and B stars and the Maia variables. Mon. Not. R. Astron. Soc. 493, 5871–5879. http://dx.doi.org/10.1093/mnras/staa670, arXiv:2001.04497.

Bass, G., Borne, K., 2016. Supervised ensemble classification of Kepler variable stars. Mon. Not. R. Astron. Soc. 459, 3721–3737. http://dx.doi.org/10.1093/mnras/stw810, arXiv:1604.01355.

Becker, W., Fenkart, R., 1971. A catalogue of galactic star clusters observed in three colours. Astron. Astrophys. Suppl. Ser. 4 (241).

Bellm, E.C., Kulkarni, S.R., Graham, M.J., Dekany, R., Smith, R.M., Riddle, R., Masci, F.J., Helou, G., Prince, T.A., Adams, S.M., Barbarino, C., Barlow, T., Bauer, J., Beck, R., Belicki, J., Biswas, R., Blagorodnova, N., Bodewits, D., Bolin, B., Brinnel, V., Brooke, T., Bue, B., Bulla, M., Burruss, R., Cenko, S.B., Chang, C.K., Connolly, A., Coughlin, M., Cromer, J., Cunningham, V., De, K., Delacroix, A., Desai, V., Duev, D.A., Eadie, G., Farnham, T.L., Feeney, M., Feindt, U., Flynn, D., Franckowiak, A., Frederick, S., Fremling, C., Gal-Yam, A., Gezari, S., Giomi, M., Goldstein, D.A., Golkhou, V.Z., Goobar, A., Groom, S., Hacopians, E., Hale, D., Henning, J., Ho, A.Y.Q., Hover, D., Howell, J., Hung, T., Huppenkothen, D., Imel, D., Ip, W.H., Ivezić, Ž., Jackson, E., Jones, L., Juric, M., Kasliwal, M.M., Kaspi, S., Kaye, S., Kelley, M.S.P., Kowalski, M., Kramer, E., Kupfer, T., Landry, W., Laher, R.R., Lee, C.D., Lin, H.W., Lin, Z.Y., Lunnan, R., Giomi, M., Mahabal, A., Mao, P., Miller, A.A., Monkewitz, S., Murphy, P., Ngeow, C.C., Nordin, J., Nugent, P., Ofek, E., Patterson, M.T., Penprase, B., Porter, M., Rauch, L., Rebbapragada, U., Reiley, D., Rigault, M., Rodriguez, H., van Roestel, J., Rusholme, B., van Santen, J., Schulze, S., Shupe, D.L., Singer, L.P., Soumagnac, M.T., Stein, R., Surace, J., Sollerman, J., Szkody, P., Taddia, F., Terek, S., Van Sistine, A., van Velzen, S., Vestrand, W.T., Walters, R., Ward, C., Ye, Q.Z., Yu, P.C., Yan, L., Zolkower, J., 2019. The zwicky transient facility: System overview, performance, and first results. Publ. Astron. Soc. Pac. 131, 018002. http://dx.doi.org/10.1088/1538-3873/aaecbe, arXiv:1902.01932.

Brasseur, C.E., Phillip, C., Fleming, S.W., Mullally, S.E., White, R.L., 2019. Astrocut: Tools for Creating Cutouts of TESS Images. Astrophysics Source Code Library, record ascl:1905.007.

Breger, M., 1979. Delta Scuti and related stars. Publ. Astron. Soc. Pac. 91, 5–26. http://dx.doi.org/10.1086/130433.

Breger, M., 2000. δ Scuti stars (review). In: Breger, M., Montgomery, M. (Eds.), Delta Scuti and Related Stars. p. 3.

Caldwell, D.A., Jenkins, J.M., Ting, E.B., 2020. Tess light curves from full frame images (tess-spoc). http://dx.doi.org/10.17909/T9-WPZ1-8S54.

Cantat-Gaudin, T., Anders, F., 2020. Clusters and mirages: cataloguing stellar aggregates in the Milky Way. Astron. Astrophys. 633, A99. http://dx.doi.org/10.1051/0004-6361/201936691, arXiv:1911.07075.

Cantat-Gaudin, T., Anders, F., Castro-Ginard, A., Jordi, C., Romero-Gómez, M., Soubiran, C., Casamiquela, L., Tarricq, Y., Moitinho, A., Vallenari, A., Bragaglia, A., Krone-Martins, A., Kounkel, M., 2020. Painting a portrait of the Galactic disc with

its stellar clusters. Astron. Astrophys. 640, A1. http://dx.doi.org/10.1051/0004-6361/202038192, arXiv:2004.07274.

Cantat-Gaudin, T., Jordi, C., Vallenari, A., Bragaglia, A., Balaguer-Núñez, L., Soubiran, C., Bossini, D., Moitinho, A., Castro-Ginard, A., Krone-Martins, A., Casamiquela, L., Sordo, R., Carrera, R., 2018. A gaia DR2 view of the open cluster population in the Milky way. Astron. Astrophys. 618, A93. http://dx.doi.org/10.1051/0004-6361/201833476, arXiv:1805.08726.

Casado, J., Hendy, Y., 2023. Discovery and description of two young open clusters in the primordial group of NGC 6871. Mon. Not. R. Astron. Soc. 521, 1399–1407. http://dx.doi.org/10.1093/mnras/stad071, arXiv:2211.12843.

Catelan, M., Smith, H.A., 2015. Pulsating Stars. Wiley-VCH, Weinheim.

Chen, X., Wang, S., Deng, L., de Grijs, R., Yang, M., Tian, H., 2020. The zwicky transient facility catalog of periodic variable stars. Astrophys. J. Suppl. 249, 18. http://dx.doi.org/10.3847/1538-4365/ab9cae, arXiv:2005.08662.

Christy, C.T., Jayasinghe, T., Stanek, K.Z., Kochanek, C.S., Thompson, T.A., Shappee, B.J., Holoien, T.W.S., Prieto, J.L., Dong, S., Giles, W., 2022. The ASAS-SN catalog of variable stars x: Discovery of 116 000new variable stars using g-band photometry. arXiv e-prints, arXiv:2205.02239, arXiv:2205.02239.

Christy, C.T., Jayasinghe, T., Stanek, K.Z., Kochanek, C.S., Thompson, T.A., Shappee, B.J., Holoien, T.W.S., Prieto, J.L., Dong, S., Giles, W., 2023. The ASAS-SN catalogue of variable stars X: discovery of 116 000 new variable stars using G-band photometry. Mon. Not. R. Astron. Soc. 519, 5271–5287. http://dx.doi.org/10.1093/mnras/stac3801, arXiv:2205.02239.

Colman, I.L., Huber, D., Bedding, T.R., Kuszlewicz, J.S., Yu, J., Beck, P.G., Elsworth, Y., García, R.A., Kawaler, S.D., Mathur, S., Stello, D., White, T.R., 2017. Evidence for compact binary systems around Kepler red giants. Mon. Not. R. Astron. Soc. 469, 3802–3812. http://dx.doi.org/10.1093/mnras/stx1056, arXiv:1705.00621.

Córsico, A.H., Uzundag, M., Kepler, S.O., Althaus, L.G., Silvotti, R., Baran, A.S., Vučković, M., Werner, K., Bell, K.J., Higgins, M., 2021. Pulsating hydrogen-deficient white dwarfs and pre-white dwarfs observed with TESS. I. Asteroseismology of the GW vir stars RX J2117+3412, HS 2324+3944, NGC 6905, NGC 1501, NGC 2371, and K 1-16. Astron. Astrophys. 645, A117. http://dx.doi.org/10.1051/0004-6361/202039202, arXiv:2011.03629.

Crawford, D.L., Barnes, J.V., 1974. Four-color and hbeta photometry for open clusters. X. The alpha Persei cluster. Astron. J. 79, 687–697. http://dx.doi.org/10.1086/111598.

Creevey, O.L., Metcalfe, T.S., Schultheis, M., Salabert, D., Bazot, M., Thévenin, F., Mathur, S., Xu, H., García, R.A., 2017. Characterizing solar-type stars from full-length Kepler data sets using the Asteroseismic Modeling Portal. Astron. Astrophys. 601, A67. http://dx.doi.org/10.1051/0004-6361/201629496, arXiv:1612.08990.

Delgado, A.J., Alfaro, E.J., Garcia-Pelayo, J.M., Garrido, R., Vidal, S., 1984. Search for variable stars in the young open cluster NGC 6871. Astron. Astrophys. Suppl. Ser. 58, 447–451.

Dias, W.S., Monteiro, H., Moitinho, A., Lépine, J.R.D., Carraro, G., Paunzen, E., Alessi, B., Villela, L., 2021. Updated parameters of 1743 open clusters based on Gaia DR2. Mon. Not. R. Astron. Soc. 504, 356–371. http://dx.doi.org/10.1093/mnras/stab770, arXiv:2103.12829.

Fetherolf, T., Pepper, J., Simpson, E., Kane, S.R., Močik, T., English, J.E., Antoci, V., Huber, D., Jenkins, J.M., Stassun, K., Twicken, J.D., Vanderspek, R., Winn, J.N., 2023. Variability Catalog of Stars Observed during the TESS Prime Mission. Astrophys. J. Suppl. 268, 4. http://dx.doi.org/10.3847/1538-4365/acdee5, arXiv:2208.11721.

Gaia Collaboration, Brown, A.G.A., Vallenari, A., Prusti, T., de Bruijne, J.H.J., Babusiaux, C., Bailer-Jones, C.A.L., Biermann, M., Evans, D.W., Eyer, L., Jansen, F., Jordi, C., Klioner, S.A., Lammers, U., Lindegren, L., Luri, X., Mignard, F., Panem, C., Pourbaix, D., Randich, S., Sartoretti, P., Siddiqui, H.I., Soubiran, C., van Leeuwen, F., Walton, N.A., Arenou, F., Bastian, U., Cropper, M., Drimmel, R., Katz, D., Lattanzi, M.G., Bakker, J., Cacciari, C., Castañeda, J., Chaoul, L., Cheek, N., De Angeli, F., Fabricius, C., Guerra, R., Holl, B., Masana, E., Messineo, R., Mowlavi, N., Nienartowicz, K., Panuzzo, P., Portell, J., Riello, M., Seabroke, G.M., Tanga, P., Thévenin, F., Gracia-Abril, G., Comoretto, G., Garcia-Reinaldos, M., Teyssier, D., Altmann, M., Andrae, R., Audard, M., Bellas-Velidis, I., Benson, K., Berthier, J., Blomme, R., Burgess, P., Busso, G., Carry, B., Cellino, A., Clementini, G., Clotet, M., Creevey, O., Davidson, M., De Ridder, J., Delchambre, L., Dell'Oro, A., Ducourant, C., Fernández-Hernández, J., Fouesneau, M., Frémat, Y., Galluccio, L., García-Torres, M., González-Núñez, J., González-Vidal, J.J., Gosset, E., Guy, L.P., Halbwachs, J.L., Hambly, N.C., Harrison, D.L., Hernández, J., Hestroffer, D., Hodgkin, S.T., Hutton, A., Jasniewicz, G., Jean-Antoine-Piccolo, A., Jordan, S., Korn, A.J., Krone-Martins, A., Lanzafame, A.C., Lebzelter, T., Löffler, W., Manteiga, M., Marrese, P.M., Martín-Fleitas, J.M., Moitinho, A., Mora, A., Muinonen, K., Osinde, J., Pancino, E., Pauwels, T., Petit, J.M., Recio-Blanco, A., Richards, P.J., Rimoldini, L., Robin, A.C., Sarro, L.M., Siopis, C., Smith, M., Sozzetti, A., Süveges, M., Torra, J., van Reeven, W., Abbas, U., Abreu Aramburu, A., Accart, S., Aerts, C., Altavilla, G., Álvarez, M.A., Alvarez, R., Alves, J., Anderson, R.I., Andrei, A.H., Anglada Varela, E., Antiche, E., Antoja, T., Arcay, B., Astraatmadja, T.L., Bach, N., Baker, S.G., Balaguer-Núñez, L., Balm, P., Barache, C., Barata, C., Barbato, D., Barblan, F., Barklem, P.S., Barrado, D., Barros, M., Barstow, M.A., Bartholomé Muñoz, S., Bassilana, J.L., Becciani, U., Bellazzini, M., Berihuete, A., Bertone, S., Bianchi, L., Bienaymé, O., Blanco-Cuaresma, S., Boch, T., Boeche, C., Bombrun, A., Borrachero, R., Bossini, D., Bouquillon, S., Bourda, G., Bragaglia, A., Bramante, L., Breddels, M.A., Bressan, A., Brouillet, N., Brüsemeister, T., Brugaletta, E., Bucciarelli, B., Burlacu, A., Busonero, D., Butkevich, A.G., Buzzi, R., Caffau, E., Cancelliere, R., Cannizzaro, G., Cantat-Gaudin, T., Carballo, R., Carlucci, T., Carrasco, J.M., Casamiquela, L., Castellani, M., Castro-Ginard, A., Charlot, P., Chemin, L., Chiavassa, A., Cocozza, G., Costigan, G., Cowell, S., Crifo, F., Crosta, M., Crowley, C., Cuypers, J., Dafonte, C., Damerdji, Y., Dapergolas, A., David, P., David, M., de Laverny, P., De Luise, F., De March, R., de Martino, D., de Souza, R., de Torres, A., Debosscher, J., del Pozo, E., Delbo, M., Delgado, A., Delgado, H.E., Di Matteo, P., Diakite, S., Diener, C., Distefano, E., Dolding, C., Drazinos, P., Durán, J., Edvardsson, B., Enke, H., Eriksson, K., Esquej, P., Eynard Bontemps, G., Fabre, C., Fabrizio, M., Faigler, S., Falcão, A.J., Farràs Casas, M., Federici, L., Fedorets, G., Fernique, P., Figueras, F., Filippi, F., Findeisen, K., Fonti, A., Fraile, E., Fraser, M., Frézouls, B., Gai, M., Galleti, S., Garabato, D., García-Sedano, F., Garofalo, A., Garralda, N., Gavel, A., Gavras, P., Gerssen, J., Geyer, R., Giacobbe, P., Gilmore, G., Girona, S., Giuffrida, G., Glass, F., Gomes, M., Granvik, M., Gueguen, A., Guerrier, A., Guiraud, J., Gutiérrez-Sánchez, R., Haigron, R., Hatzidimitriou, D., Hauser, M., Haywood, M., Heiter, U., Helmi, A., Heu, J., Hilger, T., Hobbs, D., Hofmann, W., Holland, G., Huckle, H.E., Hypki, A., Icardi, V., Janßen, K., Jevardat de Fombelle, G., Jonker, P.G., Juhász, Á.L., Julbe, F., Karampelas, A., Kewley, A., Klar, J., Kochoska, A., Kohley, R., Kolenberg, K., Kontizas, M., Kontizas, E., Koposov, S.E., Kordopatis, G., Kostrzewa-Rutkowska, Z., Koubsky, P., Lambert, S., Lanza, A.F., Lasne, Y., Lavigne, J.B., Fustec, Y.Le., Le Poncin-Lafitte, C., Lebreton, Y., Leccia, S., Leclerc, N., Lecoeur-Taibi, I., Lenhardt, H., Leroux, F., Liao, S., Licata, E., Lindstrøm, H.E.P., Lister, T.A., Livanou, E., Lobel, A., López, M., Managau, S., Mann, R.G., Mantelet, G., Marchal, O., Marchant, J.M., Marconi, M., Marinoni, S., Marschalkó, G., Marshall, D.J., Martino, M., Marton, G., Mary, N., Massari, D., Matijevič, G., Mazeh, T., McMillan, P.J., Messina, S., Michalik, D., Millar, N.R., Molina, D., Molinaro, R., Molnár, L., Montegriffo, P., Mor, R., Morbidelli, R., Morel, T., Morris, D., Mulone, A.F., Muraveva, T., Musella, I., Nelemans, G., Nicastro, L., Noval, L., O'Mullane, W., Ordénovic, C., Ordóñez-Blanco, D., Osborne, P., Pagani, C., Pagano, I., Pailler, F., Palacin, H., Palaversa, L., Panahi, A., Pawlak, M., Piersimoni, A.M., Pineau, F.X., Plachy, E., Plum, G., Poggio, E., Poujoulet, E., Prša, A., Pulone, L., Racero, E., Ragaini, S., Rambaux, N., Ramos-Lerate, M., Regibo, S., Reylé, C., Riclet, F., Ripepi, V., Riva, A., Rivard, A., Rixon, G., Roegiers, T., Roelens, M., Romero-Gómez, M., Rowell, N., Royer, F., Ruiz-Dern, L., Sadowski, G., Sagristà Sellés, T., Sahlmann, J., Salgado, J., Salguero, E., Sanna, N., Santana-Ros, T., Sarasso, M., Savietto, H., Schultheis, M., Sciacca, E., Segol, M., Segovia, J.C., Ségransan, D., Shih, I.C., Siltala, L., Silva, A.F., Smart, R.L., Smith, K.W., Solano, E., Solitro, F., Sordo, R., Soria Nieto, S., Souchay, J., Spagna, A., Spoto, F., Stampa, U., Steele, I.A., Steidelmüller, H., Stephenson, C.A., Stoev, H., Suess, F.F., Surdej, J., Szabados, L., Szegedi-Elek, E., Tapiador, D., Taris, F., Tauran, G., Taylor, M.B., Teixeira, R., Terrett, D., Teyssandier, P., Thuillot, W., Titarenko, A., Torra Clotet, F., Turon, C., Ulla, A., Utrilla, E., Uzzi, S., Vaillant, M., Valentini, G., Valette, V., van Elteren, A., Van Hemelryck, E., van Leeuwen, M., Vaschetto, M., Vecchiato, A., Veljanoski, J., Viala, Y., Vicente, D., Vogt, S., von Essen, C., Voss, H., Votruba, V., Voutsinas, S., Walmsley, G., Weiler, M., Wertz, O., Wevers, T., Wyrzykowski., Ł., Yoldas, A., Žerjal, M., Ziaeepour, H., Zorec, J., Zschocke, S., Zucker, S., Zurbach, C., Zwitter, T., 2018a. Gaia data release 2. Summary of the contents and survey properties. Astron. Astrophys. 616, A1. http://dx.doi.org/10.1051/0004-6361/201833051, arXiv:1804.09365.

Gaia Collaboration, Brown, A.G.A., Vallenari, A., Prusti, T., de Bruijne, J.H.J., Babusiaux, C., Bailer-Jones, C.A.L., Biermann, M., Evans, D.W., Eyer, L., Jansen, F., Jordi, C., Klioner, S.A., Lammers, U., Lindegren, L., Luri, X., Mignard, F., Panem, C., Pourbaix, D., Randich, S., Sartoretti, P., Siddiqui, H.I., Soubiran, C., van Leeuwen, F., Walton, N.A., Arenou, F., Bastian, U., Cropper, M., Drimmel, R., Katz, D., Lattanzi, M.G., Bakker, J., Cacciari, C., Castañeda, J., Chaoul, L., Cheek, N., De Angeli, F., Fabricius, C., Guerra, R., Holl, B., Masana, E., Messineo, R., Mowlavi, N., Nienartowicz, K., Panuzzo, P., Portell, J., Riello, M., Seabroke, G.M., Tanga, P., Thévenin, F., Gracia-Abril, G., Comoretto, G., Garcia-Reinaldos, M., Teyssier, D., Altmann, M., Andrae, R., Audard, M., Bellas-Velidis, I., Benson, K., Berthier, J., Blomme, R., Burgess, P., Busso, G., Carry, B., Cellino, A., Clementini, G., Clotet, M., Creevey, O., Davidson, M., De Ridder, J., Delchambre, L., Dell'Oro, A., Ducourant, C., Fernández-Hernández, J., Fouesneau, M., Frémat, Y., Galluccio, L., García-Torres, M., González-Núñez, J., González-Vidal, J.J., Gosset, E., Guy, L.P., Halbwachs, J.L., Hambly, N.C., Harrison, D.L., Hernández, J., Hestroffer, D., Hodgkin, S.T., Hutton, A., Jasniewicz, G., Jean-Antoine-Piccolo, A., Jordan, S., Korn, A.J., Krone-Martins, A., Lanzafame, A.C., Lebzelter, T., Löffler, W., Manteiga, M., Marrese, P.M., Martín-Fleitas, J.M., Moitinho, A., Mora, A., Muinonen, K., Osinde, J., Pancino, E., Pauwels, T., Petit, J.M., Recio-Blanco, A., Richards, P.J., Rimoldini, L., Robin, A.C., Sarro, L.M., Siopis, C., Smith, M., Sozzetti, A., Süveges, M., Torra, J., van Reeven, W., Abbas, U., Abreu Aramburu, A., Accart, S., Aerts, C., Altavilla, G., Álvarez, M.A., Alvarez, R., Alves, J., Anderson, R.I., Andrei, A.H., Anglada Varela, E., Antiche, E., Antoja, T., Arcay, B., Astraatmadja, T.L., Bach, N., Baker, S.G., Balaguer-Núñez, L., Balm, P., Barache, C., Barata, C., Barbato, D., Barblan, F., Barklem, P.S., Barrado, D., Barros, M., Barstow, M.A., Bartholomé Muñoz, S., Bassilana, J.L., Becciani, U., Bellazzini, M., Berihuete, A., Bertone, S., Bianchi, L., Bienaymé, O., Blanco-Cuaresma, S., Boch, T., Boeche, C., Bombrun, A., Borrachero, R., Bossini, D., Bouquillon, S., Bourda, G., Bragaglia, A., Bramante, L., Breddels, M.A., Bressan, A.,

Brouillet, N., Brüsemeister, T., Brugaletta, E., Bucciarelli, B., Burlacu, A., Busonero, D., Butkevich, A.G., Buzzi, R., Caffau, E., Cancelliere, R., Cannizzaro, G., Cantat-Gaudin, T., Carballo, R., Carlucci, T., Carrasco, J.M., Casamiquela, L., Castellani, M., Castro-Ginard, A., Charlot, P., Chemin, L., Chiavassa, A., Cocozza, G., Costigan, G., Cowell, S., Crifo, F., Crosta, M., Crowley, C., Cuypers, J., Dafonte, C., Damerdji, Y., Dapergolas, A., David, P., David, M., de Laverny, P., De Luise, F., De March, R., de Martino, D., de Souza, R., de Torres, A., Debosscher, J., del Pozo, E., Delbo, M., Delgado, A., Delgado, H.E., Di Matteo, P., Diakite, S., Diener, C., Distefano, E., Dolding, C., Drazinos, P., Durán, J., Edvardsson, B., Enke, H., Eriksson, K., Esquej, P., Eynard Bontemps, G., Fabre, C., Fabrizio, M., Faigler, S., Falcão, A.J., Farràs Casas, M., Federici, L., Fedorets, G., Fernique, P., Figueras, F., Filippi, F., Findeisen, K., Fonti, A., Fraile, E., Fraser, M., Frézouls, B., Gai, M., Galleti, S., Garabato, D., García-Sedano, F., Garofalo, A., Garralda, N., Gavel, A., Gavras, P., Gerssen, J., Geyer, R., Giacobbe, P., Gilmore, G., Girona, S., Giuffrida, G., Glass, F., Gomes, M., Granvik, M., Gueguen, A., Guerrier, A., Guiraud, J., Gutiérrez-Sánchez, R., Haigron, R., Hatzidimitriou, D., Hauser, M., Haywood, M., Heiter, U., Helmi, A., Heu, J., Hilger, T., Hobbs, D., Hofmann, W., Holland, G., Huckle, H.E., Hypki, A., Icardi, V., Janßen, K., Jevardat de Fombelle, G., Jonker, P.G., Juhász, Á.L., Julbe, F., Karampelas, A., Kewley, A., Klar, J., Kochoska, A., Kohley, R., Kolenberg, K., Kontizas, M., Kontizas, E., Koposov, S.E., Kordopatis, G., Kostrzewa-Rutkowska, Z., Koubsky, P., Lambert, S., Lanza, A.F., Lasne, Y., Lavigne, J.B., Fustec, Y.Le., Le Poncin-Lafitte, C., Lebreton, Y., Leccia, S., Leclerc, N., Lecoeur-Taibi, I., Lenhardt, H., Leroux, F., Liao, S., Licata, E., Lindstrøm, H.E.P., Lister, T.A., Livanou, E., Lobel, A., López, M., Managau, S., Mann, R.G., Mantelet, G., Marchal, O., Marchant, J.M., Marconi, M., Marinoni, S., Marschalkó, G., Marshall, D.J., Martino, M., Marton, G., Mary, N., Massari, D., Matijevič, G., Mazeh, T., McMillan, P.J., Messina, S., Michalik, D., Millar, N.R., Molina, D., Molinaro, R., Molnár, L., Montegriffo, P., Mor, R., Morbidelli, R., Morel, T., Morris, D., Mulone, A.F., Muraveva, T., Musella, I., Nelemans, G., Nicastro, L., Noval, L., O'Mullane, W., Ordénovic, C., Ordóñez-Blanco, D., Osborne, P., Pagani, C., Pagano, I., Pailler, F., Palacin, H., Palaversa, L., Panahi, A., Pawlak, M., Piersimoni, A.M., Pineau, F.X., Plachy, E., Plum, G., Poggio, E., Poujoulet, E., Prša, A., Pulone, L., Racero, E., Ragaini, S., Rambaux, N., Ramos-Lerate, M., Regibo, S., Reylé, C., Riclet, F., Ripepi, V., Riva, A., Rivard, A., Rixon, G., Roegiers, T., Roelens, M., Romero-Gómez, M., Rowell, N., Royer, F., Ruiz-Dern, L., Sadowski, G., Sagristà Sellés, T., Sahlmann, J., Salgado, J., Salguero, E., Sanna, N., Santana-Ros, T., Sarasso, M., Savietto, H., Schultheis, M., Sciacca, E., Segol, M., Segovia, J.C., Ségransan, D., Shih, I.C., Siltala, L., Silva, A.F., Smart, R.L., Smith, K.W., Solano, E., Solitro, F., Sordo, R., Soria Nieto, S., Souchay, J., Spagna, A., Spoto, F., Stampa, U., Steele, I.A., Steidelmüller, H., Stephenson, C.A., Stoev, H., Suess, F.F., Surdej, J., Szabados, L., Szegedi-Elek, E., Tapiador, D., Taris, F., Tauran, G., Taylor, M.B., Teixeira, R., Terrett, D., Teyssandier, P., Thuillot, W., Titarenko, A., Torra Clotet, F., Turon, C., Ulla, A., Utrilla, E., Uzzi, S., Vaillant, M., Valentini, G., Valette, V., van Elteren, A., Van Hemelryck, E., van Leeuwen, M., Vaschetto, M., Vecchiato, A., Veljanoski, J., Viala, Y., Vicente, D., Vogt, S., von Essen, C., Voss, H., Votruba, V., Voutsinas, S., Walmsley, G., Weiler, M., Wertz, O., Wevers, T., Wyrzykowski, Ł., Yoldas, A., Žerjal, M., Ziaeepour, H., Zorec, J., Zschocke, S., Zucker, S., Zurbach, C., Zwitter, T., 2018b. Gaia Data Release 2. Summary of the contents and survey properties. Astron. Astrophys. 616, A1. http://dx.doi.org/10.1051/0004-6361/201833051, arXiv:1804.09365.

Gaia Collaboration, Prusti, T., de Bruijne, J.H.J., Brown, A.G.A., Vallenari, A., Babusiaux, C., Bailer-Jones, C.A.L., Bastian, U., Biermann, M., Evans, D.W., Eyer, L., Jansen, F., Jordi, C., Klioner, S.A., Lammers, U., Lindegren, L., Luri, X., Mignard, F., Milligan, D.J., Panem, C., Poinsignon, V., Pourbaix, D., Randich, S., Sarri, G., Sartoretti, P., Siddiqui, H.I., Soubiran, C., Valette, V., van Leeuwen, F., Walton, N.A., Aerts, C., Arenou, F., Cropper, M., Drimmel, R., Høg, E., Katz, D., Lattanzi, M.G., O'Mullane, W., Grebel, E.K., Holland, A.D., Huc, C., Passot, X., Bramante, L., Cacciari, C., Castañeda, J., Chaoul, L., Cheek, N., De Angeli, F., Fabricius, C., Guerra, R., Hernández, J., Jean-Antoine-Piccolo, A., Masana, E., Messineo, R., Mowlavi, N., Nienartowicz, K., Ordóñez-Blanco, D., Panuzzo, P., Portell, J., Richards, P.J., Riello, M., Seabroke, G.M., Tanga, P., Thévenin, F., Torra, J., Els, S.G., Gracia-Abril, G., Comoretto, G., Garcia-Reinaldos, M., Lock, T., Mercier, E., Altmann, M., Andrae, R., Astraatmadja, T.L., Bellas-Velidis, I., Benson, K., Berthier, J., Blomme, R., Busso, G., Carry, B., Cellino, A., Clementini, G., Cowell, S., Creevey, O., Cuypers, J., Davidson, M., De Ridder, J., de Torres, A., Delchambre, L., Dell'Oro, A., Ducourant, C., Frémat, Y., García-Torres, M., Gosset, E., Halbwachs, J.L., Hambly, N.C., Harrison, D.L., Hauser, M., Hestroffer, D., Hodgkin, S.T., Huckle, H.E., Hutton, A., Jasniewicz, G., Jordan, S., Kontizas, M., Korn, A.J., Lanzafame, A.C., Manteiga, M., Moitinho, A., Muinonen, K., Osinde, J., Pancino, E., Pauwels, T., Petit, J.M., Recio-Blanco, A., Robin, A.C., Sarro, L.M., Siopis, C., Smith, M., Smith, K.W., Sozzetti, A., Thuillot, W., van Reeven, W., Viala, Y., Abbas, U., Abreu Aramburu, A., Accart, S., Aguado, J.J., Allan, P.M., Allasia, W., Altavilla, G., Álvarez, M.A., Alves, J., Anderson, R.I., Andrei, A.H., Anglada Varela, E., Antiche, E., Antoja, T., Antón, S., Arcay, B., Atzei, A., Ayache, L., Bach, N., Baker, S.G., Balaguer-Núñez, L., Barache, C., Barata, C., Barbier, A., Barblan, F., Baroni, M., Barrado y Navascués, D., Barros, M., Barstow, M.A., Becciani, U., Bellazzini, M., Bellei, G., García, A.Bello., Belokurov, V., Bendjoya, P., Berihuete, A., Bianchi, L., Bienaymé, O., Billebaud, F., Blagorodnova, N., Blanco-Cuaresma, S., Boch, T., Bombrun, A., Borrachero, R., Bouquillon, S., Bourda, G., Bouy, H., Bragaglia, A., Breddels, M.A., Brouillet, N., Brüsemeister, T., Bucciarelli, B., Budnik, F., Burgess, P., Burgon, R., Burlacu, A., Busonero, D., Buzzi, R., Caffau, E., Cambras, J., Campbell, H., Cancelliere, R., Cantat-Gaudin, T., Carlucci, T., Carrasco, J.M., Castellani, M., Charlot, P., Charnas, J., Charvet, P., Chassat, F., Chiavassa, A., Clotet, M., Cocozza, G., Collins, R.S., Collins, P., Costigan, G., Crifo, F., Cross, N.J.G., Crosta, M., Crowley, C., Dafonte, C., Damerdji, Y., Dapergolas, A., David, P., David, M., De Cat, P., de Felice, F., de Laverny, P., De Luise, F., De March, R., de Martino, D., de Souza, R., Debosscher, J., del Pozo, E., Delbo, M., Delgado, A., Delgado, H.E., di Marco, F., Di Matteo, P., Diakite, S., Distefano, E., Dolding, C., Dos Anjos, S., Drazinos, P., Durán, J., Dzigan, Y., Ecale, E., Edvardsson, B., Enke, H., Erdmann, M., Escolar, D., Espina, M., Evans, N.W., Eynard Bontemps, G., Fabre, C., Fabrizio, M., Faigler, S., Falcão, A.J., Casas, M.Farràs., Faye, F., Federici, L., Fedorets, G., Fernández-Hernández, J., Fernique, P., Fienga, A., Figueras, F., Filippi, F., Findeisen, K., Fonti, A., Fouesneau, M., Fraile, E., Fraser, M., Fuchs, J., Furnell, R., Gai, M., Galleti, S., Galluccio, L., Garabato, D., García-Sedano, F., Garé, P., Garofalo, A., Garralda, N., Gavras, P., Gerssen, J., Geyer, R., Gilmore, G., Girona, S., Giuffrida, G., Gomes, M., González-Marcos, A., González-Núñez, J., González-Vidal, J.J., Granvik, M., Guerrier, A., Guillout, P., Guiraud, J., Gúrpide, A., Gutiérrez-Sánchez, R., Guy, L.P., Haigron, R., Hatzidimitriou, D., Haywood, M., Heiter, U., Helmi, A., Hobbs, D., Hofmann, W., Holl, B., Holland, G., Hunt, J.A.S., Hypki, A., Icardi, V., Irwin, M., Jevardat de Fombelle, G., Jofré, P., Jonker, P.G., Jorissen, A., Julbe, F., Karampelas, A., Kochoska, A., Kohley, R., Kolenberg, K., Kontizas, E., Koposov, S.E., Kordopatis, G., Koubsky, P., Kowalczyk, A., Krone-Martins, A., Kudryashova, M., Kull, I., Bachchan, R.K., Lacoste-Seris, F., Lanza, A.F., Lavigne, J.B., Le Poncin-Lafitte, C., Lebreton, Y., Lebzelter, T., Leccia, S., Leclerc, N., Lecoeur-Taibi, I., Lemaitre, V., Lenhardt, H., Leroux, F., Liao, S., Licata, E., Lindstrøm, H.E.P., Lister, T.A., Livanou, E., Lobel, A., Löffler, W., López, M., Lopez-Lozano, A., Lorenz, D., Loureiro, T., MacDonald, I., Magalhães Fernandes, T., Managau, S., Mann, R.G., Mantelet, G., Marchal, O., Marchant, J.M., Marconi, M., Marie, J., Marinoni, S., Marrese, P.M., Marschalkó, G., Marshall, D.J., Martín-Fleitas, J.M., Martino, M., Mary, N., Matijevič, G., Mazeh, T., McMillan, P.J., Messina, S., Mestre, A., Michalik, D., Millar, N.R., Miranda, B.M.H., Molina, D., Molinaro, R., Molinaro, M., Molnár, L., Moniez, M., Montegriffo, P., Monteiro, D., Mor, R., Mora, A., Morbidelli, R., Morel, T., Morgenthaler, S., Morley, T., Morris, D., Mulone, A.F., Muraveva, T., Musella, I., Narbonne, J., Nelemans, G., Nicastro, L., Noval, L., Ordénovic, C., Ordieres-Meré, J., Osborne, P., Pagani, C., Pagano, I., Pailler, F., Palacin, H., Palaversa, L., Parsons, P., Paulsen, T., Pecoraro, M., Pedrosa, R., Pentikäinen, H., Pereira, J., Pichon, B., Piersimoni, A.M., Pineau, F.X., Plachy, E., Plum, G., Poujoulet, E., Prša, A., Pulone, L., Ragaini, S., Rago, S., Rambaux, N., Ramos-Lerate, M., Ranalli, P., Rauw, G., Read, A., Regibo, S., Renk, F., Reylé, C., Ribeiro, R.A., Rimoldini, L., Ripepi, V., Riva, A., Rixon, G., Roelens, M., Romero-Gómez, M., Rowell, N., Royer, F., Rudolph, A., Ruiz-Dern, L., Sadowski, G., Sagristà Sellés, T., Sahlmann, J., Salgado, J., Salguero, E., Sarasso, M., Savietto, H., Schnorhk, A., Schultheis, M., Sciacca, E., Segol, M., Segovia, J.C., Segransan, D., Serpell, E., Shih, I.C., Smareglia, R., Smart, R.L., Smith, C., Solano, E., Solitro, F., Sordo, R., Soria Nieto, S., Souchay, J., Spagna, A., Spoto, F., Stampa, U., Steele, I.A., Steidelmüller, H., Stephenson, C.A., Stoev, H., Suess, F.F., Süveges, M., Surdej, J., Szabados, L., Szegedi-Elek, E., Tapiador, D., Taris, F., Tauran, G., Taylor, M.B., Teixeira, R., Terrett, D., Tingley, B., Trager, S.C., Turon, C., Ulla, A., Utrilla, E., Valentini, G., van Elteren, A., Van Hemelryck, E., van Leeuwen, M., Varadi, M., Vecchiato, A., Veljanoski, J., Via, T., Vicente, D., Vogt, S., Voss, H., Votruba, V., Voutsinas, S., Walmsley, G., et al., 2016. The Gaia mission. Astron. Astrophys. 595, A1. http://dx.doi.org/10.1051/0004-6361/201629272, arXiv:1609.04153.

Gaia Collaboration, Vallenari, A., Brown, A.G.A., Prusti, T., de Bruijne, J.H.J., Arenou, F., Babusiaux, C., Biermann, M., Creevey, O.L., Ducourant, C., Evans, D.W., Eyer, L., Guerra, R., Hutton, A., Jordi, C., Klioner, S.A., Lammers, U.L., Lindegren, L., Luri, X., Mignard, F., Panem, C., Pourbaix, D., Randich, S., Sartoretti, P., Soubiran, C., Tanga, P., Walton, N.A., Bailer-Jones, C.A.L., Bastian, U., Drimmel, R., Jansen, F., Katz, D., Lattanzi, M.G., van Leeuwen, F., Bakker, J., Cacciari, C., Castañeda, J., De Angeli, F., Fabricius, C., Fouesneau, M., Frémat, Y., Galluccio, L., Guerrier, A., Heiter, U., Masana, E., Messineo, R., Mowlavi, N., Nicolas, C., Nienartowicz, K., Pailler, F., Panuzzo, P., Riclet, F., Roux, W., Seabroke, G.M., Sordo, R., Thévenin, F., Gracia-Abril, G., Portell, J., Teyssier, D., Altmann, M., Andrae, R., Audard, M., Bellas-Velidis, I., Benson, K., Berthier, J., Blomme, R., Burgess, P.W., Busonero, D., Busso, G., Cánovas, H., Carry, B., Cellino, A., Cheek, N., Clementini, G., Damerdji, Y., Davidson, M., de Teodoro, P., Nuñez Campos, M., Delchambre, L., Dell'Oro, A., Esquej, P., Fernández-Hernández, J., Fraile, E., Garabato, D., García-Lario, P., Gosset, E., Haigron, R., Halbwachs, J.L., Hambly, N.C., Harrison, D.L., Hernández, J., Hestroffer, D., Hodgkin, S.T., Holl, B., Janßen, K., Jevardat de Fombelle, G., Jordan, S., Krone-Martins, A., Lanzafame, A.C., Löffler, W., Marchal, O., Marrese, P.M., Moitinho, A., Muinonen, K., Osborne, P., Pancino, E., Pauwels, T., Recio-Blanco, A., Reylé, C., Riello, M., Rimoldini, L., Roegiers, T., Rybizki, J., Sarro, L.M., Siopis, C., Smith, M., Sozzetti, A., Utrilla, E., van Leeuwen, M., Abbas, U., Ábrahám, P., Abreu Aramburu, A., Aerts, C., Aguado, J.J., Ajaj, M., Aldea-Montero, F., Altavilla, G., Álvarez, M.A., Alves, J., Anders, F., Anderson, R.I., Anglada Varela, E., Antoja, T., Baines, D., Baker, S.G., Balaguer-Núñez, L., Balbinot, E., Balog, Z., Barache, C., Barbato, D., Barros, M., Barstow, M.A., Bartolomé, S., Bassilana, J.L., Bauchet, N., Becciani, U., Bellazzini, M., Berihuete, A., Bernet, M., Bertone, S., Bianchi, L.,

Binnenfeld, A., Blanco-Cuaresma, S., Blazere, A., Boch, T., Bombrun, A., Bossini, D., Bouquillon, S., Bragaglia, A., Bramante, L., Breedt, E., Bressan, A., Brouillet, N., Brugaletta, E., Bucciarelli, B., Burlacu, A., Butkevich, A.G., Buzzi, R., Caffau, E., Cancelliere, R., Cantat-Gaudin, T., Carballo, R., Carlucci, T., Carnerero, M.I., Carrasco, J.M., Casamiquela, L., Castellani, M., Castro-Ginard, A., Chaoul, L., Charlot, P., Chemin, L., Chiaramida, V., Chiavassa, A., Chornay, N., Comoretto, G., Contursi, G., Cooper, W.J., Cornez, T., Cowell, S., Crifo, F., Cropper, M., Crosta, M., Crowley, C., Dafonte, C., Dapergolas, A., David, M., David, P., de Laverny, P., De Luise, F., De March, R., De Ridder, J., de Souza, R., de Torres, A., del Peloso, E.F., del Pozo, E., Delbo, M., Delgado, A., Delisle, J.B., Demouchy, C., Dharmawardena, T.E., Di Matteo, P., Diakite, S., Diener, C., Distefano, E., Dolding, C., Edvardsson, B., Enke, H., Fabre, C., Fabrizio, M., Faigler, S., Fedorets, G., Fernique, P., Fienga, A., Figueras, F., Fournier, Y., Fouron, C., Fragkoudi, F., Gai, M., Garcia-Gutierrez, A., Garcia-Reinaldos, M., García-Torres, M., Garofalo, A., Gavel, A., Gavras, P., Gerlach, E., Geyer, R., Giacobbe, P., Gilmore, G., Girona, S., Giuffrida, G., Gomel, R., Gomez, A., González-Núñez, J., González-Santamaría, I., González-Vidal, J.J., Granvik, M., Guillout, P., Guiraud, J., Gutiérrez-Sánchez, R., Guy, L.P., Hatzidimitriou, D., Hauser, M., Haywood, M., Helmer, A., Helmi, A., Sarmiento, M.H., Hidalgo, S.L., Hilger, T., Hładczuk, N., Hobbs, D., Holland, G., Huckle, H.E., Jardine, K., Jasniewicz, G., Jean-Antoine Piccolo, A., Jiménez-Arranz, Ó., Jorissen, A., Juaristi Campillo, J., Julbe, F., Karbevska, L., Kervella, P., Khanna, S., Kontizas, M., Kordopatis, G., Korn, A.J., Kóspál, Á., Kostrzewa-Rutkowska, Z., Kruszyńska, K., Kun, M., Laizeau, P., Lambert, S., Lanza, A.F., Lasne, Y., Le Campion, J.F., Lebreton, Y., Lebzelter, T., Leccia, S., Leclerc, N., Lecoeur-Taibi, I., Liao, S., Licata, E.L., Lindstrøm, H.E.P., Lister, T.A., Livanou, E., Lobel, A., Lorca, A., Loup, C., Madrero Pardo, P., Magdaleno Romeo, A., Managau, S., Mann, R.G., Manteiga, M., Marchant, J.M., Marconi, M., Marcos, J., Marcos Santos, M.M.S., Marín Pina, D., Marinoni, S., Marocco, F., Marshall, D.J., Martin Polo, L., Martín-Fleitas, J.M., Marton, G., Mary, N., Masip, A., Massari, D., Mastrobuono-Battisti, A., Mazeh, T., McMillan, P.J., Messina, S., Michalik, D., Millar, N.R., Mints, A., Molina, D., Molinaro, R., Molnár, L., Monari, G., Monguió, M., Montegriffo, P., Montero, A., Mor, R., Mora, A., Morbidelli, R., Morel, T., Morris, D., Muraveva, T., Murphy, C.P., Musella, I., Nagy, Z., Noval, L., Ocaña, F., Ogden, A., Ordenovic, C., Osinde, J.O., Pagani, C., Pagano, I., Palaversa, L., Palicio, P.A., Pallas-Quintela, L., Panahi, A., Payne-Wardenaar, S., Peñalosa Esteller, X., Penttilä, A., Pichon, B., Piersimoni, A.M., Pineau, F.X., Plachy, E., Plum, G., Poggio, E., Prša, A., Pulone, L., Racero, E., Ragaini, S., Rainer, M., Raiteri, C.M., Rambaux, N., Ramos, P., Ramos-Lerate, M., Re Fiorentin, P., Regibo, S., Richards, P.J., Rios Diaz, C., Ripepi, V., Riva, A., Rix, H.W., Rixon, G., Robichon, N., Robin, A.C., Robin, C., Roelens, M., Rogues, H.R.O., Rohrbasser, L., Romero-Gómez, M., Rowell, N., Royer, F., Ruz Mieres, D., Rybicki, K.A., Sadowski, G., Sáez Núñez, A., Sagristà Sellés, A., Sahlmann, J., Salguero, E., Samaras, N., Sanchez Gimenez, V., Sanna, N., Santoveña, R., Sarasso, M., Schultheis, M., Sciacca, E., Segol, M., Segovia, J.C., Ségransan, D., Semeux, D., Shahaf, S., Siddiqui, H.I., Siebert, A., Siltala, L., Silvelo, A., Slezak, E., Slezak, I., Smart, R.L., Snaith, O.N., Solano, E., Solitro, F., Souami, D., Souchay, J., Spagna, A., Spina, L., Spoto, F., Steele, I.A., Steidelmüller, H., Stephenson, C.A., Süveges, M., Surdej, J., Szabados, L., Szegedi-Elek, E., Taris, F., Taylor, M.B., Teixeira, R., Tolomei, L., Tonello, N., Torra, F., Torra, J., Torralba Elipe, G., Trabucchi, M., Tsounis, A.T., Turon, C., Ulla, A., Unger, N., Vaillant, M.V., van Dillen, E., van Reeven, W., Vanel, O., Vecchiato, A., Viala, Y., Vicente, D., Voutsinas, S., Weiler, M., Wevers, T., Wyrzykowski, Ł., Yoldas, A., Yvard, P., Zhao, H., Zorec, J., Zucker, S., Zwitter, T., 2023. Gaia Data Release 3. Summary of the content and survey properties. Astron. Astrophys. 674, A1. http://dx.doi.org/10.1051/0004-6361/202243940, arXiv:2208.00211.

Ginsburg, A., Sipőcz, B.M., Brasseur, C.E., Cowperthwaite, P.S., Craig, M.W., Deil, C., Guillochon, J., Guzman, G., Liedtke, S., Lian Lim, P., Lockhart, K.E., Mommert, M., Morris, B.M., Norman, H., Parikh, M., Persson, M.V., Robitaille, T.P., Segovia, J.C., Singer, L.P., Tollerud, E.J., de Val-Borro, M., Valtchanov, I., Woillez, J., Astroquery Collaboration, a subset of astropy Collaboration, 2019. astroquery: An Astronomical Web-querying Package in Python. Astron. J. 157, 98. http://dx.doi.org/10.3847/1538-3881/aafc33, arXiv:1901.04520.

Guzik, J.A., Kaye, A.B., Bradley, P.A., Cox, A.N., Neuforge, C., 2000. Driving the Gravity-Mode Pulsations in γ Doradus Variables. Astrophys. J. Lett. 542, L57–L60. http://dx.doi.org/10.1086/312908.

Handberg, Rasmus, Lund, Mikkel, Huber, Daniel, Buzasi, Derek, 2019. Tess data for asteroseismology lightcurves (tasoc). http://dx.doi.org/10.17909/T9-4SMN-DX89.

Handler, G., 2009. Delta scuti variables. In: Guzik, J.A., Bradley, P.A. (Eds.), Stellar Pulsation: Challenges for Theory and Observation. pp. 403–409. http://dx.doi.org/10.1063/1.3246528, arXiv:2110.09806.

Harris, C.R., Millman, K.J., van der Walt, S.J., Gommers, R., Virtanen, P., Cournapeau, D., Wieser, E., Taylor, J., Berg, S., Smith, N.J., Kern, R., Picus, M., Hoyer, S., van Kerkwijk, M.H., Brett, M., Haldane, A., del Río, M., Peterson, P., Gérard-Marchant, K., Reddy, T., Weckesser, W., Abbasi, H., Gohlke, C., Oliphant, T.E., 2020. Array programming with NumPy. Nature 585, 357–362. http://dx.doi.org/10.1038/s41586-020-2649-2.

Hedges, C., 2021. Vetting: A Stand-alone Tool for Finding Centroid Offsets in NASA Kepler, K2, and TESS, Alerting the Presence of Exoplanet False Positives. Res. Notes Am. Astron. Soc. 5, 262. http://dx.doi.org/10.3847/2515-5172/ac376a.

Hedges, C., Saunders, N., Martínez-Palomera, J., 2021. Contaminante: A Tool for Automatically Finding a Close-to-optimal Aperture for Transiting Signals in Kepler, K2, and TESS Data. Res. Notes Am. Astron. Soc. 5, 260. http://dx.doi.org/10.3847/2515-5172/ac3765.

Heinze, A.N., Tonry, J.L., Denneau, L., Flewelling, H., Stalder, B., Rest, A., Smith, K.W., Smartt, S.J., Weiland, H., 2018. A First Catalog of Variable Stars Measured by the Asteroid Terrestrial-impact Last Alert System (ATLAS). Astron. J. 156, 241. http://dx.doi.org/10.3847/1538-3881/aae47f, arXiv:1804.02132.

Higgins, M.E., Bell, K.J., 2023. Localizing Sources of Variability in Crowded TESS Photometry. Astron. J. 165, 141. http://dx.doi.org/10.3847/1538-3881/acb20c, arXiv:2204.06020.

Huang, C.X., 2020. Tess lightcurves from the mit quick-look pipeline (qlp). http://dx.doi.org/10.17909/T9-R086-E880.

Hunter, J.D., 2007. Matplotlib: A 2d graphics environment. Comput. Sci. Eng. 9, 90–95. http://dx.doi.org/10.1109/MCSE.2007.55.

Jeffery, C.S., 2008. The impact of asteroseismology on the theory of stellar evolution. Commun. Asteroseismol. 157, 240–248.

Jeon, Y.B., Lee, U., Park, Y.H., Kim, D., Jang, H., Cho, S., 2012. Variable Stars in the Region of CYG OB3 Association Centered on the Open Cluster NGC 6871 I: δ Scuti Type Stars. Publ. Korean Astron. Soc. 27, 399–409. http://dx.doi.org/10.5303/PKAS.2012.27.5.399.

Jørgensen, B.R., Lindegren, L., 2005. Determination of stellar ages from isochrones: Bayesian estimation versus isochrone fitting. Astron. Astrophys. 436, 127–143. http://dx.doi.org/10.1051/0004-6361:20042185.

Kahraman Aliçavuş, F., Handler, G., Chowdhury, S., Niemczura, E., Jayaraman, R., De Cat, P., Ozuyar, D., Aliçavuş, F., 2024. On the existence of maia variables. arXiv e-prints, arXiv:2404.16988, arXiv:2404.16988.

Kang, Y.B., Kim, S.L., Rey, S.C., Lee, C.U., Kim, Y.H., Koo, J.R., Jeon, Y.B., 2007. Variable Stars in the Open Cluster NGC 2099 (M37). Publ. Astron. Soc. Pac. 119, 239–250. http://dx.doi.org/10.1086/513883, arXiv:astro-ph/0702675.

Kjeldsen, H., 2000. CCD studies of delta scuti stars in open clusters. In: Szabados, L., Kurtz, D. (Eds.), IAU Colloq. In: The Impact of Large-Scale Surveys on Pulsating Star Research, vol. 176, pp. 415–420.

Kurtz, D.W., Shibahashi, H., Murphy, S.J., Bedding, T.R., Bowman, D.M., 2015. A unifying explanation of complex frequency spectra of γ Dor, SPB and Be stars: combination frequencies and highly non-sinusoidal light curves. Mon. Not. R. Astron. Soc. 450, 3015–3029. http://dx.doi.org/10.1093/mnras/stv868, arXiv:1504.04245.

Lenz, P., Breger, M., 2005. Period04 User Guide. Commun. Asteroseismol. 146, 53–136. http://dx.doi.org/10.1553/cia146s53.

Lightkurve Collaboration, Cardoso, J.V.d.M., Hedges, C., Gully-Santiago, M., Saunders, N., Cody, A.M., Barclay, T., Hall, O., Sagear, S., Turtelboom, E., Zhang, J., Tzanidakis, A., Mighell, K., Coughlin, J., Bell, K., Berta-Thompson, Z., Williams, P., Dotson, J., Barentsen, G., 2018. Lightkurve: Kepler and TESS Time Series Analysis in Python. Astrophysics Source Code Library, arXiv:1812.013.

Loktin, A.V., Matkin, N.V., Gerasimenko, T.P., 1994. The characteristics of open star clusters from UBV data. Astron. Astrophys. Trans. 4, 153–165. http://dx.doi.org/10.1080/10556799408205372.

Masci, F.J., Laher, R.R., Rusholme, B., Shupe, D.L., Groom, S., Surace, J., Jackson, E., Monkewitz, S., Beck, R., Flynn, D., Terek, S., Landry, W., Hacopians, E., Desai, V., Howell, J., Brooke, T., Imel, D., Wachter, S., Ye, Q.Z., Lin, H.W., Cenko, S.B., Cunningham, V., Rebbapragada, U., Bue, B., Miller, A.A., Mahabal, A., Bellm, E.C., Patterson, M.T., Jurić, M., Golkhou, V.Z., Ofek, E.O., Walters, R., Graham, M., Kasliwal, M.M., Dekany, R.G., Kupfer, T., Burdge, K., Cannella, C.B., Barlow, T., Van Sistine, A., Giomi, M., Fremling, C., Blagorodnova, N., Levitan, D., Riddle, R., Smith, R.M., Helou, G., Prince, T.A., Kulkarni, S.R., 2019. The zwicky transient facility: Data processing, products, and archive. Publ. Astron. Soc. Pac. 131, 018003. http://dx.doi.org/10.1088/1538-3873/aae8ac, arXiv:1902.01872.

Massey, P., Johnson, K.E., Degioia-Eastwood, K., 1995. The Initial Mass Function and Massive Star Evolution in the OB Associations of the Northern Milky Way. Astrophys. J. 454 (151), http://dx.doi.org/10.1086/176474.

MAST Team, 2021a. Tess fast light curves - all sectors. http://dx.doi.org/10.17909/T9-ST5G-3177.

MAST Team, 2021b. Tess light curves - all sectors. http://dx.doi.org/10.17909/T9-NMC8-F686.

McQuillan, A., Mazeh, T., Aigrain, S., 2014. Rotation Periods of 34 030Kepler Main-sequence Stars: The Full Autocorrelation Sample. Astrophys. J. Suppl. 211, 24. http://dx.doi.org/10.1088/0067-0049/211/2/24, arXiv:1402.5694.

Meynet, G., Mermilliod, J.C., Maeder, A., 1993. New dating of galactic open clusters. Astron. Astrophys. Suppl. Ser. 98, 477–504.

Nemec, J.M., Nemec, A.F.L., Lutz, T.E., 1994. Period-luminosity-metallicity relations, pulsation modes, absolute magnitudes, and distances for population II variable stars. Astron. J. 108, 222. http://dx.doi.org/10.1086/117062.

Nielsen, M.B., Gizon, L., Schunker, H., Karoff, C., 2013. Rotation periods of 12 000 main-sequence Kepler stars: Dependence on stellar spectral type and comparison with v sin i observations. Astron. Astrophys. 557, L10. http://dx.doi.org/10.1051/0004-6361/201321912, arXiv:1305.5721.

Oelkers, R.J., Stassun, K.G., 2018. Precision Light Curves from TESS Full-frame Images: A Different Imaging Approach. Astron. J. 156, 132. http://dx.doi.org/10.3847/1538-3881/aad68e, arXiv:1803.02316.

Ofek, E.O., Soumagnac, M., Nir, G., Gal-Yam, A., Nugent, P., Masci, F., Kulkarni, S.R., 2020. A catalogue of over 10 million variable source candidates in ZTF Data Release 1. Mon. Not. R. Astron. Soc. 499, 5782–5790. http://dx.doi.org/10.1093/mnras/staa2814, arXiv:2007.01537.

Paegert, M., Stassun, K.G., Collins, K.A., Pepper, J., Torres, G., Jenkins, J., Twicken, J.D., Latham, D.W., 2021. TESS input catalog versions 8.1 and 8.2: Phantoms in the 8.0 catalog and how to handle them. arXiv e-prints, arXiv:2108.04778, arXiv:2108.04778.

Palakkatharappil, D.B., Creevey, O.L., 2023. Asteroseismic age constraints on the open cluster NGC 2477 using oscillating stars identified with TESS FFI. Astron. Astrophys. 674, A146. http://dx.doi.org/10.1051/0004-6361/202243624, arXiv:2303.12205.

Pamos Ortega, D., García Hernández, A., Suárez, J.C., Pascual Granado, J., Barceló Forteza, S., Rodón, J.R., 2022. Determining the seismic age of the young open cluster α Per using δ Scuti stars. Mon. Not. R. Astron. Soc. 513, 374–388. http://dx.doi.org/10.1093/mnras/stac864, arXiv:2203.14256.

Paunzen, E., Heiter, U., Netopil, M., Soubiran, C., 2010. On the metallicity of open clusters. I. Photometry. Astron. Astrophys. 517, A32. http://dx.doi.org/10.1051/0004-6361/201014131, arXiv:1008.3476.

Pedersen, M.G., Bell, K.J., 2023. Contamination in TESS Light Curves: The Case of the Fast Yellow Pulsating Supergiants. Astron. J. 165, 239. http://dx.doi.org/10.3847/1538-3881/accc31, arXiv:2304.05706.

Pietrukowicz, P., Soszyński, I., Netzel, H., Wrona, M., Udalski, A., Szymański, M.K., Poleski, R., Kozłowski, S., Skowron, J., Ulaczyk, D., Skowron, D.M., Mróz, P., Rybicki, K., Iwanek, P., Gromadzki, M., 2020. Over 10000 δ Scuti Stars toward the Galactic Bulge from OGLE-IV. Acta Astronomica 70, 241–263. http://dx.doi.org/10.32023/0001-5237/70.4.1, arXiv:2103.10436.

Prša, A., Kochoska, A., Conroy, K.E., Eisner, N., Hey, D.R., IJspeert, L., Kruse, E., Fleming, S.W., Johnston, C., Kristiansen, M.H., LaCourse, D., Mortensen, D., Pepper, J., Stassun, K.G., Torres, G., Abdul-Masih, M., Chakraborty, J., Gagliano, R., Guo, Z., Hambleton, K., Hong, K., Jacobs, T., Jones, D., Kostov, V., Lee, J.W., Omohundro, M., Orosz, J.A., Page, E.J., Powell, B.P., Rappaport, S., Reed, P., Schnittman, J., Schwengeler, H.M., Shporer, A., Terentev, I.A., Vanderburg, A., Welsh, W.F., Caldwell, D.A., Doty, J.P., Jenkins, J.M., Latham, D.W., Ricker, G.R., Seager, S., Schlieder, J.E., Shiao, B., Vanderspek, R., Winn, J.N., 2022. TESS Eclipsing Binary Stars. I. Short-cadence Observations of 4584 Eclipsing Binaries in Sectors 1-26. Astrophys. J. Suppl. 258, 16. http://dx.doi.org/10.3847/1538-4365/ac324a, arXiv:2110.13382.

Reimann, H.G., 1989. UVBY photometry of open clusters. II. NGC 6871. Astron. Nachr. 310, 273–280. http://dx.doi.org/10.1002/asna.2113100407.

Ricker, G.R., Winn, J.N., Vanderspek, R., Latham, D.W., Bakos, G.Á., Bean, J.L., Berta-Thompson, Z.K., Brown, T.M., Buchhave, L., Butler, N.R., Butler, R.P., Chaplin, W.J., Charbonneau, D., Christensen-Dalsgaard, J., Clampin, M., Deming, D., Doty, J., De Lee, N., Dressing, C., Dunham, E.W., Endl, M., Fressin, F., Ge, J., Henning, T., Holman, M.J., Howard, A.W., Ida, S., Jenkins, J.M., Jernigan, G., Johnson, J.A., Kaltenegger, L., Kawai, N., Kjeldsen, H., Laughlin, G., Levine, A.M., Lin, D., Lissauer, J.J., MacQueen, P., Marcy, G., McCullough, P.R., Morton, T.D., Narita, N., Paegert, M., Palle, E., Pepe, F., Pepper, J., Quirrenbach, A., Rinehart, S.A., Sasselov, D., Sato, B., Seager, S., Sozzetti, A., Stassun, K.G., Sullivan, P., Szentgyorgyi, A., Torres, G., Udry, S., Villasenor, J., 2015. Transiting Exoplanet Survey Satellite (TESS). J. Astron. Telesc. Instrum. Syst. 1, 014003. http://dx.doi.org/10.1117/1.JATIS.1.1.014003.

Ricker, G.R., Winn, J.N., Vanderspek, R., Latham, D.W., Bakos, G.Á., Bean, J.L., Berta-Thompson, Z.K., Brown, T.M., Buchhave, L., Butler, N.R., Butler, R.P., Chaplin, W.J., Charbonneau, D., Christensen-Dalsgaard, J., Clampin, M., Deming, D., Doty, J., De Lee, N., Dressing, C., Dunham, E.W., Endl, M., Fressin, F., Ge, J., Henning, T., Holman, M.J., Howard, A.W., Ida, S., Jenkins, J., Jernigan, G., Johnson, J.A., Kaltenegger, L., Kawai, N., Kjeldsen, H., Laughlin, G., Levine, A.M., Lin, D., Lissauer, J.J., MacQueen, P., Marcy, G., McCullough, P.R., Morton, T.D., Narita, N., Paegert, M., Palle, E., Pepe, F., Pepper, J., Quirrenbach, A., Rinehart, S.A., Sasselov, D., Sato, B., Seager, S., Sozzetti, A., Stassun, K.G., Sullivan, P., Szentgyorgyi, A., Torres, G., Udry, S., Villasenor, J., 2014. Transiting exoplanet survey satellite (TESS). In: Oschmann, Jacobus M.J., Clampin, M., Fazio, G.G., MacEwen, H.A. (Eds.), Space Telescopes and Instrumentation 2014: Optical, Infrared, and Millimeter Wave. 914320. http://dx.doi.org/10.1117/12.2063489, arXiv:1406.0151.

Skarka, M., Henzl, Z., 2024. Periodic variable A-F spectral type stars in the southern TESS continuous viewing zone. http://dx.doi.org/10.48550/arXiv.2406.12578, arXiv e-prints, arXiv:2406.12578.

Skarka, M., Žák, J., Fedurco, M., Paunzen, E., Henzl, Z., Mašek, M., Karjalainen, R., Sanchez Arias, J.P., Sódor, Á., Auer, R.F., Kabáth, P., Karjalainen, M., Liška, J., Štegner, D., 2022. Periodic variable A-F spectral type stars in the northern TESS continuous viewing zone. I. Identification and classification. Astron. Astrophys. 666, A142. http://dx.doi.org/10.1051/0004-6361/202244037, arXiv:2207.12922.

Slawson, R.W., Prša, A., Welsh, W.F., Orosz, J.A., Rucker, M., Batalha, N., Doyle, L.R., Engle, S.G., Conroy, K., Coughlin, J., Gregg, T.A., Fetherolf, T., Short, D.R., Windmiller, G., Fabrycky, D.C., Howell, S.B., Jenkins, J.M., Uddin, K., Mullally, F., Seader, S.E., Thompson, S.E., Sanderfer, D.T., Borucki, W., Koch, D., 2011. Kepler Eclipsing Binary Stars. II. 2165 Eclipsing Binaries in the Second Data Release. Astron. J. 142, 160. http://dx.doi.org/10.1088/0004-6256/142/5/160, arXiv:1103.1659.

Soderblom, D.R., 2010. The Ages of Stars. Annu. Rev. Astron. Astrophys. 48, 581–629. http://dx.doi.org/10.1146/annurev-astro-081309-130806, arXiv:1003.6074.

Soszyński, I., Pietrukowicz, P., Skowron, J., Udalski, A., Szymański, M.K., Skowron, D.M., Poleski, R., Kozłowski, S., Mróz, P., Ulaczyk, K., Rybicki, K., Iwanek, P., Wrona, M., Gromadzki, M., 2021. Over 24 000 δ Scuti Stars in the Galactic Bulge and Disk from the OGLE Survey. Acta Astronomica 71, 189–204. http://dx.doi.org/10.32023/0001-5237/71.3.1, arXiv:2111.03072.

Southworth, J., Maxted, P.F.L., Smalley, B., 2004. Eclipsing binaries in open clusters - II. V453 Cyg in NGC 6871. Mon. Not. R. Astron. Soc. 351, 1277–1289. http://dx.doi.org/10.1111/j.1365-2966.2004.07871.x, arXiv:astro-ph/0403572.

Tadross, A.L., 2003. Metallicity distribution on the galactic disk. New Astron. 8, 737–744. http://dx.doi.org/10.1016/S1384-1076(03)00062-9.

Tadross, A.L., 2011. A Catalog of 120 NGC Open Star Clusters. J. Korean Astron. Soc. 44, 1–11. http://dx.doi.org/10.5303/JKAS.2011.44.1.001, arXiv:1108.2134.

Ulla, A., Creevey, O.L., Álvarez, M.A., Andrae, R., Bailer-Jones, C.A.L., Bellas-Velidis, I., Brugaletta, E., Carballo, R., Dafonte, C., Delchambre, L., Dharmawardena, T., Drimmel, R., Fouesneau, M., Frémat, Y., Garabato, D., Hatzidimitriou, D., Heiter, U., Kordopatis, G., Korn, A.J., Lanzafame, A., Lobel, A., Manteiga, M., Marshall, D.J., Pailler, F., Pallas-Quintela, L., Recio-Blanco, A., Rybizki, J., Sarro Baro, L.M., Schultheis, M., Sordo, R., Soubiran, C., Thévenin, F., Vallenari, A., 2022. Gaia DR3 documentation chapter 11: Astrophysical parameters. In: Gaia Data Processing and Analysis Consortium. Gaia DR3 documentation, European Space Agency.

Uytterhoeven, K., Moya, A., Grigahcène, A., Guzik, J.A., Gutiérrez-Soto, J., Smalley, B., Handler, G., Balona, L.A., Niemczura, E., Fox Machado, L., Benatti, S., Chapellier, E., Tkachenko, A., Szabó, R., Suárez, J.C., Ripepi, V., Pascual, J., Mathias, P., Martín-Ruíz, S., Lehmann, H., Jackiewicz, J., Hekker, S., Gruberbauer, M., García, R.A., Dumusque, X., Díaz-Fraile, D., Bradley, P., Antoci, V., Roth, M., Leroy, B., Murphy, S.J., De Cat, P., Cuypers, J., Kjeldsen, H., Christensen-Dalsgaard, J., Breger, M., Pigulski, A., Kiss, L.L., Still, M., Thompson, S.E., van Cleve, J., 2011. The Kepler characterization of the variability among A- and F-type stars. I. General overview. Astron. Astrophys. vol. 534, A125. http://dx.doi.org/10.1051/0004-6361/201117368, arXiv:1107.0335.

Virtanen, P., Gommers, R., Oliphant, T.E., Haberland, M., Reddy, T., Cournapeau, D., Burovski, E., Peterson, P., Weckesser, W., Bright, J., van der Walt, S.J., Brett, M., Wilson, J., Millman, K.J., Mayorov, N., Nelson, A.R.J., Jones, E., Kern, R., Larson, E., Carey, C.J., Polat, İ., Feng, Y., Moore, E.W., VanderPlas, J., Laxalde, D., Perktold, J., Cimrman, R., Henriksen, I., Quintero, E.A., Harris, C.R., Archibald, A.M., Ribeiro, A.H., Pedregosa, F., van Mulbregt, P., SciPy 1.0 Contributors, 2020. SciPy 1.0: Fundamental algorithms for scientific computing in python. Nature Methods vol. 17, 261–272. http://dx.doi.org/10.1038/s41592-019-0686-2.

Viskum, M., Hernandez, M.M., Belmonte, J.A., Frandsen, S., 1997. A search for delta Scuti stars in northern open clusters. I. CCD photometry of NGC 7245, NGC 7062, NGC 7226 and NGC 7654. Astron. Astrophys. 328, 158–166.

Xiong, D.R., Deng, L., Zhang, C., Wang, K., 2016. Turbulent convection and pulsation stability of stars - II. Theoretical instability strip for δ Scuti and γ Doradus stars. Mon. Not. R. Astron. Soc. vol. 457, 3163–3177. http://dx.doi.org/10.1093/mnras/stw047, arXiv:1808.09621.

Zhou, A.Y., 2023a. Identifying superwasp detected candidate variables with TESS. In: Research Notes of the AAS, vol. 7, p. 227. http://dx.doi.org/10.3847/2515-5172/ad06b9.

Zhou, A.Y., 2023b. New pulsating variable stars and eclipsing binaries in NGC 6871. In: Research Notes of the AAS, vol. 7, p. 262. http://dx.doi.org/10.3847/2515-5172/ad12a3.

Zhou, A.Y., 2023c. Variability census of legacy catalogs: I. 1800+ new δ scuti and γ doradus stars. Res. Notes Am. Astron. Soc. 7, 210. http://dx.doi.org/10.3847/2515-5172/acffc2.

Zhou, A.Y., 2024. Unveiling δ Scuti and γ Doradus hybrid pulsation of HD 53166 and HD 53349 plus rich frequencies in HD 52788. New Astron. 105, 102081. http://dx.doi.org/10.1016/j.newast.2023.102081, arXiv:2301.08355.

Zhou, A.Y., Liu, Z.L., Du, B.T., 2001a. Bi-modal pulsation of the delta Scuti star V1821 Cygni. Astron. Astrophys. 371, 233–239. http://dx.doi.org/10.1051/0004-6361:20010375.

Zhou, A.Y., Rodríguez, E., Liu, Z.L., Du, B.T., 2001b. Multiperiodicity and physical nature of the δ Sct star GSC 2683-3076. Mon. Not. R. Astron. Soc. 326, 317–325. http://dx.doi.org/10.1046/j.1365-8711.2001.04604.x.